Investigating the effects of cholesterol on phospholipid bilayer with molecular dynamics simulations

Chen, Xia

Investigating the effects of cholesterol on phospholipid bilayer with molecular dynamics simulations

By Xia Chen

Supervisors: Professor Wen Wang
Professor Martin Dove

Submitted for the Degree of Doctor of Philosophy

Institute of Bioengineering
Queen Mary University of London

2015

Declaration

I, Xia Chen, declare that the work include in this thesis is performed by myself, unless clearly acknowledged otherwise, during the course of my PhD period at Queen Mary University of London.

I accept that the College has the right to use plagiarism detection software to check the electronic version of the thesis.

I confirm that this thesis has not been submitted for the award of a degree at this or any other university

Signature: Xia Chen

Acknowledgements

I would like to thank Professor Wen Wang and Professor Martin Dove for all their supervision, invaluable advice, and encouragements during my PhD study.

I would also like to thank all the people who have provided me useful advice on simulation and programming techniques, especially to Dr. Mario Orsi, Ms. Min Gao, Mr. Wei Ding.

Many thanks to the current and former group membrane for sharing your happiness and giving warmth to me during my study: Dr. Yiling Lu, Dr. Yankai Liu, Dr. Ke Bai, Dr. Hong Chang, Dr. Lin Qiu, Dr. Weiqi Li Dr. Xiaotian Yu, Dr. Devendra inder Deo, Dr. Zhengjun Lv, Ms. Miao Lin, Ms. Rebecca Jane Norton, Ms. Junyao Yang, Ms. Baoqi Yu, Ms. Pioapiao Luo and Mr. Wenjie Zhu.

At last, I would express my great gratitude to my family, especially to my wife, Dan Xu. I could not have completed my PhD without her love and support.

Abstract

This PhD project studies the effects of cholesterol in phospholipid bilayer using molecular dynamics (MD) simulations. Dipalmitoylphosphatidylcholine (DPPC) bilayers with cholesterol concentrations between 0% and 40% were simulated using all-atom CHARMM36 force filed. The main concerned aspects of the lipid bilayer with cholesterol include structural properties, the lipid dynamics and mechanical properties of the bilayer. It was found that the lipid bilayer was condensed when it was embedded with cholesterol molecules. Addition of cholesterol in bilayer systems induced a smaller average surface area occupied by DPPC molecules, a more ordered hydrocarbon chains of DPPC molecules, and a thickened bilayer. The effects of cholesterol on dynamics properties of lipid bilayer were also observed as a decrease in the lateral diffusion coefficients for both cholesterol and DPPC in DPPC-cholesterol mixture bilayer. Furthermore, lateral pressure profiles were calculated to look into the local stress distribution along the bilayer norm. It was found that cholesterol introduced extra contraction troughs in the profiles at the position under the head groups of DPPC, which explained the structural changes observed in the study. Bending moduli of the bilayer with and without cholesterol were estimated by calculating the splay modulus of pairs of each bilayer components. It was found that the involvement of cholesterol reduced the splay angles of each pair of bilayer component,

resulting in a higher bending modulus of the structure.

Table of Contents

List of Figures and Tables

List of Abbreviation

DPPC	Dipalmitoylphosphatidylcholine
DMPC	Dimyristoylphosphatidylcholine
DOPC	Dioleoylphosphatidylcholine
SM	Sphingomyelin
PC	Phosphatidylcholine
PE	Phosphatidylethanolamine
PS	Phosphatidylserine
MD	Molecular dynamics
NMR	Nuclear magnetic resonance
NpT	Constant number of particles, pressure, and temperature
PPPM	Particle-Particle Particle-Mesh
PBC	Periodic boundary condition
EDP	Electron density profile
LPP	Lateral pressure profile
ACF	Autocorrelation function
MSD	Mean square displacement
PMF	Potential of mean force
T_m	Transition temperature
L_d	Liquid-disorder phase

L_o	Liquid-order phase
S_o	Gel phase
Å	Angstrom
k_B	Boltzmann constant
atm	Atmosphere

Chapter 1 Introduction

1.1 Cell membrane and lipid bilayer

Cell membrane is a biological membrane that separates cellular interiors from extracellular environment. Biological membrane controls movement of substances across the structure, and gets involved in a variety of cellular processes such as cell adhesion, ion conductivity and mechanotransduction of cells.

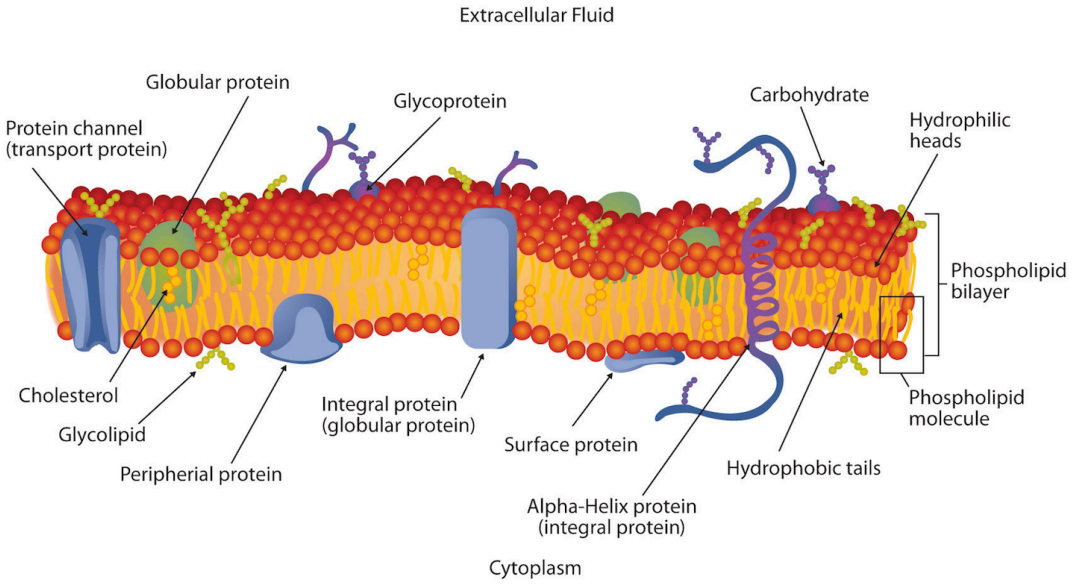

Figure 1 Plasma membrane diagram.

The image was adopted from the textbook (David W. Ball, 2011)

Singer and Nicolson (1972) proposed the first comprehensive model of the plasma membrane with the fluid-mosaic model (shown in Figure 1). The model described a complicated asymmetric, possibly heterogeneous distribution of

lipids forming a fluid substrate in which the proteins and other membrane substances are embedded. In the two-dimensional liquid substrate, lipids, proteins and other membrane components can diffuse around to some extent within the planar structure. The fundamental fluid-like structure is a lipid bilayer, and the key materials forming a bilayer are phospholipids. Physically, phospholipids molecules aggregate into a two-lipids thick layer spontaneously with their hydrophilic groups pointing outward the water phase and the hydrophobic groups pointing inward the centre of the bilayer. The outer side of the lipid bilayer is covered with glycocalyx complex, which is a macromolecular film consisting of glycoproteins and proteoglycans with glycosaminoglycans chains attached to their core proteins. On the inner side of the bilayer, the structure is connected and supported by the membrane-associated cytoskeleton, in particular to actin filaments.(Cantor, 1999b)

Though lipid bilayer only occurs a small fraction of the total mass of most membranes, particularly compared to membrane proteins, it is the structural matrix for other membrane components to be arranged in or around. The bilayer structure is formed via self-assembly with a complex mixture of the lipids. The driving forces for forming the bilayer structure arise from the Van der Waals, electrostatic, hydrogen bond, and other inter-molecular interactions. The hydrophobic effect is considered as the major factor to form the bilayer structure, since the non-polar hydrocarbon chains of phospholipids are repulsed by water

molecules and packed into a nearly insulated environment away from water, and the hydrophilic polar head of lipids are arranged in line via energetically favourable interactions with water molecules or other molecules in the aqueous environment (Yeagle, 1989).

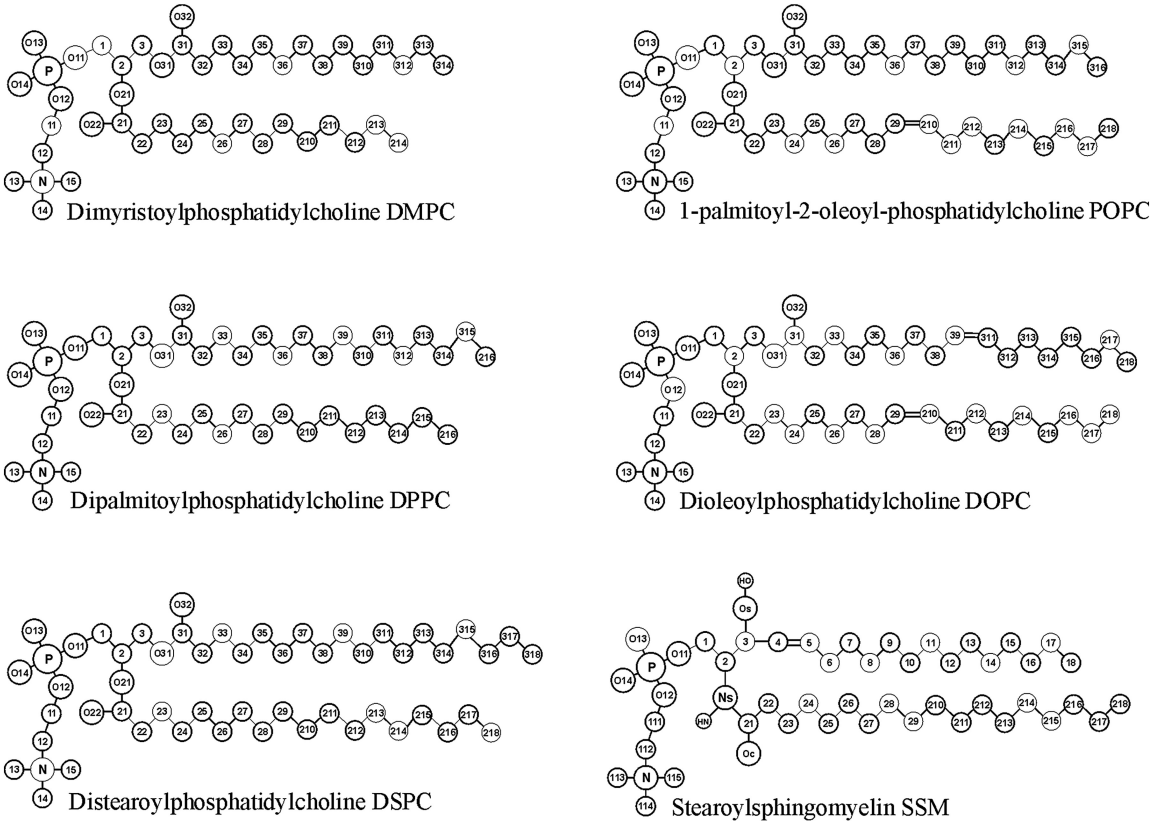

Figure 2 Chemical structral of phosphlipids in model membrane.
Carbon atoms in each molecule are numbered. The figure was adopted from reference (Rog et al., 2009)

1.1.1 Phospholipids

In a real plasma membrane, the lipids species involved of forming the lipid bilayer are of enormous diversity. For instance, in a recent study, thousands of

lipids species were found in a single sample of adipose tissue (Pietilainen et al., 2011, Rog and Vattulainen, 2014). The huge diversity comes from variations in different parts of the phospholipids molecules. For example, a glycerol-phospholipid molecule can be considered with three different compositional parts. Firstly, the glycerol group is located at the centre part of the molecule, acting as the backbone, to which two hydrophobic fatty acid hydrocarbon chains are attached at the position *sn*-1 and *sn*-2, respectively, and a phosphoric group is attached at position *sn*-3. The group attached to the phosphoric acid can be various such as choline, ethanolamine, serine, glycerol or inositol (Yeagle, 1989). The attached group and the phosphoric acid group together are called the head group of phospholipid. Based on the added group in head group, the glycerol-phospholipids are named more specifically, such as Phosphatidyl-cholines (PC), phosphatidyl-ethanolamines (PE), Phosphatidyl-serines (PS). Aside from the diversity of the head group, the two hydrocarbon chains at *sn*-1 and *sn*-2 can vary in both length and saturation state (number of double bonds in chains) (Yeagle, 1989). Based on the saturation in the hydrocarbon chains, phospholipids can also be categorized into saturated lipids and unsaturated lipids. Besides the glycerol-phospholipids, other backbone groups can replace the backbone glycerol and result in other lipid species (Yeagle, 1989) as well. For example, sphingomyelin (SM) is one of the most studied phosphosphingolipids, and the SM molecule is synthesized from the sphingosine group rather than glycerol group. Due to complex compositions

of a real cell membrane, a model membrane system consisting of one or more lipid types is often constructed with fundamental features in laboratory or in computer simulation for cell membrane study. Figure 2 shows several popular phospholipids used in modelling a membrane because of their representative chemical structure among the huge diversity of the phospholipid species in nature. In present study, the dipalmitoylphosphatidylcholine (DPPC, 16:0/16:0), which is composed of a choline phosphoric head group, glycerol and two saturated fatty acid tails, is used as the constituent of the modelled lipid membrane, because it is an artificially synthesized lipid species for research purposes in studying liposomes, lipid bilayers and biological membrane model. Since it has been studied widely in both experiments and computer simulations, DPPC lipid bilayer has been regarded as a benchmark for the membrane modelling.

1.1.2 Cholesterol

Besides phospholipids, cholesterol is one of the most important lipid species in nature, it occurs at relatively high concentrations in animal cell membranes. Typically, the cholesterol concentration is about 20-30 mol% in biological membranes, and it is found as much as 50 mol% in red blood cell (Sackmann, 1995). Cholesterol plays numerous important roles in membranes. Physiologically, cholesterol is one important precursor to hormones and

vitamins. Physically, it gets involved in modulating mechanical properties of membranes and controlling thermodynamics phase states of a lipid bilayer (Rog et al., 2009).

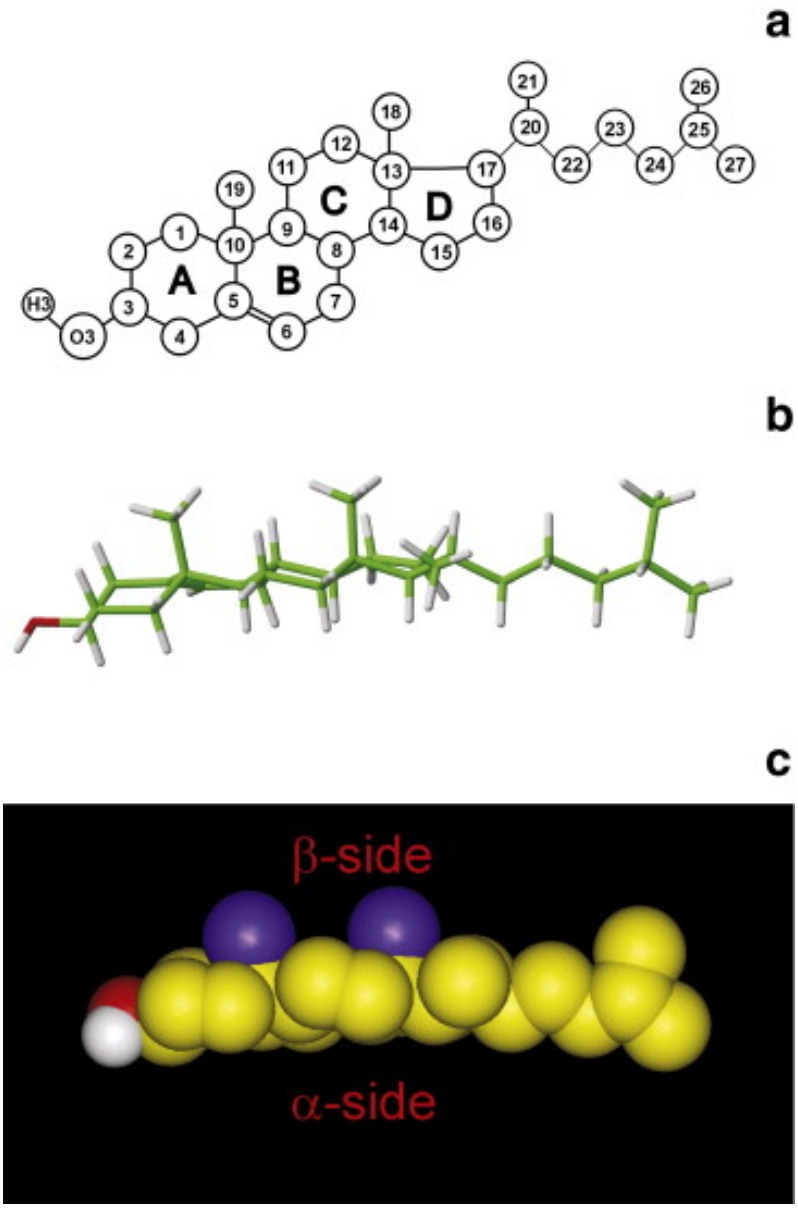

Figure 3 Structure of cholesterol molecule.

(a) The numbering of carbon atoms and rings (labelled with A, B, C, D); (b) The stick model of three-dimensional structure of cholesterol; (c) The space-filling model of cholesterol, with the smooth α side, and the rough β side labeled. Figure was adopted from reference (Rog et al., 2009)

As to the chemical structure shown in Figure 3, cholesterol is composed of a tetracyclic fused ring backbone, with a single hydroxyl group at carbon 3, a double bond between carbons 5 and 6, and a short hydrocarbon side chain at carbon 17. The rings are *trans* fused into multi-ring structure and it is flat and rigid, which characterises cholesterol and most of its analogues. From the three-dimensional view (see Figure 3 (c)), it is worth mentioning that the hydroxyl (-OH) group, the two individual methyl groups C18 and C19, attached at positions 10 and 13 respectively, are positioned on the same side of the ring skeleton in *cis* orientations, and this face of the ring structure is called β-side or rough side of cholesterol. Accordingly, the flat side of cholesterol is commonly known as α-side. In the cholesterol molecule the only additional group is the 3β-hydroxyl group, while in other sterols there are many possible substituents oriented toward α- or β-side. Most part of cholesterol is hydrophobic except the polar hydroxyl group, which adds hydrophilic property to cholesterol, so cholesterol is also an amphiphilic molecule similar with phospholipids. In a lipid membrane with cholesterol, cholesterol molecules are found to be oriented parallel to phospholipids and aligned with the polar hydroxyl group pointing outward to head groups of phospholipids molecules and no-polar part buried in the hydrocarbon chains of the phospholipids (Ohvo-Rekila et al., 2002).

1.1.3 Thermodynamics phase behaviours of lipid bilayer and cholesterol's effect

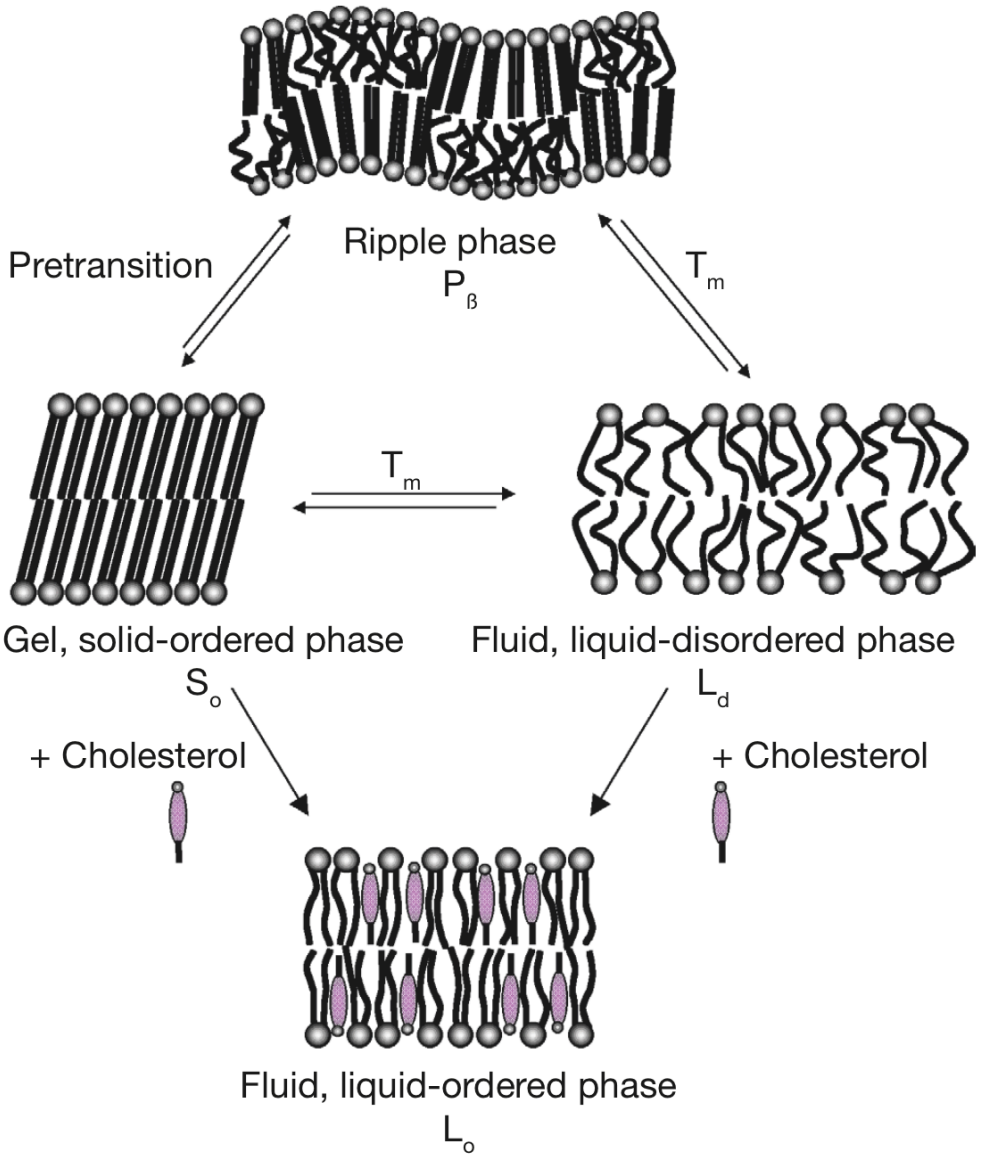

Figure 4 Thermodynamics states of a lipid bilayer in fluid environment.

Scheme demonstrating the different phase behaviours of a lipid bilayer, and the water regions are not shown in the figure for clarity. Note: T_m refers to the transition temperature. The figure was adopted from reference (Eeman and Deleu, 2010)

One of the most important properties of a lipid bilayer is the fluidity. A lipid molecule in a bilayer can move around laterally in plane and rotate on its site, and the mobility of molecules is affected by temperature and composition of the lipid bilayer. The phase behaviour of a lipid bilayer is commonly categorised with the ordering state of the hydrocarbon chain quantitatively. As seen in Figure 4, a pure lipid bilayer is characterised with a transition temperature at which bilayer undergo transition from the gel phase S_o to fluid phases L_d. In the gel or solid-ordered phase, the tails of the lipids are ordered and tilted slightly with respect to the bilayer normal, and the mobility of the lipids in bilayer is restricted to the slowest level. Upon heating the bilayers, some of the lipids become active and the tails of them become disordered, and the bilayer occurs ripple structure on the surface. Then when it is above the main phase transition temperature (T_m), the hydrocarbon chains of lipids become fully melted into liquid like conformation with relatively higher degrees of rotational and translational freedom. A lipid bilayer at a temperature above the T_m is often called a fluid or liquid-like lipid bilayer, which is mainly considered phase behaviour in lipid bilayer research. (Karplus and McCammon, 2002)

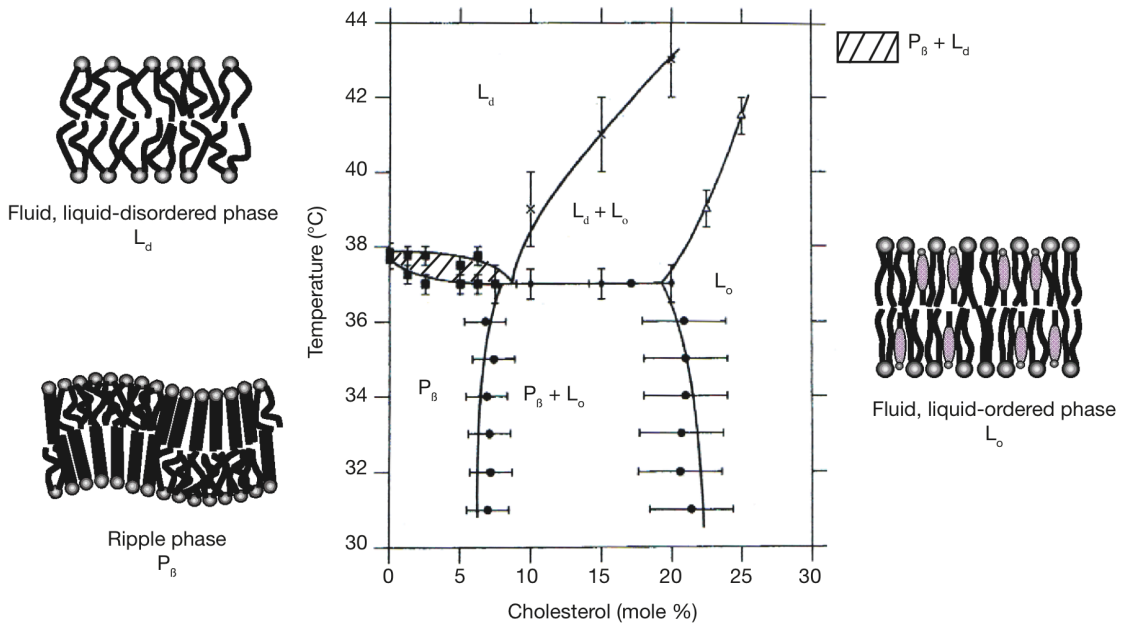

Figure 5 Phase behaviours diagrams for binary mixture of cholesterol and DPPC in water environment.

Cholesterol induces co-existence of liquid-disordered L_d and liquid-ordered L_o thermodynamics states at temperatures above main transition temperature, and it also induces transition phase with ripple phase P_β and liquid-ordered L_o phase at lower temperatures. The figure was adapted from reference (Eeman and Deleu, 2010, Vist and Davis, 1990) Copyright © 1990, American Chemical Society.

Besides the bilayer-forming lipids, cholesterol by itself doesn't form bilayer phases, but it induces an intermediate state, the liquid-ordered phase L_o, in a lipid bilayer (see Figure 4). This remarkable phase not only has a high ordering state like a bilayer in solid phase, but also features with a relatively high translational mobility of a bilayer in fluid phase. In a phospholipids bilayer with cholesterol (see Figure 5), the gel-fluid transition phase of the bilayer was broadened upon heating the system. At a certain temperature below T_m, the

lipid bilayer in gel or ripple phase undergoes transition into a liquid-ordered thermodynamics state L_o with increasing cholesterol concentration. At temperatures above the main T_m, upon adding cholesterol into the bilayer system the fluid lipid bilayer occurs a co-existence of the liquid-ordered and liquid-disordered states ($L_d + L_o$). At cholesterol concentrations 25 mol% or even higher, the disordered phospholipids are further restricted and they are arranged into more ordered or aligned configurations. Briefly speaking, cholesterol increases the fluidity of the hydrocarbon chains and prevents phospholipids from forming gel phase at low temperature. By contrast, cholesterol decreases the membrane fluidity and induces more aligned packing state among the hydrocarbon chains of lipids at high temperature (Ohvo-Rekila et al., 2002, Bennett and Tieleman, 2013, Yeagle, 1989).

1.1.4 Lipid Rafts

As cholesterol affects physical properties of lipid membrane, cholesterol is also involved of manipulating the functions of proteins embedded in the membrane via direct or indirect approach. Many membrane proteins, including ion channels, membrane receptors and enzymes, are found to be sensitive to mechanical modification of the surrounding domains. Some proteins are found to interact with cholesterol molecules to manipulate either activation or inactivation. The mediation of the activity of the cholesterol-regulated proteins is probably

associated with sterol-sensing domains. In addition, some proteins that are compartmentalized into lipid rafts are also dependent on cholesterol, since cholesterol is involved of lipid raft formation. (Simons and Ikonen, 1997, Gullingsrud and Schulten, 2004, Ohvo-Rekila et al., 2002)

Lipid rafts are commonly referred to micro-domains enriched with cholesterol and sphingolipids in a lipid membrane. These highly ordered domains provide platforms where specific proteins are concentrated and segregated from the surrounding bilayer (Simons and Ikonen, 1997). While the relevance of such domains and their roles in modulating the functions of the proteins are still much debated, though lipid rafts are believed to be important for many biological processes including neurotransmission (Allen et al., 2007) and amyloid diseases (Bucciantini et al., 2014). In contrary, the integral membrane proteins also affect the dynamics of the surrounding lipids. The motional freedom of the lipids neighbouring the proteins is constrained due to their direct interactions with the protein. These lipids are known as annular lipids. Additionally, lipids may also reside in non-annular sites such as clefts on the protein surface or in the space between protein subunits. These lipids, known as non-annular lipids, may interact with the protein with a higher affinity, and have less accessibility to the bulk lipids. Compared to the annular lipids, the non-annular lipids are less possible to exchange with lipids from the bulk regions.

It has been observed that non-annular lipids may participate in mediating protein function and oligomerization. (Paila and Chattopadhyay, 2010, Grouleff et al., 2015)

1.2 Molecular scale study of lipid membrane

Molecular scale interactions of membrane components drive the membrane lipid bilayer self-assembly and functioning of the living cells. Chemical structures of the involved molecules are of great importance in the interactions. Therefore, the knowledge of the steric structure of lipids at atomic level resolution is essential for a complete understanding of their functional role. It is very helpful to deepen our understandings on lipid conformations, molecular interactions and membrane dynamics in biological membrane study.

1.2.1 Experimental techniques to characterise lipid bilayer

Experimental techniques such as X-ray crystallography and nuclear magnetic resonance (NMR) are used to produce the detailed structure of the biological macromolecules, like lipids, proteins, peptides, DNA and RNA. For example, X-ray crystallography is the primary technique to derive the three-dimensional

structure in the solid state. It is capable to determine the relative positions of the atoms in space finely, and yield bond length, angles, and torsion angles. More information about packing arrangement of molecules and distances between molecules can be obtained as well. But the picture derived from X-ray crystallography and NMR reveals an averaged static state of the matter. In the equilibrium structure, biological macromolecules undergo substantial fluctuations, and the equilibrium structure can be altered greatly when compared to the static picture taken by structural imaging techniques. In lipid membrane, the function of the membrane is closely associated with the dynamic alterations in the lipid bilayer. (Yeagle, 2004)

Alterations in lipid dynamics influence various cellular functions such as mechanical signal transduction, substances transportation across the structure and lateral diffusion of membrane component in the bilayer (Yeagle, 2004, Yeagle, 1989). Therefore, measuring the dynamics properties of bio-membranes is critical in studying the biological function. However, due to the limitation of current experimental techniques, molecular dynamics of membrane is not comprehensively investigated in experiments. In previous literatures, Fluorescence spectroscopy is a widely used technique to characterize the dynamics of bio-membranes. Nevertheless, the spatial and temporal resolution

of the technique is not capable enough to resolve the details of biomembrane at molecular level.

1.2.2 Computational techniques to model lipid membrane

In biophysics, biological membranes can be treated at different scale levels. At the cellular scale or macroscopic level, the membrane is regarded as a thin pseudo planar film, and its properties and characteristics can be extensively understood in terms of phenomenological elastic models. Moving a little closer into the membrane, the membrane appears as the 'fluid mosaic'. Different lipid blocks form a matrix with embedded proteins. At the molecular level, the view of cell membrane becomes a broad, hydrophilic surface that creates an interfacial barrier between the aqueous solvent and the hydrophobic membrane interior. From the microscopic view, the membrane is a collection of molecules, and each molecule is composed of a group of atoms. The macroscopic properties of membrane have been extensively investigated by experiments and continuum model. However, the atomic level structural and dynamical information of membranes are fragmentary. It is mainly because there is no existing experimental technique that can directly reveal the positions and motions of atoms. The situation has been improved since more powerful computers became

available to boost the development of computational study. Molecular dynamics simulation has become a powerful complementary technique to experiments, and the method shed light on understanding the mechanical and dynamical properties of the lipid membrane. With molecular dynamics simulations, details of a computer-based lipid membrane model at the microscopic level (molecular or atomic level) can be explored explicitly, including the positions of each particle in the system at every moment with system evolvement. Also the corresponding velocities of the particle and the forces exerted on each particle at each time point can be obtained from the computer simulation. From the movement of each particle in the system, the dynamics properties of each molecule or the whole system itself can be evaluated. Moreover, the microscopic information can be converted into macroscopic observables such as pressure, energy, heat capacities, etc. via statistical mechanics. (Tieleman et al., 1997)

Molecular dynamics simulations have been extensively used in cell membrane research (Tieleman et al., 1997, Scott, 2002, Saiz et al., 2002, Rog and Vattulainen, 2014, Rog et al., 2009). They are capable to provide atomic level information that helps understand the mechanisms behind the behaviours, which are not accessible by any current experimental techniques. Moreover, as experimental measurements sometimes need probes, which may perturb the system and lead inaccuracy in results. While measurements by MD simulations do not require additional probes, and MD simulations can even investigate effects of the probes

in experiments (Repakova et al., 2006, Stimson et al., 2007). Furthermore, MD simulation is capable to provide insights into a lipid membrane. An example of such observable is the lateral pressure profile inside a lipid bilayer, which provide important information about the, but it is very hard to gauge in experiments. Combining the MD simulations and experiments provides a comprehensive understanding on the behaviours of the system at different length and timescale since different methods can be correlated with each other(Rog et al., 2009).

1.3 Aim of current study

The aim of the study is to investigate the effect of cholesterol on the physical properties of the DPPC bilayer with all-atom molecular dynamics simulation method. A series of simulations of DPPC bilayer at various cholesterol concentrations are performed to study the effects of cholesterol on lipid bilayer from various concerned aspects:

- Structural properties of the lipid bilayer
- Lipid dynamics in the bilayer
- Effect of cholesterol on lateral pressure profile
- Mechanical properties of the lipid bilayer

Though the most PC lipids in nature are unsaturated and most saturated lipids are sphingolipids, DPPC is a good candidate for bilayer simulation from many aspects considerations. First, saturated PC has been investigated in majority of the experiments, and the available experimental data are supportive for force field development and refinement. Second, most lipids in membrane have at least one saturated hydrocarbon chain, as it was reported that interactions of cholesterol with saturated chain is essential to affect the overall structural properties. Third, there have been a plenty of simulations for saturated PC lipids with cholesterol in literatures using different force fields, and the simulation results can be used to validate our model and compare our results.

The recently updated all-atom CHARMM force field sets for DPPC (Klauda et al., 2010) and cholesterol (Lim et al., 2012) are employed in our simulations. The improved parameters were reported to show better accuracy and consistency with experimental data. To my knowledge, the updated force fields haven't been used for a systematic study of properties of DPPC bilayer containing cholesterol.

Chapter 2 Molecular dynamics method

In computational experiments, simulations are used to study virtually all kinds of systems in many scientific disciplines. Roughly, computer simulations can be performed on continuum model and particle-based model to solve different problems. Continuum simulations are usually used for the dynamics of fields consisting of a large number of particles. Particle-based simulations usually focus on the motion of discrete constituents, and the particle can be either an atom or a coarse-grained bead representing a group of atoms.

2.1 Molecular dynamics

In an all-atom molecular dynamics (MD) simulation, each atom in a simulated system is modelled as one particle, and interactions between any two atoms are defined by energy potential function. The position and velocities of the atoms evolve according to the Newton's equation of motion (Tildesley, 1987). In a phospholipid bilayer model, assuming the system consisting of a collection of N atoms with each mass m_i for atom i, the equations of motion of the N particles can be expressed with Newton's second law,

$$m_i \frac{\mathrm{d}^2 r_i}{\mathrm{d}t^2} = m_i a_i = F_i , \quad i = 1,2,3 \dots \dots , N. \tag{2.1}$$

Where a_i is the acceleration of atom i, r_i is the position (x_i, y_i, z_i) of atom i in

space at a given time instant, and F_i is the force exerted on atom *i*.

The individual forces F_i acting on atom *i* in the system can also be expressed by the gradient of the potential energy,

$$F_i = -\nabla_i U = -\frac{\mathrm{d}U}{\mathrm{d}r_i} \tag{2.2}$$

Combing the equations (2.1) and equation (2.2) yields:

$$-\frac{\mathrm{d}U}{\mathrm{d}r_i} = m_i \frac{\mathrm{d}^2 r_i}{\mathrm{d}t^2} \tag{2.3}$$

Where U is the potential energy of the system. The negative signs in the equations (2.2) and (2.3) indicate the system tends to move towards a configuration with relatively lower potential energy.

The differential equations of motion are integrated with some designed numerical algorithms such as the Verlet algorithm and its modifications (Tildesley, 1987, Swope et al., 1982). According to the integration algorithm, the positions and velocities of each particle are updated. For instance, the velocity Verlet algorithm describes the equations of motion with

$$r_i(t + \Delta t) = r_i(t) + v_i(t)\Delta t + \frac{F_i(t)}{2m_i}\Delta t^2 \tag{2.4a}$$

$$v_i(t + \Delta t) = v_i(t) + \frac{F_i(t + \Delta t) + F_i(t)}{2m_i}\Delta t \tag{2.4b}$$

where Δt is the time step used to propagate the equations of motion. For all-atom MD simulations, the time step Δt is 1 fs in common, and it can be

doubled to be 2 fs with constrained bond lengths to boost simulation efficiency.

2.2 Force field

In classic mechanics, the forces between atoms depend only on the position of the atoms, and are not explicit on time. The forces can be determined from the gradient of a potential function as shown in equation (2.2). In order to define the physical model of an atomic system, the potential energy function describing pairwise interactions of all atoms has to be given or approximated, and the potential function is the so-called force field.

Classically, the total potential of a system of N atoms can be divided into two categories, namely, the bonded and the non-bonded interactions terms. The bonded interactions, referring to interactions among atoms that are connected with each other by covalent bonds, include bond, angle and dihedral terms. Non-bonded interactions include the electrostatics and van der Waals forces terms. Hence, a general form of the potential energy function consists of several terms with a simple expression: (Tildesley, 1987)

$$U_{\text{total}} = U_{\text{bond}} + U_{\text{angle}} + U_{\text{dihedral}} + U_{\text{electrostatics}} + U_{\text{vdW}} \qquad (2.5)$$

The equation (2.5) shows the different contributors to the total potential energy U_{total}. The bond and angle term are often modelled with harmonic potentials,

$$U_{\text{bond}} = \sum \frac{1}{2} \mathrm{k}_{ij}^{b} \left(r_{ij} - r_{ij}^{0}\right)^{2} \tag{2.6}$$

$$U_{\text{angle}} = \sum \frac{1}{2} \mathrm{k}_{ijk}^{\theta} \left(\theta_{ijk} - \theta_{ijk}^{0}\right)^{2} \tag{2.7}$$

where r_{ij} is the distance between atom *i* and *j*, θ_{ijk} is the angle between atoms *i*, *j* and *k*; The equilibrium distances and angles, r_{ij}^{0} and θ_{ijk}^{0} ,and the force constants, k_{ij}^{b} and $\mathrm{k}_{ijk}^{\theta}$, are fit parameters, respectively. The dihedral angle energy is given with a cosine expansion,

$$U_{\text{dihedral}} = \sum \mathrm{k}^{\phi} \left(1 + \cos\left(n(\phi - \phi^{0})\right)\right) \tag{2.8}$$

where ϕ is the value of the dihedral angle , the equilibrium value ϕ^{0} and the force constant k^{ϕ} determining the energy barrier height and the multiplicity *n* giving the number of the corresponding energy minima states as the bond is rotated through 360°. The electrostatic interaction is defined with the Coulombic term,

$$U_{\text{electrostatics}} = \sum_{i<j} \frac{q_i q_j}{4\pi\mathcal{E}_0 r_{ij}} \tag{2.9}$$

where q_i and q_j are partial charges of atoms *i* and *j*, and $\mathcal{E}_0$is the vacuum permittivity. The van der Walls interaction between atoms, describing the strong repulsion at very short distances and the London dispersion forces at long distances, is often modelled with the famous Lennard-Jones (LJ) potential,

$$U_{\mathrm{vdW}} = \sum_{i<j} \frac{\mathrm{A}_{ij}}{r_{ij}^{12}} - \frac{\mathrm{B}_{ij}}{r_{ij}^{6}} \tag{2.10}$$

where A_{ij} and B_{ij} are Lennard–Jones fit parameters describing the interaction strength of repulsion and dispersion, respectively.

2.3 Ensembles

An ensemble refers to a conceptual collection of a large number of identical systems. Each participant in the ensemble is characterized with its microscopic parameters. In classical MD simulation, each particle in the system has the positions and velocities, but all of the particles share the same macroscopic parameters. A MD simulation with standard equations of motion samples the trajectory in the microcanonical ensemble (NVE). The system is a collection of particles with different positions and velocities, but it is specified with the same number of particles, N, volume, V, and total energy, E. The NVE ensemble is useful to check integration accuracy and energy conservation, however it is not quite related with the experimental conditions. In membrane simulations, it is more common to control the absolute temperature T with a thermostat, and thus to produce the standard canonical ensemble (NVT). In both NVE and NVT ensembles, the volume of the system is required to be constant, and it is problematic in the mixtures of various lipid species membrane system since the accurate data for the surface area per lipid and the thickness of the membrane

are unknown in most cases. The constant volume may cause unnatural dimensions of the system, and unphysical fluctuations in membrane due to inflexible boundaries. Of further interest are simulations in the isothermal-isobaric ensemble (NpT) where the pressure and temperature are controlled to be constant, and the simulation box size must be allowed to change to obtain desired pressure in NpT ensemble. The most popular NpT methods used in membrane simulation are the scaling algorithm of Berendsen et al. (1984) and the Nose-Hoover method (Nose and Klein, 1983, Hoover, 1985). In fact, the Berendson weak-coupling algorithm doesn't produce an NpT ensemble, but it is usually most efficient in reaching desired reference values. The Nose-Hoover method results in an NpT ensemble by coupling system to an external temperature and pressure bath, but it can undergo unnecessary oscillating movements when the system is started far from equilibrium. Therefore, a good way to perform a membrane simulation in NpT ensemble is to use a Berendsen algorithm for system equilibration and a Nose-Hoover method for production simulations.

2.4 Limitations of molecular dynamics simulations

2.4.1 Reliability of energy potential function

Description of the potential energy of the interactions of all atoms in the systems requires a large number of parameters. The current available force fields haven't achieved to mimic all the forces experienced by the 'real' atoms. Force field parameters are often empirically obtained from experiments and quantum mechanics calculations. Ideally, empirical force fields should be transferable and applicable to many systems under different conditions. However, parameters in different force field sets are usually self-consistent, which means parameters in one set are normally used for specific molecules or systems. Because force fields are often parameterized and refined by fitting the model to the available experimental data on specific system. Therefore different force fields may not be compatible to each other. The available force fields, such as AMBER (Dickson et al., 2014), CHARMM (Vanommeslaeghe et al., 2010) or GROMOS (Baran and Mazerski, 2002) have proved to be pretty accurate regarding kinetic and thermodynamics properties for proteins, nucleic acids, and lipids.

The classical force fields are approximated form of the potential energy functions. Simulations performed by classical interactions can predict many important motions of atoms and dynamical properties of the system, while these simulations are poorly suitable to study chemical events such as bond breaking

and bond making where quantum effects are essential. Aside from that, another event involved of quantum mechanical effect, electronic polarization, which is caused by the uneven distribution of electrons between one nucleus and another covalently bonded nucleus among groups of atoms, is generally not taken into account in the force fields. In classical description, each atom is distributed with a fixed partial charge throughout the simulation. However, in reality, the electron clouds around atoms are constantly shifting in response to their environments, so the partial charges of atoms in force fields would better be dynamic and responsive. With fixed partial charge, average effects of polarization are retained while detailed effects are poorly represented. At present, however, a generally recognized polarizable force field is still not available.(Tieleman et al., 1997, Tildesley, 1987)

2.4.2 Length scale and timescale limitations

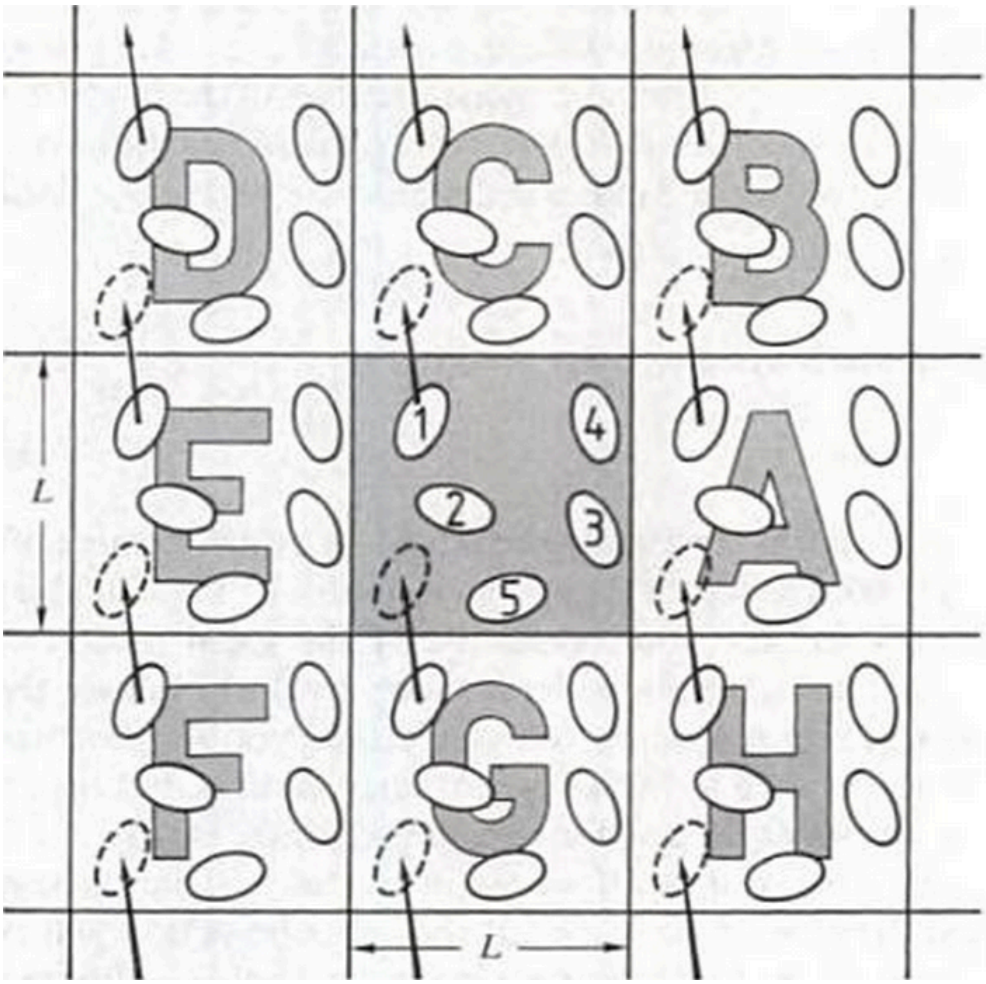

Figure 6 A two-dimensional periodic system.
Molecules can enter and leave each box across each of the four edges. Adapted from the book (Tildesley, 1987)

Another principal limitation of MD method is the high computational expenses. The size and duration of the modelled system is often limited to be small compared to the natural system, which is greatly restrained by the high computational demands to perform MD simulations. However, with dramatic increase in the computational power in the past decade, it is now possible to run

simulations for more than one millisecond on high performance computers (Shaw et al., 2008). But most routine simulations are still limited under one microsecond due to the high computational demand. For example, it takes several months to complete a one-microsecond simulation of a relatively small system (approximately 25,000atoms) on a powerful computer with 24 cores (Durrant and McCammon, 2011). In terms of system size limitation, the solution is to apply periodic boundary condition on the system, and it in effects extends the system into infinite periodic lattices. As a two-dimensional version of the periodic boundary conditions is shown in Figure 6, the original box containing *N* atoms is replicated in the plane to form an infinite plane. In a simulation, as a particle moves in the original box (the central one), its imaginary atoms in each of the neighbouring boxes move in exactly the same way. Thus, as the atom moves across the boundary of the original box, one of its images will re-enter through the opposite side. However, this treatment can introduce artefacts into the system, especially for non-bonded forces calculations. The size of simulation system must be big enough to prevent periodic artefacts, since if the box is too small, a macromolecule may interact with its own imaginary molecule in a neighbouring box. (Tildesley, 1987, Tieleman et al., 1997)

2.4.3 Treatment of long-range interactions

The calculations of the non-bonded interactions (in equations (2.9) and (2.10)) are most expensive as such calculations should be performed between all atoms of the simulated system. A system with N atoms leads to a computational complexity that increases as N^2, and the N is pretty large for the biological systems. To achieve fast calculations, various methods, such as truncation, the Ewald summation and its modifications are often applied to reduce the complexity of the simulation algorithm. For Lennard-Jones (LJ) interactions, a truncation can be defined to neglect the interactions outside the cutoff distance. As the LJ interactions are fairly short-ranged, a cutoff around 1.0 nm is typically enough to minimize truncation artifacts if shifted-force algorithm is used to make the potential go smoothly to zero at the cutoff distance. The evaluation of Coulombic interactions is more problematic. As the potential energy decays as r^{-1} and it is still substantial even at a pretty long distance. If the electrostatics interactions are truncated like LJ interactions, truly bad situation can occur, such as accumulation of charges at the cutoff boundary or significantly wrong energies. The problem has severely restricted to MD simulations for a long time. Currently, one of the best approaches for long-range interactions is based on the Ewald summation (Darden et al., 1993, Essmann et al., 1995), which is an efficient method to calculate the interactions between a charged particle and its imaginary copies in the infinite periodic boxes. The calculation is divided into

two parts. One short-ranged part converges quickly in real space, and the other long-ranged part is solved quickly in Fourier space. Also, Fast Fourier Transforms (FFT) algorithm can be used to accelerate the Fourier calculations (Deserno and Holm, 1998).

Chapter 3 Effects of cholesterol on structural properties of DPPC bilayer

3.1 Introduction

Many cell membrane activities are associated with the structural properties of the phospholipids bilayer. Therefore membrane structural parameters have been defined to estimate structural properties of the membrane, including average surface area per lipid, thickness of the hydrophobic region, overall thickness of the bilayer, and deuterium order parameters. These structural parameters obtained from experimental data can be used to validate simulated bilayer systems (Nagle and Tristram-Nagle, 2000).

One of most important cholesterol effects on bilayer structure is ordering effect. For a lipid bilayer in the fluid phase, the acyl chains of lipid molecules are pretty flexible and disordered to some extent. Embedding cholesterol molecules into the system induces increased ordering of the hydrocarbon chains of lipids, which is called ordering effect of cholesterol. Ordering effect is a generic effect of cholesterol on a lipid bilayer under the physiologically relevant fluid phase, and it was observed in experiments with various experimental techniques such as X-ray crystallography, NMR, fluorescence spectroscopy and so on (Rog et al.,

2009). In MD simulations, the ordering of the lipid's acyl chains can be quantitatively evaluated by order parameter, which is a parameter that can be calculated from deuterium NMR experiments. Therefore, the order parameter from simulations can be directly compared to experimental data. Basically, the order parameter reflects how much the acyl chains align along the bilayer norm. Higher values of order parameter indicate the hydrocarbon tails means more aligned and less flexible, and lower values mean hydrophobic region of the bilayer is more flexible and less ordered. Aside of the order parameter, ordering effects can also be evaluated by other way such as analysing tilt angles of lipid molecules respect to the bilayer norm. Probability distribution of tilt angles explores the preferred orientation of the molecules respect to the bilayer norm, and therefore shows how the molecules are aligned in a bilayer structure, which can be analysed pretty straightforward for MD simulations (Rog and Vattulainen, 2014) .

Another widely discussed effect of cholesterol is condensing effect. Interpretations of condensing effect can be different depending on how it is evaluated. Initially, condensing effect was defined as cholesterol increases the packing density of membrane surface regions (Marsh and Smith, 1973), but then it has been interpreted as cholesterol leads reduction of the surface area occupied by PC lipid (Phosphatidylcholine) molecules in cholesterol-containing bilayers (Yeagle, 1985) .

In a single component bilayer, calculating the surface area occupied by one lipid molecule is as simple as dividing the overall surface area of one leaflet by number of lipids. However, it is not an easy task in bilayer composed of more than two components. In mixed bilayer with cholesterol, to evaluate the condensing effect needs consider the areas per PC lipid ($<A_{PC}>$) as well as the areas per cholesterol ($<A_{Chol}>$). A series of experimental studies by Smaby et al. (1997, 1994, 1996) on monolayer systems proposed a method to derive area per phospholipid by assuming the area per cholesterol to be a constant value (0.39 nm^2), which is measured from monolayer studies (Hyslop et al., 1990). However it may not be fully justified at all times. It was argued that the surface area taken by cholesterol varies depending on the distance of the steroid ring of cholesterol from bilayer centre (Rog and Vattulainen, 2014).

Condensing effects is also reflected to the thickness of the bilayer. As the bilayer is a relative soft structure with no obvious boundary, there are several ways to define and measure the thickness of bilayer. In simulations, the most common approach is to average the distance between phosphorus atoms of the PC lipids in opposite monolayers. An alternative approach is to calculate electron density profile (EDP) of water and lipids along the bilayer norm, and then to measure the distance between the crossing points where the densities of water and lipids molecules are equal. The two planes along the bilayer surface at the crossing

points represent the interfacial surfaces between bilayer and bulk water. A series of simulations of lipid bilayers containing cholesterol showed an increase in thickness as cholesterol concentration increases, and it was observed in experiments (Gallova et al., 2004, McIntosh, 1978) and simulations (Hofsass et al., 2003).

In this chapter, the effects of cholesterol on structural properties of the DPPC/cholesterol mixture bilayer systems are investigated with MD simulations. The mainly concerned parameters are studied in this chapter, such as area per lipid, order parameters and so on. Moreover, Voronoi tessellation method (Lukat et al., 2013) was used to investigate the area distribution among DPPC and cholesterol molecules.

3.2 Computational details

3.2.1 Initial structure assembly

There are six DPPC/cholesterol bilayer systems with different concentrations of cholesterol at 0%, 5%, 10%, 20%, 30%, and 40%. Each bilayer system contains 128 lipid molecules (DPPC and cholesterol), and each bilayer system was hydrated with 3840 water molecules.

The initial lipid bilayer configurations were constructed from DPPC and cholesterol molecules. The single molecular structures of DPPC and cholesterol were obtained from CHARMM36 force field package (Klauda et al., 2010), and they were replicated and assembled into the initial bilayer configuration using Packmol program (Martinez et al., 2009). The lipids molecules were distributed randomly with their polar part orienting outward from the bilayer centre in each leaflet, and water molecules were allocated above the upper leaflet and below the lower leaflet, respectively. For example, in the DPPC bilayer system containing 40% cholesterol molecules, each leaflet contains 26 cholesterols and 38 DPPCs, and 1920 water molecules were generated into layers along polar surface of each leaflet, respectively. Atomic CHARMM36 lipid parameter set was used for DPPC and standard CHARMM TIP3P water model (Klauda et al., 2010). For cholesterol, a recent modified description based on CHARMM36 for cholesterol C36c was applied in simulations (Lim et al., 2012). At last, the assembled configuration files and force field CHARMM36 parameters files were integrated and converted into LAMMPS input files using *charmm2lammps* tool from LAMMPS toolbox kit (*LAMMPS website*, Plimpton, 1995).

3.2.2 MD Simulation conditions

Prior to all actual MD simulations, energy minimization was performed on all initial structure using conjugate gradient algorithm to remove any bad steric

contacts between atoms. The simulations were carried out using LAMMPS molecular dynamics simulator package (9-Dec2014 version) (*LAMMPS website*, Plimpton, 1995), on a Cray XC30 supercomputer (Archer, the UK National Supercomputing service).

Periodic boundary conditions were applied in all three directions of the simulation box. SHAKE algorithm (Andersen, 1983) was used to constrain the bond length and angular values involving hydrogen atom. With the SHAKE constraints, the time step was set to 2 fs with integration algorithm. The Van der Waals interactions were described by Lennar-Jones potentials. A force-based switching function was applied to smoothly decay the energy and force to zero between 8 Å and 12 Å. For electrostatic interaction, Particle-Particle Particle-Mesh (PPPM) method (Hockney and Eastwood, 1988) was used with truncation radius at 12 Å. All the simulations were carried out in the NpT ensemble with constant pressure at 1 atm and constant temperature at 323k. During the equilibration period, Langevin thermostat (Schneider and Stoll, 1978) was used to control temperature at 323k with relaxation time at 2ps. The pressure was maintained at 1 atm using semi-isotropic berendsen barostat (Berendsen et al., 1984) with x-direction and y-direction coupled together to fluctuate independently from z-direction, and relaxation time was set to 2 ps. For production simulations, the temperature and pressure were controlled using Nose-Hoover algorithm with a damping time of 0.1ps and 1ps, respectively, and

xy plane of the simulation box fluctuates independently from Z direction like equilibration runs. Each of the systems was equilibrated at least 120 ns, and then 60 ns production simulations were performed as production period for data collection. As some analyses are based on analysing the trajectory of the atoms in the systems, coordinates of all of the atoms in every system were saved every 10 ps over the production simulation.

3.3 Analysis

3.3.1 Area

In order to investigate the effects of cholesterol on the structural properties, several parameters were employed to analyse the changes led by cholesterol molecules. Surface area is a fundamental parameter to characterise the state of lateral packing of the bilayer structure. In pure DPPC bilayer system, the area per DPPC refers to the projected area on xy plane of bilayer structure. It was simply calculated by dividing the xy-plane area ($L_x \times L_y$) of simulation box by the number of DPPC molecules (N_{DPPC}) in one leaflet.

In DPPC/cholesterol mixture bilayer systems, it is not straightforward to know how the area of simulation box is distributed for DPPC and cholesterol molecules. To calculate area per DPPC and area per cholesterol, Voronoi tessellation method

was employed to revolve the structural organisation of the bilayer structure using APL@Voro software (Lukat et al., 2013). To perform Voronoi tessellation analysis, C1, C21, C31 atoms in DPPC molecules and O3, C2, C4 atoms in cholesterol molecules were selected as key atoms for DPPC and cholesterol respectively. In each configuration of the trajectory, two-dimensional Voronoi diagram was constructed in each monolayer by projecting the selected key atoms' coordinates to xy bilayer plane and assigning a polygon to each atom. As three atoms were selected for DPPC and cholesterol, respectively, the area of the three corresponding polygons is considered as the area of one molecule. The area per DPPC and area per cholesterol is obtained by averaging over all polygons in both monolayers for each configuration and over all configurations of production simulations.

3.3.2 Thickness

Along the direction of bilayer norm, thickness (D) of the bilayer is the most evaluated parameter for bilayer. Various definitions were proposed for thickness for bilayer, because there are no apparent boundaries for this dynamic structure hydrated with water. In this study, thickness of bilayer was simply defined as the distance between phosphorus atoms of DPPC molecules in opposite leaflets.

3.3.3 Electron Density Profile

Besides thickness, additional structural information in the direction of bilayer norm can be obtained by computing electron density profiles for the whole systems, specific type of component or certain atoms. The profiles provide insights on atoms distribution in the norm direction. The electron density profiles were obtained by dividing simulation box into bins along z-direction. Then the number of electrons located in each bin was counted, and the electron density in each bin can be derived from dividing the total number of electrons by the volume of the bin. At last, the electron density distribution along the normal direction of a bilayer can be obtained as a profile.

3.3.4 Order parameter

Conformational changes in lipid hydrocarbon chains led by cholesterol can be monitored by deuterium order parameter (S_{CD}), which is measured by deuterium NMR experiments. Order parameter characterises the order of lipid bilayer, and it can be calculated for each $\mathrm{CH_2}$ group in lipid chains as:

$$S_{\mathrm{CD}} = \left\langle \frac{1}{2}(3\cos^2\theta_{\mathrm{CD}} - 1) \right\rangle, \tag{3.1}$$

where θ is the angle between a carbon-deuterium (CD) bond vector (in the experiment) or a CH-bond (in the simulation) and the bilayer norm, and the angular bracket indicates ensemble average over two bonds in each $\mathrm{CH_2}$, all

DPPC lipids and the production period. The CH_2 groups are numbered from 2 to 15 according to the carbon atoms position in each chain. As carbon number 1 refers to carbonyl group and number 16 refers to the CH_3 group at the end of each chain, they are not included in order parameter calculations.

3.3.5 Electrostatics potential

The electrostatics potential across the lipid bilayer was calculated by double integration of Poisson's equation with the charge density across the bilayer. The equation of electrostatic potential is written as,

$$\phi(z) - \phi(z_0) = -\frac{1}{\epsilon_0}\int_{z_0}^{z} dz' \int_{z_0}^{z'} \rho(z'')dz'' \qquad (3.2)$$

with ρ is charge density, ϵ_0 is the permittivity of free space, z is the coordinate along the z-axis. The charge density was calculated as the partial charges of all atoms in each bin along z-axis divided by the volume of its bin, and then numerically integrating the charge densities twice over the simulation box.

3.4 Results and discussion

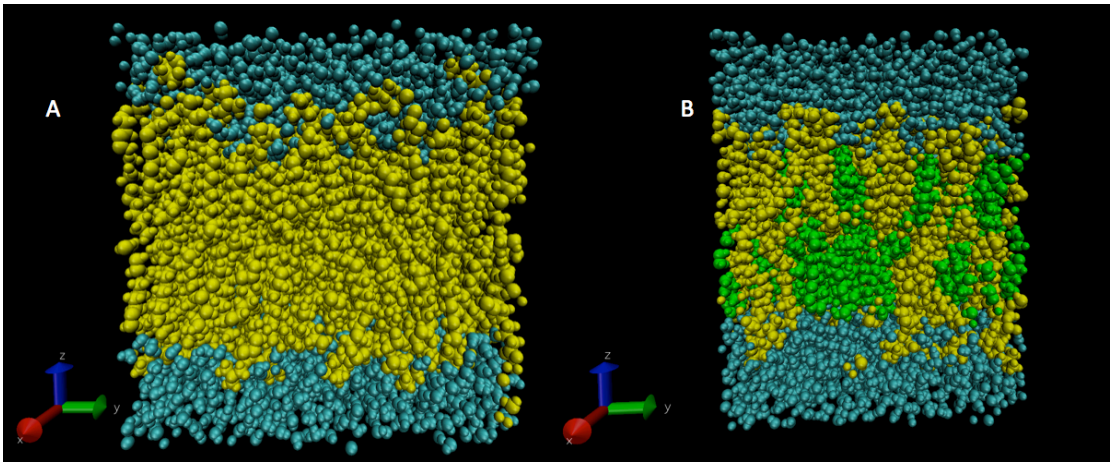

Figure 7 The snapshots of the equilibrated bilayer systems.
(A) on the left is the DPPC bilayer without cholesterol molecules , and (B) on the right is the DPPC bilayer with 40% cholesterol molecules. The cyan molecules represent water molecules, the yellow molecules represent DPPC molecules, and the green molecules in (B) represent cholesterol molecules.

All systems were simulated for equilibration over 140ns before collecting data from the production period, and only the last 60ns simulation data were used for data analysis. The snapshots of the equilibrated DPPC bilayer systems with 0% and 40% cholesterol were shown in Figure 7.

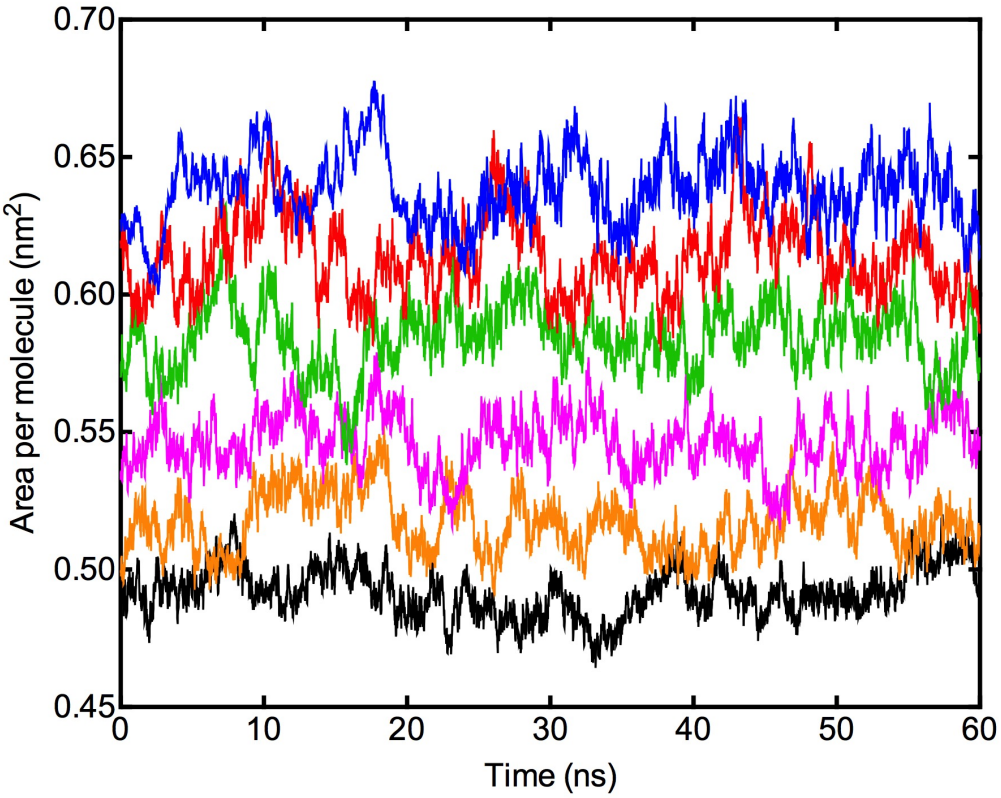

Figure 8 Area per molecule evolves with simulation time.

Plots in different colour represent different cholesterol concentration in the bilayers: 0 mol% (blue), 5 mol% (red), 10 mol% (green), 20 mol% (magenta), 30 mol% (orange), 40 mol% (black) cholesterol.

3.4.1 Area and thickness of the simulated DPPC bilayers

Area per molecule, which was calculated in the same way as deriving area per DPPC in cholesterol-free bilayer, was used to examine the equilibrium of each system. Figure 8 shows the evolution of area per molecule for each system over the last 60 ns production simulations, and all area plots are considered as

converged. In addition, the amplitudes of fluctuating curves of the area indicate the level of stability of the systems, and it is noted that fluctuation is less pronounced with higher cholesterol content. The decrease in area per molecule with addition of cholesterol may suggest condensing effect.

Table 1 Averages areas and thickness in all bilayer systems with different cholesterol concentrations.

	0%	5%	10%	20%	30%	40%
Area/molecule (nm^2)	0.638 ±0.0002	0.615 ±0.0002	0.584 ±0.0002	0.546 ±0.0001	0.517 ±0.0001	0.492 ±0.0001
Area/DPPC (nm^2)	0.638 ±0.0002	0.623 ±0.0001	0.604 ±0.0001	0.582 ±0.0003	0.566 ±0.0200	0.552 ±0.0002
Area/cholesterol (nm^2)	N/A	0.429 ±0.0006	0.421 ±0.0003	0.408 ±0.0002	0.402 ±0.0002	0.403 ±0.0001
Thickness (nm)	3.812 ±0.0006	3.863 ±0.0006	3.944 ±0.0006	4.052 ±0.0006	4.120 ±0.0006	4.139 ±0.0006

To further examine condensing effect led by cholesterol, the surface area taken by DPPC and cholesterol needs to be found out. The obtained areas for DPPC and cholesterol by Voronoi analysis are listed in Table 1. The average of the area occupied by one DPPC molecule decreases from 0.638 nm^2 to 0.552 nm^2 gradually with cholesterol concentration increasing from 0% to 40%. The

condensing effect led by cholesterol is observed in our simulated bilayer-cholesterol systems. As for area taken by cholesterol (see Table 1), the value of the area is not obviously influenced by the cholesterol concentration, as it decreases only by 0.026 nm^2 from 5% to 40% cholesterol systems. It is worth mentioning that the value remains at the same level about 0.40 nm^2 at higher cholesterol concentrations. It means that area per cholesterol is barely affected by the amount of itself in the systems at high cholesterol concentrations.

In comparison with experimental data, results observed here show good agreements. As there are no available experimental data for DPPC-cholesterol bilayers currently, only area per DPPC for pure bilayer system is available in experiment. A recent experiment study of fluid pure DPPC bilayer at 323K found that the area per molecule was 0.631 nm^2 (Kucerka et al., 2011), which is in good agreement with 63.8 nm^2 obtained here. As for area per cholesterol, the area obtained in present simulations are in range of 0.40 to 0.43 nm^2, which agrees well with the area in the range of 0.39-0.41 nm^2 observed in experiments of pure cholesterol monolayer (Brzozowska and Figaszewski, 2002, Hyslop et al., 1990). Furthermore, the observed small range of area per cholesterol in my study (see Table 1) is supportive with the fact that many researchers used the assumed constant value 0.39 nm^2 for cholesterol to estimate the area assigned to the rest DPPC molecules.

In comparison with previous simulation studies, different levels of condensing effect on DPPC bilayer were observed. Chiu et al. (2002) carried out similar simulations study of DPPC-cholesterol bilayer systems. Their results have showed more apparent condensing effect, as the area per molecule decreased to about 0.40 nm^2 at 33% cholesterol, which is much smaller than 0.492 nm^2 obtained from my simulation at 40% cholesterol concentration. In their simulations, external surface tension was applied on each monolayer to contract the surface plane of bilayer to the area per molecule in agreement with experimental result. However, the tension force were adjusted and determined only in pure DPPC bilayer, and the same tension was applied to all cholesterol-containing systems. That is reasonable for pure DPPC bilayer, but it may cause problem for DPPC-cholesterol bilayer systems. Because cholesterol may break the previous dynamic balance artificially achieved in a pure DPPC bilayer system. In my case, no external tension forces were applied on bilayers and the final results are only determined by the interactions between molecules. In a recent review paper (Rog et al., 2009), the author argued that the degree of condensation in DPPC bilayer is a bit too high in previous simulation studies (Chiu et al., 2002, Hofsass et al., 2003, Patra, 2005), because the area per DPPC is below the area observed in gel-phase bilayer.

3.4.2 Electron density profiles across the membrane systems

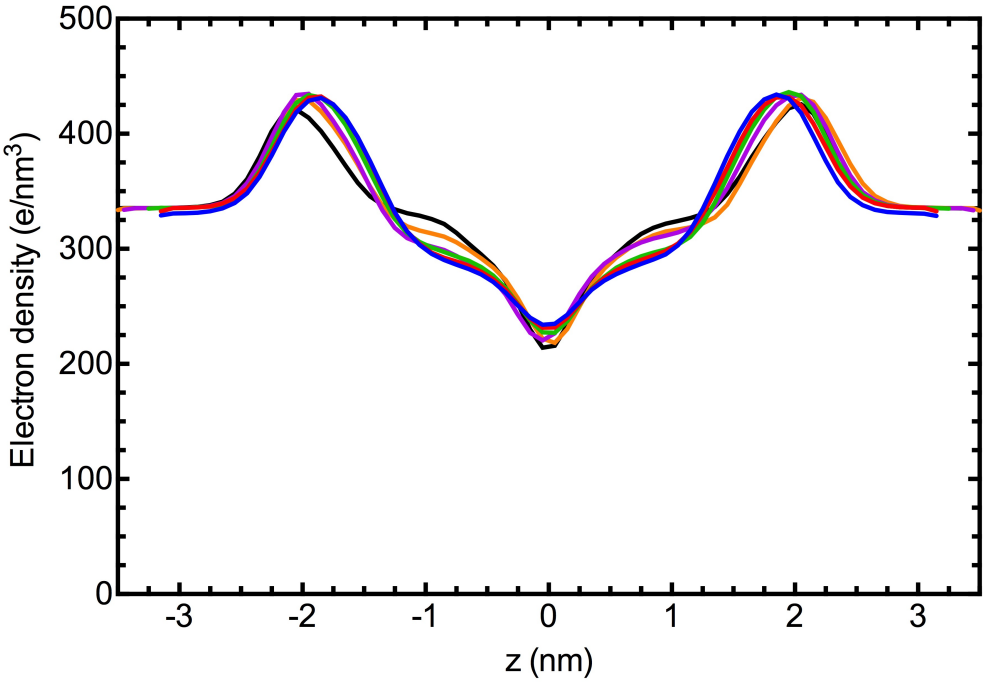

Figure 9 electron density profiles of DPPC bilayer with 0 (blue), 5 (red), 10 (green), 20 (magenta), 30 (orange), and 40 (black) mol% cholesterol.

Condensation of bilayer is also reflected on changes in thickness of bilayer and density profile along bilayer norm. As the lateral packing density increases, the thickness of the structure increases. Besides thickness, electron densities distribution along bilayer norm provide additional information, and the profiles obtained from simulations can be directly compared to results obtained by x-ray and neutron diffraction experiment. Figure 9 shows the total electron densities profiles for DPPC bilayers with different cholesterol concentrations. The two maxima in each curve are observed at the approximate locations of the

phosphate groups, and the trough occurs at the centre of the bilayer, where the terminal carbon groups reside. With increasing cholesterol concentration, the two peaks in each curve were shifted away from the bilayer centre, which indicate that the bilayer is thickened. At the bilayer centre, the densities gradually decrease with more cholesterol involved, while densities around regions at ±1 nm show a monotonic increase. These regions are locations of the cholesterol fused ring structure in each leaflet, since the rigid fused rings structure is of a higher electron density compared to the flexible hydrocarbon chains of DPPC molecules.

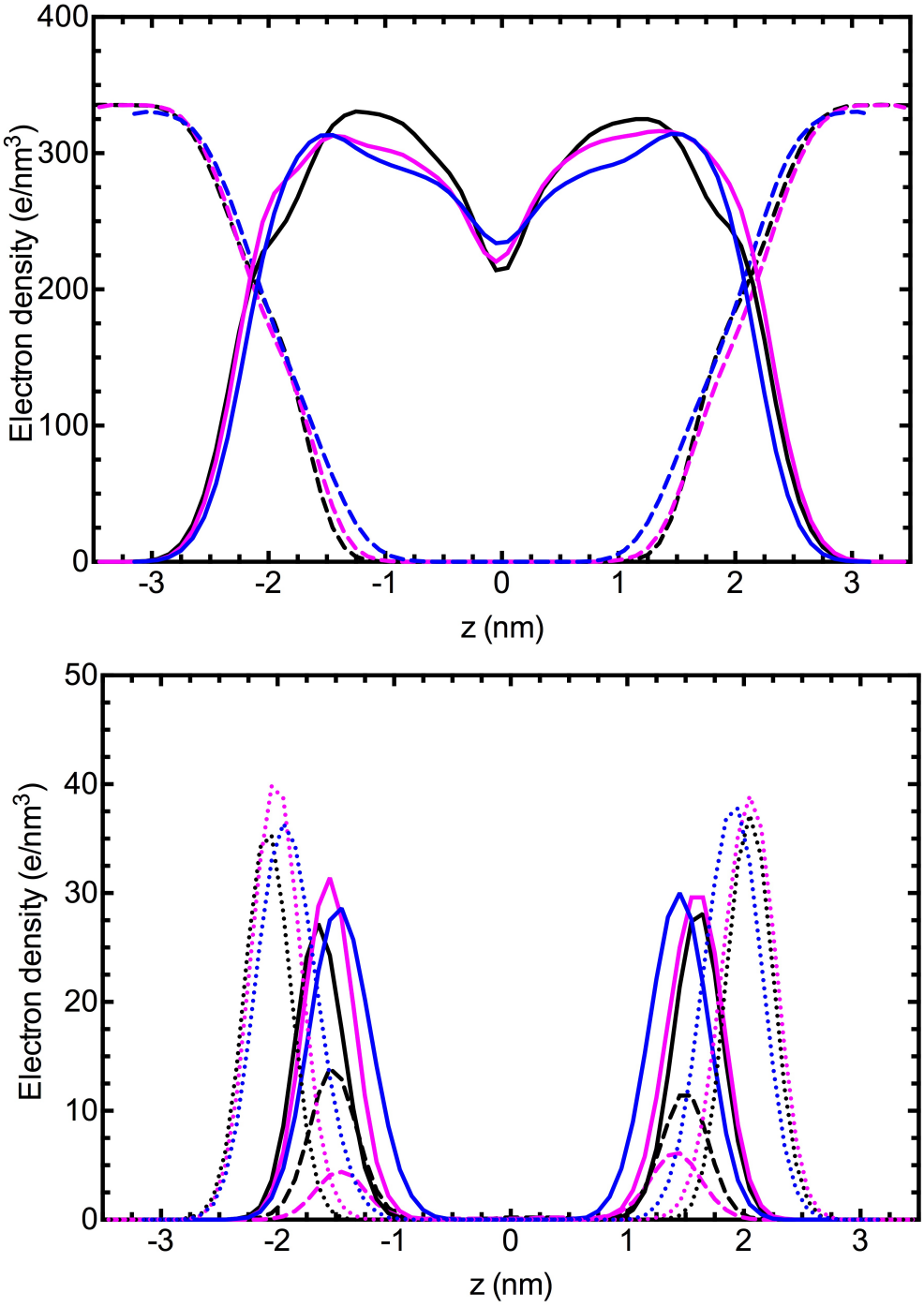

Figure 10 Partial electron density profiles.

The upper plot shows partial electron density profiles of lipid bilayer (solid line) and water (dashed); the lower plot shows the density profiles of phosphorus (dotted line) and carbonyl carbon atoms (solid line) of DPPC and hydroxyl oxygen (dashed line) of cholesterol in bilayer systems with 0 (blue), 20 (magenta), and 40 mol% cholesterol (blue).

Furthermore, it is interesting to see partial density profile of specific molecules or specific atoms to the overall electron density profiles, which cannot be easily assessed by experiments. It is clearly shown in Figure 10 that all profiles are shifted toward bulk water region, which is consistent with the increase of bilayer thickness with cholesterol embedded. The density profiles of water molecules indicate that it becomes more difficult to penetrate into bilayer. As it is well known that the hydrophobic region is repulsive to water molecules because of unfavourable energetic interactions. In presence of cholesterol, the hydrophobic interior of the bilayer, which roughly refers to the distance between maxima in the density profiles of the carbonyl carbon atoms, is thickened, and also the increase in electron density near the boundaries of hydrophobic region can further restrict water molecules penetrating. As shown in the lower plot in Figure 10, the hydroxyl oxygen atoms of cholesterol molecules reside slightly closer to the bilayer centre compared to the carbonyl carbon atoms of DPPC, hence cholesterol molecules are located in the hydrophobic region just under DPPC's head groups.

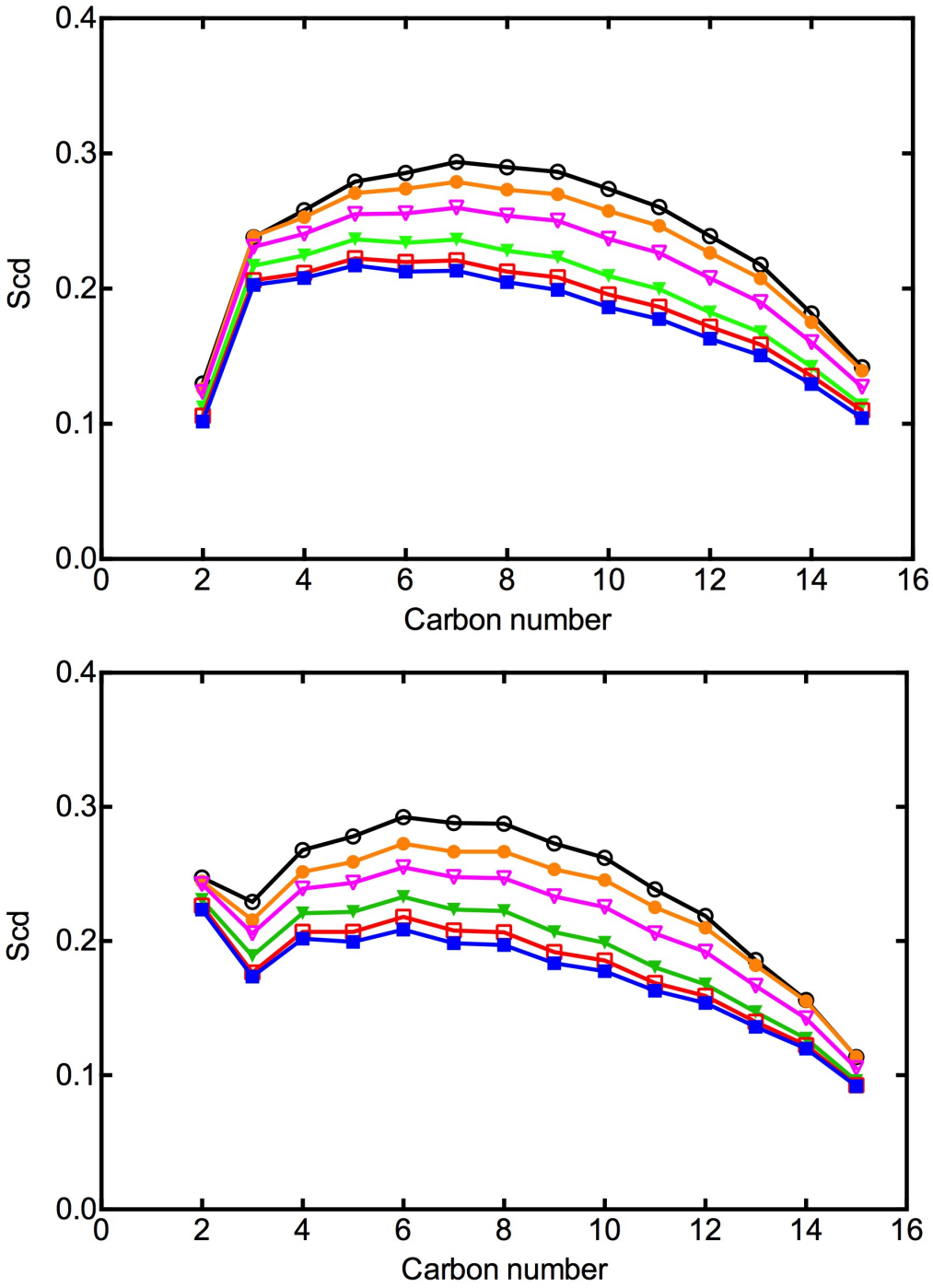

Figure 11 Order parameter profiles for each chain.

Upper plots are for sn-1 chains and lower plots are for sn-2 chains of DPPC at different cholseterol concentrations: 0 (blue), 5 (red), 10 (green), 20 (magenta), 30 (orange), and 40 (black) mol% cholesterol.

3.4.3 Order parameters of the hydrocarbon tails of the DPPC molecules

Another main effect of cholesterol is ordering effect in bilayer, which is closely related with condensing effect. The order in bilayer is often characterized by order parameters in acyl chains in DPPC bilayer. Order parameters versus carbon atoms' position in two chains of DPPC molecules were computed and plotted in Figure 11. It is clearly visible that quantities of order parameters area increased in both tails upon more cholesterol getting involved, and the increase in order parameters of each methylene group is almost linear, which is in agreement with the observation in experiment study by Pare and Lafleur (1998). The characteristic plateau region for pure DPPC is observed in the upper and middle part of the tails, where the order parameters vary slightly. With cholesterol concentration increasing, the plateau disappears gradually. In addition, more pronounced ordering effects were observed in the upper and middle segments for carbon number 5 to10. The ordering effects in the rest methylene groups are comparatively modest. Apparently, it is the rigid ring structure in cholesterol that orders the flexible hydrocarbon chains of the neighbouring DPPC. That is because the location of the rigid structure of cholesterol in bilayer is at similar depth of bilayer with the upper and middle part of the chains. By contrast, smaller ordering effect occurs at the end of the chains, which probably only interact with the flexible tail of cholesterol.

In comparison with previous studies of pure DPPC bilayer, the order parameter profiles of both chains are in good agreement with experiments and simulations (Falck et al., 2004, Hofsass et al., 2003, Petrache et al., 2000). As for the cholesterol containing systems, it was found in the experiment by Pare and Lafleur (1998) that the order parameters were increased almost by a factor of 2 when 33% of the DPPC molecules area replaced by cholesterol at temperature of 323 K, and similar results were obtained in other experiments or simulations. Compared to these studies, the ordering effect in present study seems to be weaker, and it was also mentioned in the paper for introducing the updated CHARMM36 force field (Klauda et al., 2010). But the overall progression of the changes in the order parameters profiles is consistent with other simulation studies (Chiu et al., 2002, Hofsass et al., 2003)].

3.4.4 Electrostatics potential of the bilayer

The electrostatics potential, also known as dipole potential, arises from the non-random orientation of the lipids molecules and water molecules in the interfacial region of bilayer. Figure 12 shows the overall and partial electrostatic potential profiles for the systems with various cholesterol concentrations. For all electrostatics potential profiles, the potential rises at the interfacial region of lipids and water, and the overall potential is mostly determined in this region. The experimentally measured dipole potential for pure DPPC bilayer was in the

range of 220-280mV (Siu et al., 2008, Clarke, 2001). All of the dipole potentials in bilayer centre in present studies were over 600 mV, which is in agreement with other simulation studies (Hofsass et al., 2003, Chiu et al., 2002, Robinson et al., 2011), but all simulation results are overestimated compared to experimental data.

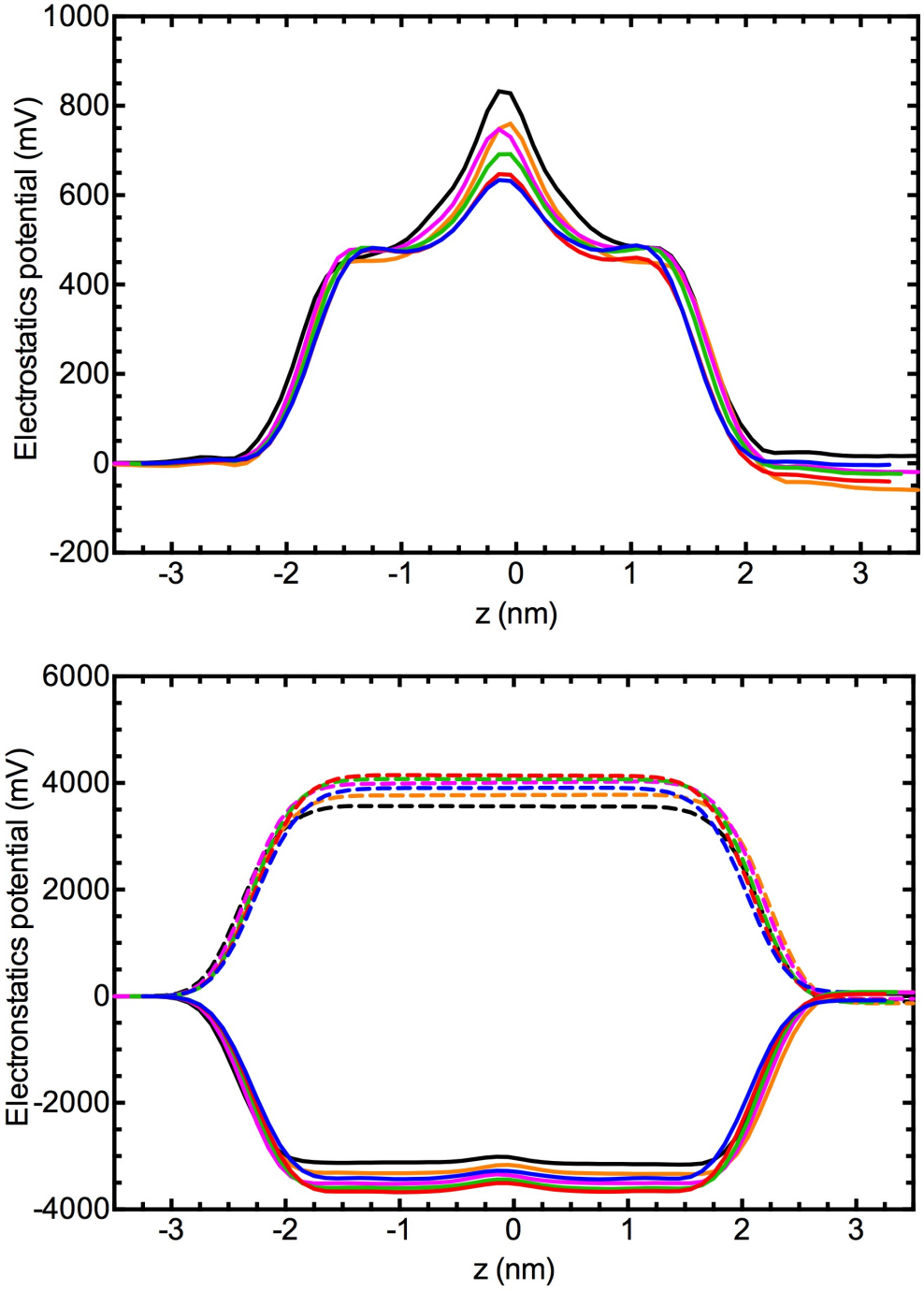

Figure 12 Electrostatics potential profiles across bilayer.

Total Electrostatics potential (upper plot), and partial contributions (lower panel) of lipid dipoles (solid line) and water dipole (dashed line), in bilayers with 0 (blue), 5 (red), 10 (green), 20 (magenta), 30 (orange), and 40 (black) mol% cholesterol.

It is clearly seen in Figure 12 that the total dipole potential at bilayer centre monotonically increased by about 200 mV, with cholesterol concentration from 0% to 40%, which is reasonably consistent with the gradient difference measured in experiments (McIntosh et al., 1989). It seems that the overall potential was increased by cholesterol molecule, and it can be explained as the cholesterol induced higher packing density in the bilayer interior so that the contribution of the overall dipole potential from the lipid region was enhanced.

3.5 Summary

The most important ordering effect and condensing effect of cholesterol on lipid bilayer were observed in current study, and obtained results are in good agreement with data from experiments and simulations. Moreover, the values of the obtained surface areas appear to be more reasonable than previous studies. It may be related to the method used for deriving partial areas for DPPC and cholesterol, and also it is likely to be attributed to the CHARMM36 force field. The findings here suggest that the bilayer model is reasonably assembled and equilibrated, and the obtained structural parameters are in good consistency with previous studies.

Chapter 4 Effect of cholesterol on the dynamic properties of DPPC bilayer

4.1 Introduction

Membrane dynamics plays important roles in a variety of cellular activities such as signalling, substances transportation across membrane, and formation of lipid rafts. The effects of cholesterol on the properties of phospholipid bilayer are diverse. In terms of lipid dynamics, it was reported that cholesterol suppressed lateral diffusion of lipid molecules in bilayers, and changed the fluidity states of the membrane in experiments and simulations (Almeida et al., 1992, Polson et al., 2001, Hofsass et al., 2003, Falck et al., 2004, Lindblom and Oradd, 2009).

Moreover, the dynamics properties of lipid bilayer can be reasonably related with the structural properties of the lipid bilayer, based on the free area theory (Falck et al., 2004, Kupiainen et al., 2005). Free area refers to the unoccupied space by molecules, and the theory suggests that the amount and distribution of the free area in membrane are correlated with the dynamics properties of bilayer, such as permeability and lateral diffusion. More specifically, lipid diffusion in bilayer requires occurrence of the free area adjacent to the diffusing molecule, and the unoccupied area should be larger than some critical value. In

addition, before long-distance diffusion occurs, the molecule usually takes relatively long time to rattle in the cage formed by the neighbours (Tieleman et al., 1997, Falck et al., 2004, Vattulainen and Mouritsen, 2004, Kupiainen et al., 2005).

In this chapter, the effects of cholesterol on dynamics properties of the DPPC bilayer were studied from two aspects, the lipid lateral diffusion rate in bilayer and the intra-molecular reorientation dynamics.

4.2 Method

4.2.1 Lateral diffusion

The lipid diffusion in the plane of the bilayer is evaluated by the lateral diffusion coefficient. Traditionally in experiments, several techniques were often used to evaluate lateral diffusion such as the nuclear magnetic resonance, fluorescence recovery after photo bleaching, and single-particle tracking (Vattulainen and Mouritsen, 2004). In simulation, the motion of the single particle in the plane of the bilayer can be quantified by the lateral diffusion coefficient *D*, defined with:

$$D = \lim_{t\to\infty} \frac{1}{2dt} \langle |\vec{r}(t)|^2 \rangle \qquad (4.1)$$

where d=2 is the dimension of the bilayer and $\langle |\vec{r}(t)|^2 \rangle$ is the averaged mean squared displacement (MSD) over M atoms of the given molecule species and N

molecules in the bilayer system. Calculation of the $\langle|\vec{r}(t)|^2\rangle$ is expressed with:

$$\langle|\vec{r}(t)|^2\rangle \equiv \frac{1}{N\times M}\sum_{i=1}^{N}\sum_{j=1}^{M}\langle\left|\vec{r}_{ij}(t)-\vec{r}_{ij}(0)\right|^2\rangle \qquad (4.2)$$

where $\vec{r}_{ij}(t)$ is the position of the atom *j* in the molecule *i* at time *t* .

It is worth noted that the centre of mass (CM) of the either monolayer in a bilayer may drift during the simulations. If the monolayer's drifts were not taken into account, the results may reflect the motions of the monolayer rather than diffusion of the lipid molecule in the leaflet. Therefore the motion of each particle with respect to the corresponding monolayer was calculated by subtracting the monolayer's CM motion. Similar methods for treating the monolayer's drifts were reported in literatures (Falck et al., 2004, Ollila et al., 2007b).

In current study, only the last 60 ns simulation trajectories of each system were divided into 6 blocks for MSD calculations. Block average over the 6 blocks was performed to obtain converged result, since the randomness of the lipid motions introduces great uncertainties in the results, and the simulation time and system size is not long and big enough to offset these fluctuations. Similar approach for the calculation was reported in literature (Siu et al., 2008).

4.2.2 Rotational diffusion

In experiments, nuclear magnetic resonance (NRM) technique was often used to

study intra-molecular dynamics. Computational studies using rotational autocorrelation functions can provide complementary data for experimental results. To look insight into the effect of cholesterol on lipid orientational dynamics, the autocorrelation functions of different vectors for DPPC were considered in present study. Three vectors were selected for DPPC: (a) The P-N vector was used to represent head groups of DPPC, (b) the vector (C21-C31) joining the respective carbonyl carbon atom in *sn*-1 and *sn*-2 tails represents the glycerol backbone, (c) C2-C216 represent the *sn*-2 hydrocarbon chain, where C2 is the carbon in glycerol group connecting the *sn*-2 chain, and C216 is the terminal carbon in *sn*-2 chain. In practice, the second-order reorientation autocorrelation function was employed:

$$C_2(t) = \frac{1}{2}\langle 3[\vec{\mu}(t) - \vec{\mu}(0)]^2 - 1\rangle \qquad (4.3)$$

where $\vec{\mu}(t)$ is a unit vector that describes the chosen rotational mode.

4.3 Results and discussion

4.3.1 Lateral mean square displacement of DPPC and cholesterol

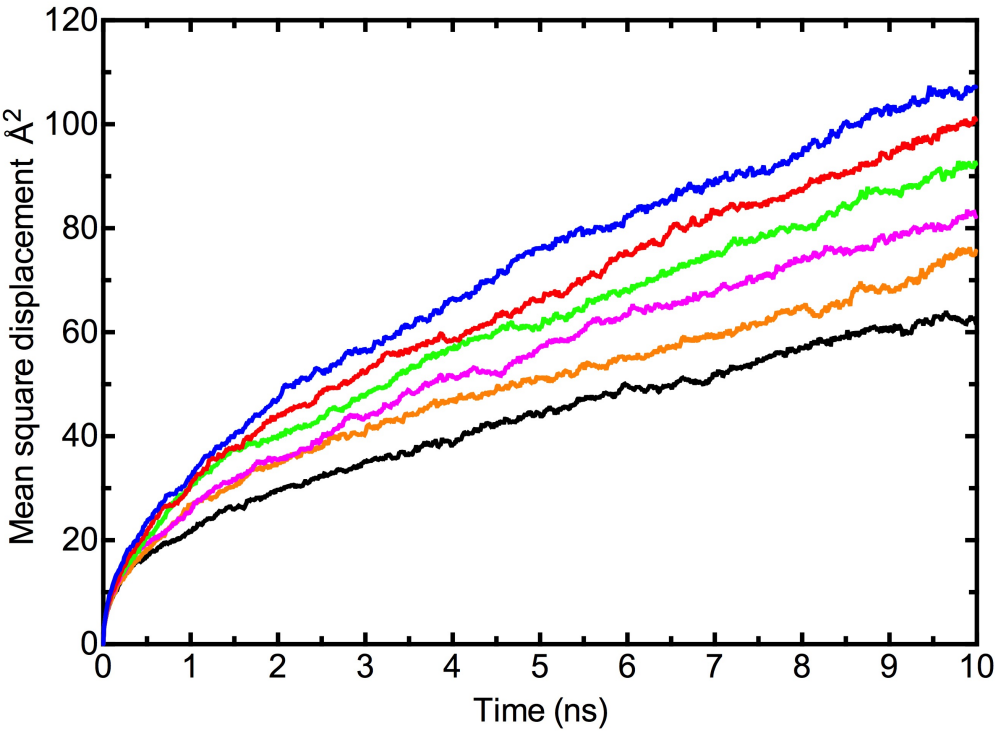

Figure 13 The MSD of DPPC in the bilayer at various cholesterol concentrations. Cholesterol concentrations: 0 % (blue), 5 % (red), 10 % (green), 20 % (magenta), 30 % (orange), 40 % (black) cholesterol in a DPPC bilayer. Note: the last 60 ns trajectory was divided into six blocks and the MSD was calculated separately in each blocks and then averaged as the result shown here.

Lipids in the bilayer at liquid crystalline state diffuse laterally in the plane due to the intermolecular interactions. The lipid diffusion can be roughly classified into two regimes. One is the fast fluctuation of lipid in the cage formed by the

neighbouring lipids and solvation, and this kind of motion is often known as the rattling in a cage. Another regime is the long distance but slow lateral diffusion in the bilayer, which comes from the Brownian motion of lipids in a viscous fluid.

As shown in Figure 13, the lateral MSD curves of DPPC for all simulated bilayer systems show the existence of both classified lipid diffusive behaviours. At the beginning stage with timescale of 0 to 2 ns, a nonlinear rapid increase is observed in MSD, and it indicates the fast rattling motion of DPPC in a cage. Then, the increasing trend of MSD is slowed, and it implies that DPPC molecule escapes from the cage and switches to the slow diffusion mode, where the MSD increases with time linearly. As for the trend for increasing cholesterol content, the obtained results suggest that cholesterol weakens the lateral mobility of DPPC molecules for both motion modes. The effect of cholesterol on the lateral motion is closely related to the distributed surface area, or the volume of the cage. As it was discussed in Chapter 3 that cholesterol reduced the distributed surface area for each molecule, the occurrence of vacancy defect for lateral diffusion is further limited correspondingly. The more cholesterol molecules are involved in the bilayer, the less lateral mobility the molecules can achieve. In addition to the indirect effect of cholesterol, cholesterol may also directly affect the diffusion by forming complex with the saturated DPPC molecules. As cholesterol is short in size and buried under the head groups of DPPC molecules with the rigid ring structure contacting the upper segment of the tails of DPPC, two types of lipids

may form a complex and jointly move together rather than independently. Therefore the mobility of a jointly combined group is likely to be hindered due to larger structure. Evidences for forming complexes among cholesterol and phospholipids in bilayer have been found in both experiments and simulation studies (Lindblom and Oradd, 2009, Rog et al., 2009).

As for the motion of cholesterol in the bilayers, aside from its lateral diffusion within one leaflet, cholesterol can also occasionally translocate its position from one leaflet to the opposite leaflet. This rare occurring event is known as cholesterol flip-flop, and the evidence of occurrence of flip-flop motion is discussed later. Here, the existence of translocation between the two monolayers can result in somewhat improper results of the lateral MSD for cholesterol. To consider the individual molecule's motion with respect to the collective motion of the monolayer, the CM (centre-of-mass) motion of the monolayer was subtracted from the MSD for the individual cholesterol. However, it is confusing about which monolayer's motion is considered for the flip-flopping cholesterol. In practice, the MSD of cholesterol was considered with respect to the instantaneous monolayer's CM motion. For example, one cholesterol molecule was originally located in the upper monolayer for a period of time, so the upper monolayer's CM motion was considered during this period. Then the cholesterol is tumbled and transferred to the opposite monolayer, and the corresponding CM motion of this monolayer was considered. Apparently, it is no

a good solution to address this issue, however, it is reasonable for most cases because the flip-flop event is rare to occur. Even if it might not reveal the actual diffusive behaviour, it is still suggestive for the lateral motions of cholesterol in lipid bilayer.

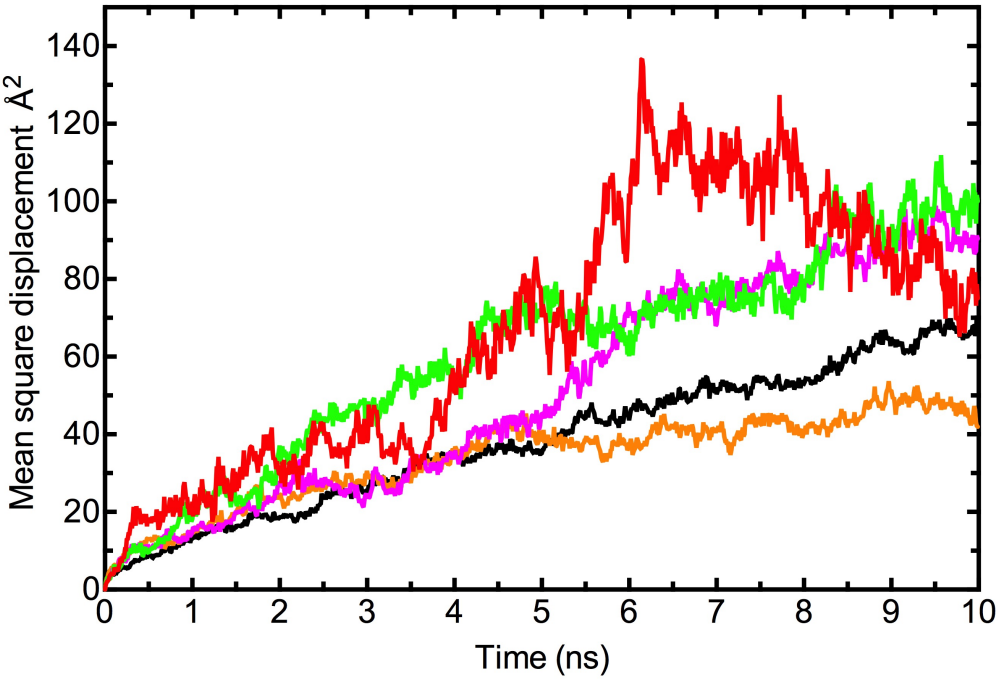

Figure 14 The MSD of cholesterol in the DPPC bilayer at various cholesterol concentrations.

Cholesterol concentrations: 5% (red), 10% (green), 20% (magenta), 30% (orange), 40% (black) Note: the last 60 ns trajectory was divided into six blocks and the MSD was calculated separately in each blocks and then averaged as the result shown here.

As seen in Figure 14, the obtained MSD curves of cholesterol are more fluctuating than those of DPPC in Figure 13, especially in the bilayer systems

with low cholesterol content. These remarkable fluctuations may be attributed to two factors. One is that the poor sampling due to insufficient amount of cholesterol in system. As it is observed that the curves become increasingly less fluctuating upon increasing cholesterol concentration. Interestingly, at 40% cholesterol concentration, the MSD (the black curve in Figure 13) is almost linear over the whole timescale. Another possible factor may be associated with flip-flop translocation of cholesterol between two leaflets of the bilayer. The cholesterol can exist in the bilayer centre and orient itself perpendicular to the bilayer normal. Due to less restriction from surrounding molecules, the rotational and lateral diffusion can occur much easier compared with being oriented parallel to the bilayer normal.

In addition to the fluctuation, the motions of cholesterol seem to be absent from the stage of rattling motion in a cage, which was observed in the MSD of DPPC (see Figure 13). Besides the 5% cholesterol system, the MSD of cholesterol increases at a steady pace rather than the rapid increase at beginning and slow down later. This is probably because cholesterol molecules are mostly located in the hydrophobic region of bilayer, where less restriction was applied from the neighbouring flexible hydrocarbon chains of DPPC, and also cholesterol molecules are barely affected by water molecules. As for the overall trend of the MSD of cholesterol, the obtained results (in Figure 14) indicate that cholesterol's motion in the lateral plane is slowed by its concentration, which is consistent

with the findings for that of DPPC.

4.3.2 The lateral diffusion of DPPC is slowed down in presence of cholesterol

To quantify the lateral motions along the bilayer surface, the diffusion coefficient can be derived from the lateral MSD. As it was mentioned that the fast rattling motion in a cage is more closely related to the volume of the cage, only the long-range lipid diffusive behaviours are concerned here. In practice, the DPPC diffusion coefficient was determined from the MSD by linear fitting over the time window of 5 to 10 ns. The chosen time scale, where MSD increases almost linearly with time, is more closely related to the long-time diffusive behaviour (Patra et al., 2004, Siu et al., 2008, Ollila et al., 2007b, Terama et al., 2008). As for cholesterol, the linear fitting for the diffusion coefficient was performed over the timescale of 0 to 5 ns to avoid fluctuating segments. During this period, each cholesterol molecule in all cases has approximately moved about 6 angstroms or more. This is roughly the distance between two lipids in cholesterol-free bilayer, and the distance can be even shorter in presence of cholesterol. Moreover, the MSD segment in this time interval is reasonably linear with fewer fluctuations than rest parts.

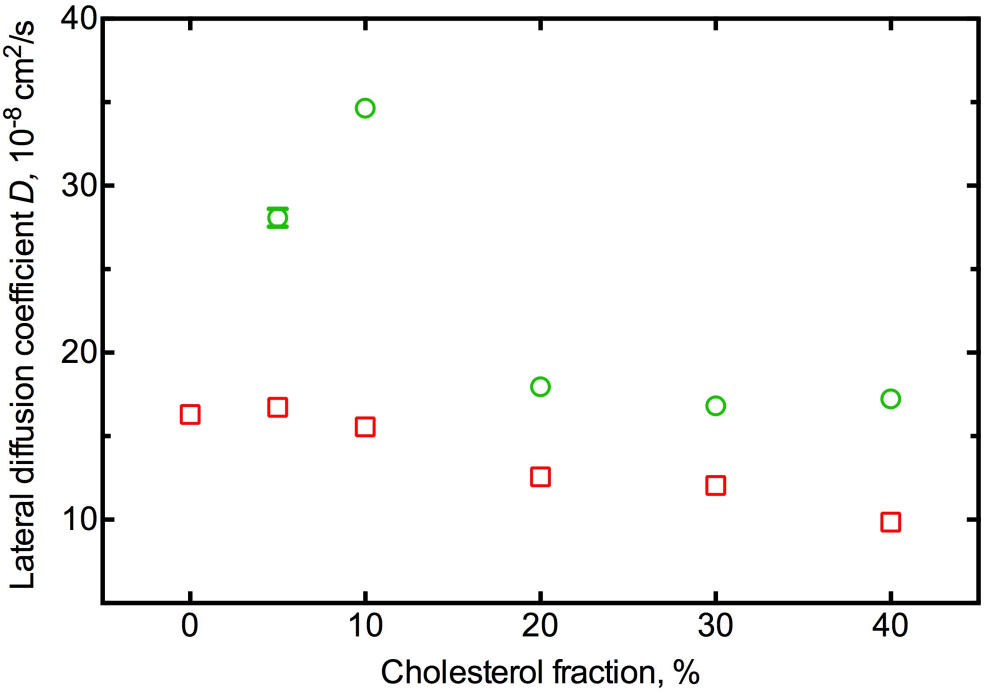

Figure 15 Lateral diffusion coefficients *D* for DPPC (red square) and cholesterol (green circle) in the bilayer systems at different cholesterol concentrations.
The errors were estimated from the linear fitting, and most of the added error bars were overlapped by the symbols.

Figure 15 showed that the obtained lateral diffusion coefficient of DPPC and cholesterol. In all cases, the lateral diffusion of cholesterol is faster than that of DPPC, and similar trend was also found in previous simulation study (Hofsass et al., 2003). The slowed diffusion of DPPC can be explained from several aspects. First, the location of cholesterol molecule is in the hydrophobic region just under head groups of DPPC molecules, where the electron density of the region cholesterol molecules reside is lower than the membrane-water interfacial region. It's sensible to argue that the vacancy defects are more likely to occur in

less crowd region, and those free transient spaces facilitate lipid diffusion. So cholesterol is more likely to take up to free space to diffuse faster. In addition, the DPPC got large dipole moment that that of cholesterol, it was believed that the electrostatics interactions among head groups and water molecules are essential to slow down the lateral diffusion of DPPC (Hofsass et al., 2003) Another possible reason for the faster motion of cholesterol is the effect of entanglements. The lateral motion of lipids with long enough chains is slowed due to the chains entangled with other chains. So cholesterol is less likely to be entangled among chains due to its short chain.

Comparing the obtained results (see Figure 15) with the experimental studies, the results here are in good agreement with the study by Lindblom et al. (2006), who systematically measured the lateral diffusion in single component DPPC bilayer and cholesterol-containing systems based on pulsed-field gradient NMR technique. For the pure DPPC system, the obtained lateral diffusion coefficient of DPPC here is 16.3×10^{-8} cm^2/s in reasonably agreement with 14×10^{-8} cm^2/s measured in their experimental study at 323 K. As for the system in presence of cholesterol, Filippov et al. found a lateral diffusion coefficient of 7.2×10^{-8} cm^2/s at 31% cholesterol concentration (Lindblom et al., 2006). The decreasing trend in experiment is in reasonable agreement with the simulation results here. However, in the previous similar simulation study by Falck et al. (2004), they found that the lateral diffusion coefficient of DPPC was

decreased almost by a factor of 10 at 30% cholesterol. Considering the compared experimental results above (Lindblom et al., 2006), the damping effect of cholesterol on lipid lateral diffusion was suggested to be overestimated in their findings. Moreover, it is not surprising about the overestimation, since it has been discussed in literature that the condensing effect of cholesterol in their study was too high (Rog et al., 2009, Edholm and Nagle, 2005). Therefore, the results in present study are more reasonable than previous similar simulation works (Hofsass et al., 2003, Falck et al., 2004).

4.3.3 Cholesterol Flip-Flop motion

In addition to lateral diffusion, cholesterol also undergoes intra-membrane exchange, which is often called flip-flop of cholesterol. Since the cholesterol's flip-flop motion is less concerned in present study, I attempted a very simple way to track down the motion of the flip-flopped cholesterol molecule.

In practice, a direction vector for cholesterol is defined between the oxygen atom (O) and the carbon atom (C25) in the hydrocarbon chain of cholesterol. Then the orientation of each cholesterol molecule in each bilayer system during the last 60 ns simulation were monitored and analysed. Among the cholesterol molecules, the one, which switched its direction along z-axis most frequently, was chosen as the molecule that possibly flip-flopped during the simulation. Details about the

screening procedure can be found in the in my self-coded program in **Appendix A.**

Figure 16 shows the positions and the orientations of the chosen cholesterol molecule in the DPPC bilayer with 5% cholesterol. It shows that the cholesterol molecule evidently flip-flopped from the lower monolayer to the opposite layer one time during the simulation, and the tumbling process lasts about 10 ns. During the midway of the flip-flop process, the molecule oscillated a few nanoseconds in the liquid-like tail-tail interfacial region at the bilayer centre, where the cholesterol molecule can move freely with least restrictions from surrounding molecules, and it tumbled around before diffuse into the opposite layer. In terms of the flip-flop rate, the chosen cholesterol molecule is pretty active over the simulation period, but only one complete the flip-flop process has been observed, which indicate the cholesterol flip-flop a rare event.

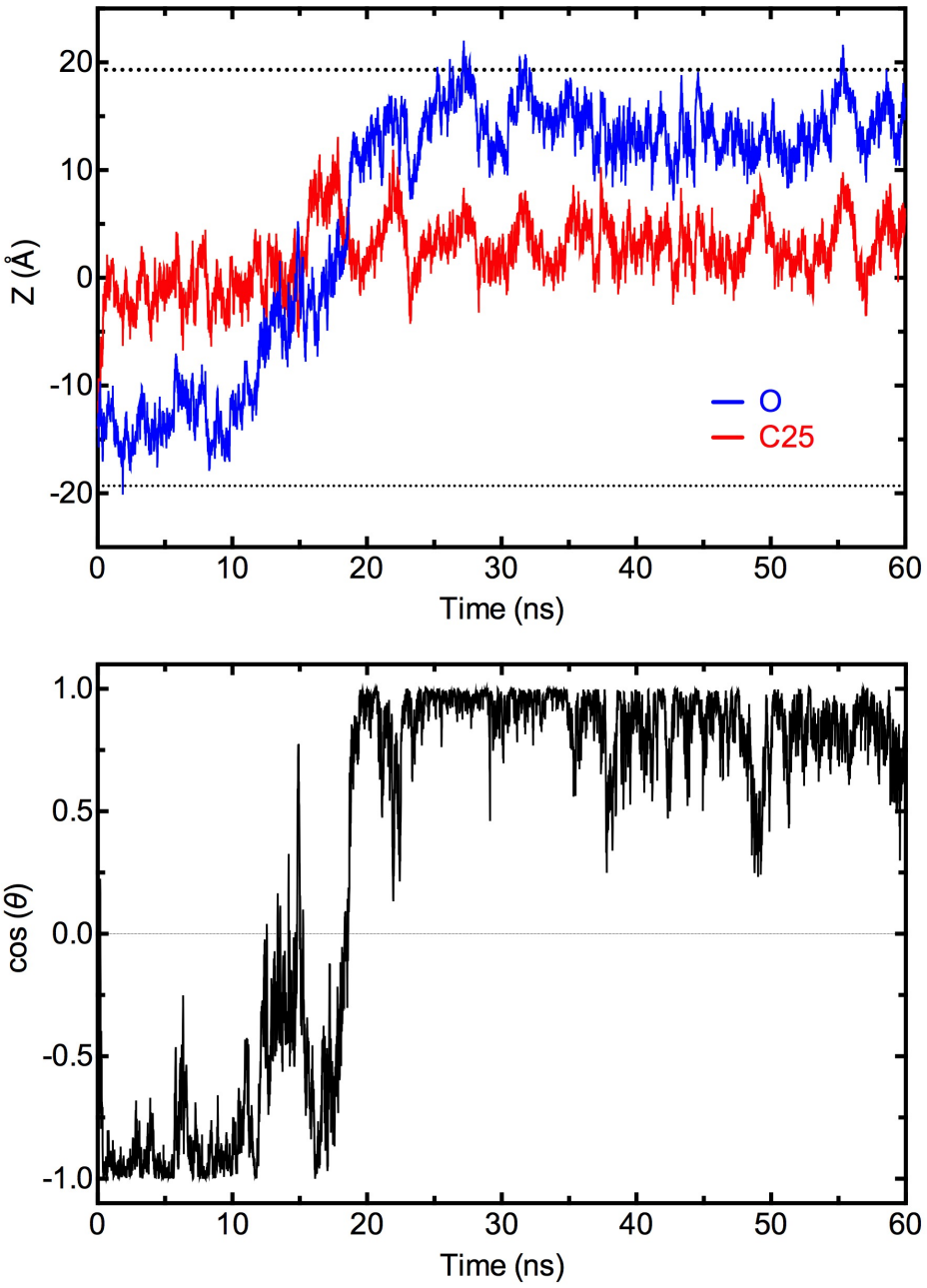

Figure 16 The flip-flop motion of the chosen cholesterol molecule in 5% cholesterol bilayer system.

The upper panel shows the z-axis positions of oxygen O (blue) and carbon atom C25 (red) in the hydrocarbon chain over the simulation period, and the two dashed lines indicate the average position of phosphorus in each monolayer. The lower panel shows the cosine of the angle θ between the direction vector of cholesterol connecting O and C25 and the z-axis unit vector pointing upward ([0,0,1]).

In the DPPC bilayer with 40% cholesterol, more interesting flip-flop event was found. As introduced, the selected cholesterol is the most active one among the molecules in the bilayer. As seen in Figure 17, the cholesterol molecule was reoriented towards the opposite direction in the time interval between 25 and 30 ns, whereas the molecule still stays in the upper leaflet where it was. The way the cholesterol presents is energetically unfavourable, since the polar hydroxyl group of cholesterol is positioned in the hydrophobic bilayer centre, and the hydrocarbon tail is very close to the head groups of the DPPC molecules. This bizarre phenomenon is probably related to the structure of the bilayer with high cholesterol content. At 40% cholesterol, the DPPC molecules are much ordered and the bilayer is packed tighter with reduced area per molecule. As it was discussed in Chapter 3, the electron density in the region where cholesterol resides increased remarkably. Then when the cholesterol undergoes tumbling motion and attempts to diffuse to the opposite layer, no enough free space is available to fit it in. Theoretically, provided the simulation continues for longer time, the cholesterol should be able to transfer to the opposite layer, or switch its orientation into the energetically favourable way. However, the cholesterol flip-flop is not the mainly concerned aspect in present study. Anyway, the illustrated cases have provided evidences of the occurrence of the cholesterol flip-flop motion.

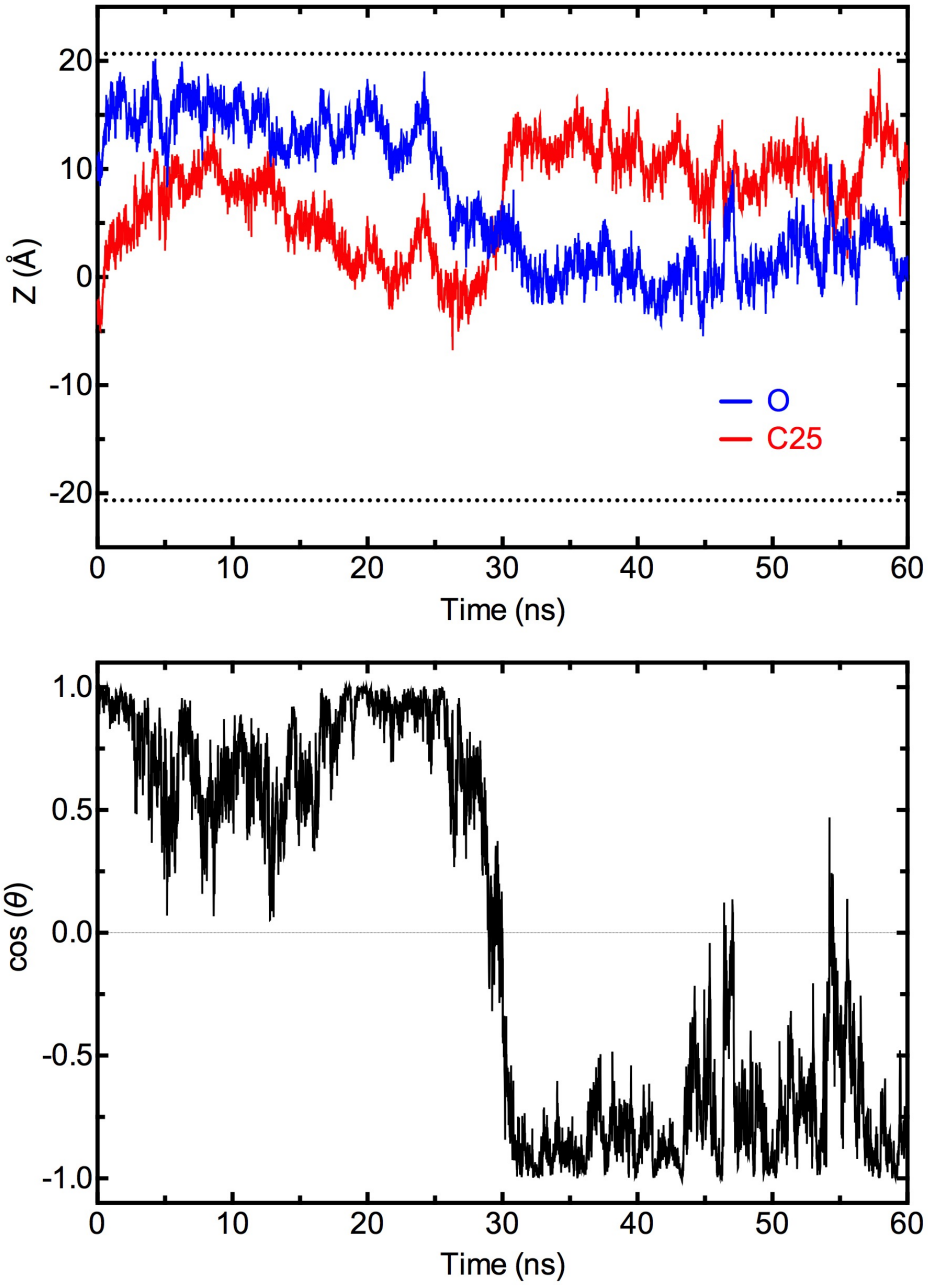

Figure 17 The flip-flop motion of the chosen cholesterol molecule in 40% cholesterol bilayer system.

The upper panel shows the z-axis positions of oxygen O (blue) and carbon atom C25 (red) in the hydrocarbon chain over the simulation period, and the two dashed lines indicate the average position of phosphorus in each monolayer. The lower panel shows the cosine of the angle θ between the direction vector of cholesterol connecting O and C25 and the z-axis unit vector pointing upward ([0,0,1]).

4.3.4 Dual effects of cholesterol on rotational dynamics of DPPC

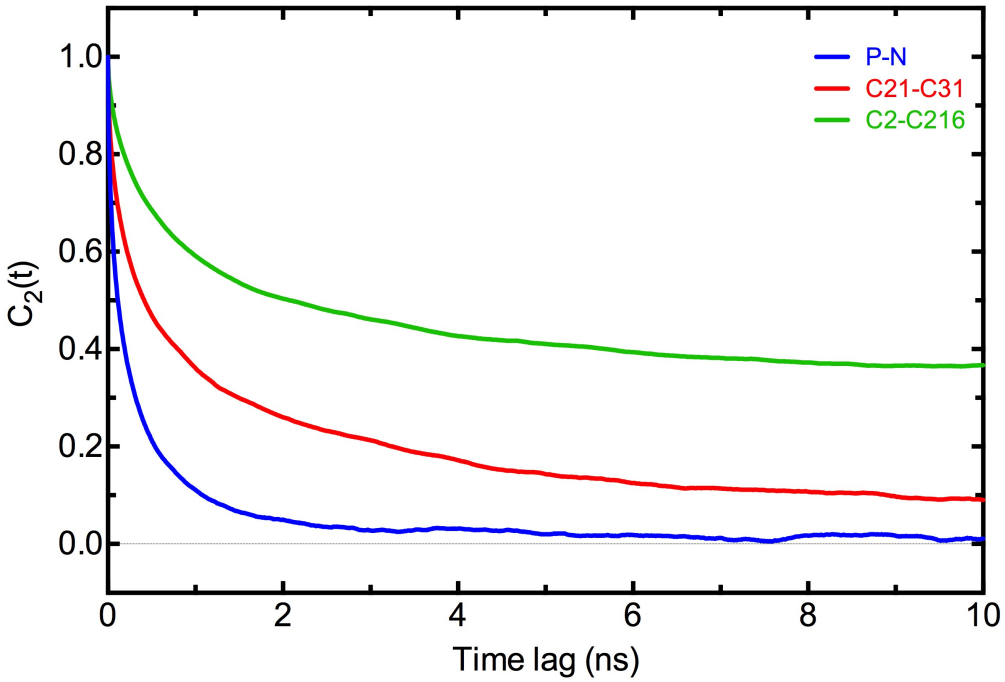

Figure 18 Rotational autocorrelation functions for different vector in the DPPC molecule.

Vectors include P-N in head group, the C21-C31 joining the carbonyl carbon in *sn*-1 and *sn*-2 chain, and the vector C2-C216 for the *sn*-2 chain of DPPC.

To look insight into the intra-molecular lipid dynamics, the rotational autocorrelation functions (Equation 4.3) of the chosen vectors describing the lipids were considered to reveal the re-orientational dynamics in different parts of the lipids. As shown in Figure 18, the autocorrelation functions (ACF) of the three representative vectors for DPPC in the cholesterol-free bilayer system show different decaying trends with development of time lag. The ACF of the P-N

vector in the head group of DPPC molecule decays fastest, and it means the head group is the most dynamic in re-orienting. Then the C21-C31 vector for the middle part of DPPC comes in the second place, and the slowest ACF decaying occurs in the vector joining the C2 in glycerol group and the terminal carbon in *sn*-2 chain. The finding here is consistent with recent simulations(Yang et al., 2014, Ollila et al., 2007b, Terama et al., 2008).

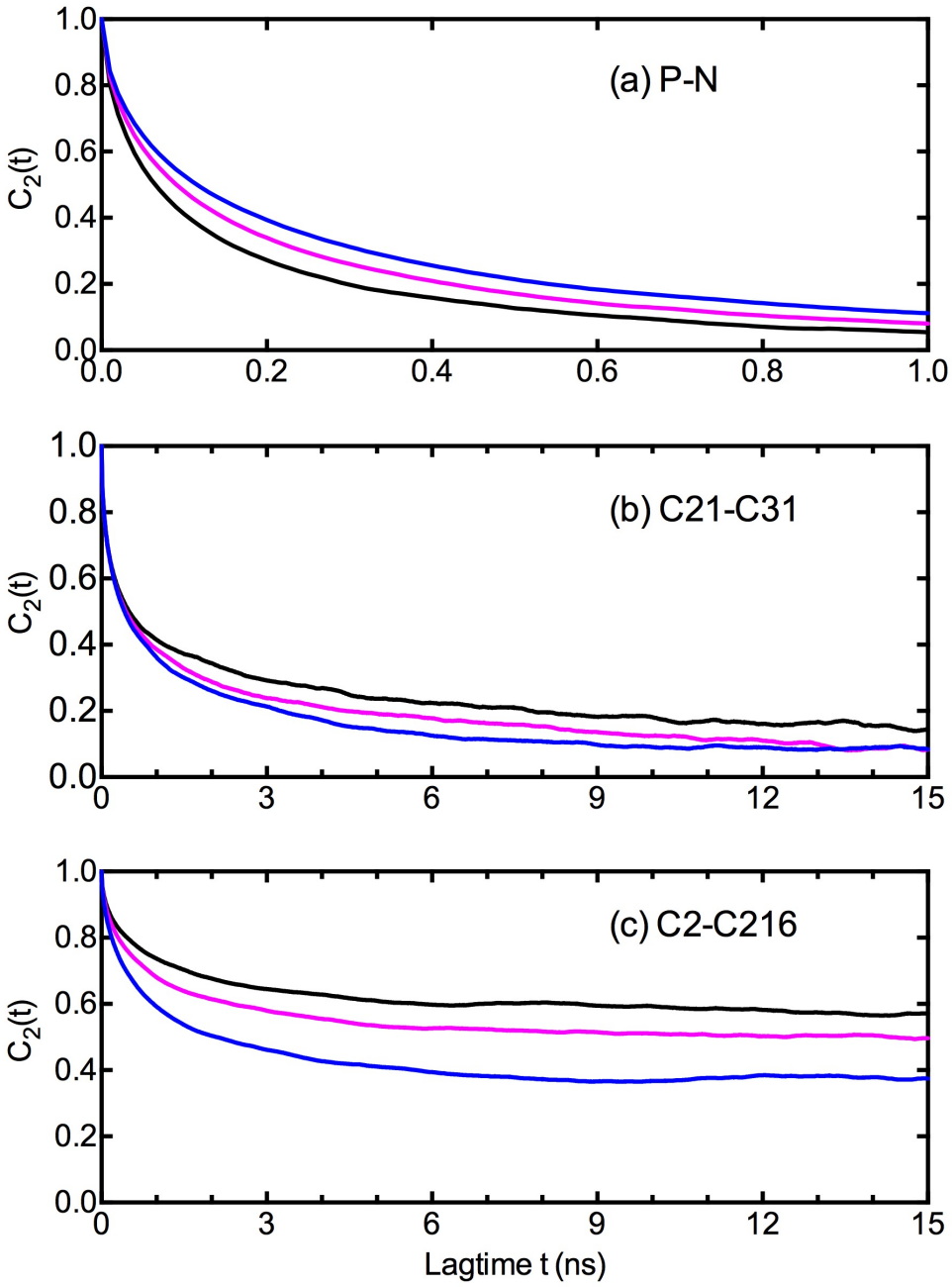

Figure 19 Rotational autocorrelation functions for the vectors of DPPC.

(a) P-N, (b) C21-C31, (c) C2-C216 in the DPPC bilayer with 0% (blue), 20% (magenta), 40% cholesterol (black). For simplicity, the results of the rest systems are not shown.

The effect of cholesterol on rotation dynamics of different parts of DPPC can be

opposite. As seen in Figure 19, the correlation times in the ACF of the P-N vector decrease monotonically with increasing cholesterol concentration, which means cholesterol enhances the rotation dynamics of the head group of DPPC. By contrast, opposite trend is observed in the ACFs for the other two vectors for DPPC, hence it indicates that cholesterol damps the rotation dynamics of the backbone region and *sn*-2 chain of DPPC.

The dual effects of cholesterol on the rotation dynamics of DPPC are closely associated with the location of cholesterol in the lipid bilayer. In lipid bilayer, cholesterol is located under the head groups of DPPC, neighbouring the carbonyl groups and the hydrocarbon chains. The hydrocarbon chains of DPPC become more aligned along the bilayer normal in presence of cholesterol, and then less space is available for rotational motion. So the damping effect of cholesterol on rotational dynamics of DPPC is sensibly associated with the condensing effect of cholesterol. The reason for the damped dynamics is similar with the slowed lipid lateral diffusion, which is that the lipid dynamics is closely related to the free space for motion. In addition, the decrease of correlation times due to cholesterol seems to be larger for the *sn*-2 tail vector C2-C216 vector than the laterally oriented C21-C31 vector close to the backbone region. Obviously, it is determined by the vector's definition. The rotational dynamics of *sn*-2 tail largely indicates the tail's tilting motion, while the carbonyl carbons vector mostly reflects the DPPC's rotating around the axis of DPPC. Cholesterol is more

restrictive to the tilting motion of DPPC then the self-rotating mode, since the tilting motion requires more space.

However, the enhancing effect of cholesterol on dynamics of the head region of DPPC is tricky to explain, since it seems to be inconsistent with the well-known condensing effect of cholesterol. One possible explanation is that the enhanced dynamics is associated with hydrogen bonding between the head groups and water molecules. As the polar hydroxyl in cholesterol may form hydrogen bonds with either the DPPC head groups or the water molecules, and hence it perturbs the interactions between water and DPPC, this may speed up the dynamics of the head group. The regime on enhanced dynamics of lipid molecules was suggested in recent simulations of the lipid bilayer with ethanol (Terama et al., 2008).

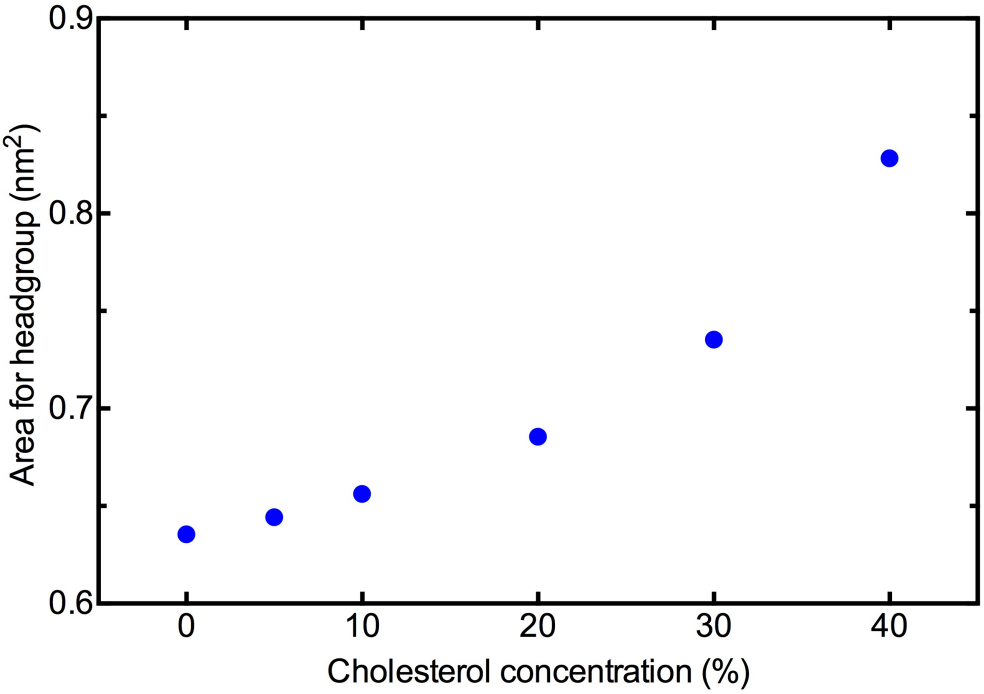

Figure 20 The effective average area for the head groups of each DPPC molecule in the systems with various cholesterol concentrations.

In addition to that, another reasonable explanation for the enhanced dynamics is actually attributed to the increased effective area for the head groups of DPPC molecules. The conventional approach for evaluating the distributed area for each molecule takes cholesterol into account. Therefore, the obtained average area actually reflects the cross-sectional area of the region below head groups of DPPC. In fact, if one only concerns the distributed area for each molecule in the hydrophilic cross-sectional region, the contribution of cholesterol can simply ignored because cholesterol molecules are mainly located in the hydrophobic region of lipid bilayer. Based on that assumption, the area distributed for each DPPC is the effective area for the head groups of DPPC. As shown in Figure 20,

the effective area for DPPC increases with increasing cholesterol content, and it is consistent with the enhanced dynamics of the head groups of DPPC. In addition, it suggests that the dynamics of the hydrophilic part of DPPC are influenced by cholesterol in an unspecific regime.

4.4 Summary

In this chapter, I focus on the effect of cholesterol on the lipid dynamics from two aspects, the lipid lateral diffusion, and rotation dynamics. It was found cholesterol slowed down the lateral diffusion rate of DPPC and that of cholesterol. In addition, occurrence of flip-flop motion of cholesterol was identified in some of the present simulations. Lastly, cholesterol is found to play dual role in affecting rotation dynamics of DPPC. The rotation motion of the backbone and tail region of DPPC is damped in presence of cholesterol, while the head groups of DPPC is influenced in an opposite way.

Chapter 5 The effect of cholesterol on lateral pressure profiles

5.1 Introduction of lateral pressure in membrane

Simons and Ikonen (1997) proposed lipid raft model for the structure, which is typically enriched in cholesterol, sphingomyelin and saturated phospholipids, and cholesterol was suggested to be the central part in formation of the lipid rafts. Lipid rafts were found to be closely associated with many cellular activities such as signal transduction, regulating functionalities of integral proteins, and cholesterol was suggested to be crucial in many of these activities. As the fact that the bilayer compositional change can alter the structural properties was believed to have impacts on the embedded proteins (Bloom et al., 1991, Cantor, 1999a), Cantor (1997) proposed an indirect mechanism that changes in the lateral pressure profile of a lipid membrane may affect the activities of membrane proteins, such as mechanosensitive channels (Cantor, 1999a). The lateral pressure profile depicts the distribution of the local lateral pressure in a lipid bilayer, and can provide microscopic interpretations for many macroscopic measureable properties of lipid bilayer, such as the surface tension, surface free energy, and spontaneous curvature (Tildesley, 1987, Safran, 1994, Cantor, 1999b, Jensen et al., 2001)

The lateral pressure has been suggested to play important biological roles in, for example, the phenomena as general anaesthesia (Cantor, 1997, Eckenhoff, 2001, Terama et al., 2008), or regulation of protein function (deKruijff, 1997, Cantor, 1999a, Samuli Ollila et al., 2007). However, gauging lateral pressure profiles is very difficult due to absence of good probes in experiments. Only one experiment study was reported by Templer et al. (1998) at present. Molecular dynamics simulations of lipid bilayer have shed light on estimation of the lateral pressure inside the bilayer structure. Several previous studies have revealed that the pressure profiles are pretty complex and the local pressures can be various depending on the compositions. In addition, quantities of the local pressure can be as high as the order of 1000 bars (Lindahl and Edholm, 2000b, Samuli Ollila et al., 2007), and it is evident that it is capable to influence proteins by favouring a certain conformation. Moreover, it was found that the lateral pressure profiles of the lipid bilayer with polyunsaturated lipids are notably different from the profiles of saturated lipid bilayer. With increasing the number of double bonds, the peak in the middle becomes less repulsive (Carrillo-Tripp and Feller, 2005, Ollila et al., 2007b). In terms of cholesterol related studies, Patra (2005) carried out the first study on the effect of cholesterol on lateral pressure profile in phospholipid bilayer and found that the cholesterol induced qualitatively changes in regional pressures inside the bilayer at higher cholesterol concentrations (over 20%). In DPPC-cholesterol bilayer, extra positive pressure

regional peaks and negative troughs were introduced in the pressure profile compared to the pressure profile found in pure DPPC bilayer, and the magnitudes of local lateral pressure become higher with increasing the cholesterol content (Patra, 2005). Later, Samuli Ollila et al. (2007) compared the lateral pressure profiles in the lipid membranes with different sterol types, and it was found that the lateral pressure profiles were sensitive to the sterol type, though these sterols have very similar chemical structure with cholesterol.

In this Chapter, I focused on investigating the lateral pressure in the DPPC bilayer with and without cholesterol molecules. Since most of the previous studies on the similar topic used simplified united-atom force fields, the present study using the recently improved all-atom CHARMM36 force field (Klauda et al., 2010, Lim et al., 2012) is necessary to fill the gap.

5.2 Calculations of the lateral pressure profile

In present study, the pressure tensor was computed with the built-in function of the LAMMPS package (Plimpton, 1995), and the data were collected during the last 20 ns simulation. To obtain the lateral pressure profile, the simulation box was divided into thin slabs at 1 Å width along bilayer normal (z-axis), and then the local lateral pressure $P(z)$ in each slab is defined as:

$$P(z) = \frac{P_{xx}(z) + P_{yy}(z)}{2} - P_{zz}(z) \tag{5.1}$$

where $P_{xx}(z), P_{yy}(z), P_{zz}(z)$ are the diagonal elements of the local pressure tensor in slab s. The expression describes the difference between the lateral pressure $(P_L = (P_{xx}(z) + P_{yy}(z))/2)$ and the normal pressure $(P_N = P_{zz}(z))$ components of the pressure tensor, which actually is not the lateral pressure itself but rather equivalent to the surface tension inside the bilayer (Lindahl and Edholm, 2000b, Patra, 2005). However, the expression is still conventionally named as the lateral pressure profile. Quantitatively, the positive $P(z)$ means that a bilayer tends to expand along the membrane plane (x-y plane) in slab s and the negative $P(z)$ means a contraction in this slab.

As it was noted in the LAMMPS manual, the overall pressure can be decomposed into two partial terms:

$$P(z) = P^{KE}(z) + P^{VIR}(z) \tag{5.2}$$

where the $P^{KE}(z)$ refers to a kinetic energy term, and the $P^{VIR}(z)$ refers to a virial term. Moreover, $P^{KE}(z)$ was calculated with:

$$P^{KE}(z) = \frac{1}{V}\langle \sum_i m_i v_i \otimes v_i \rangle \tag{5.3}$$

where the $\otimes$ sign denotes tensor product, m_i and v_i are the mass and velocity of atom i, respectively, and V is the volume for the corresponding slab. All angular brackets in present and following equations in this section represent an average over the simulation time.

The virial term includes all potential energy terms except kinetic energy term, and the general form can be expressed in terms of atomistic positions, velocities and forces as:

$$P^{VIR}(z) = \frac{1}{V}\langle \sum_{\substack{i<j \\ i\in V}} f_{ij} \otimes r_{ij} \rangle \tag{5.4}$$

For example, the pairwise non-bonded term, which includes Lennard-Jones and electrostatics interactions, $P^{NB}(z)$ is calculated with:

$$P^{NB}(z) = \frac{1}{2V}\langle \sum_{\substack{i \\ i\in V}} \sum_{\substack{j \\ j\neq i}} (r_i f_{ij} + r_j f_{ji}) \rangle \tag{5.5}$$

where r_i and r_j are the positions of atom i and atom j, f_{ij} is the force exerted on atom i ,and f_{ji} is the corresponding opposite force on atom j. Note that atom i belongs the volume V.

The bonded interaction $P^B(z_s)$ between atom i and atom j is similarly computed with:

$$P^B(z_s) = \frac{1}{2V_s}\langle \sum_{\substack{i \\ i\in Vs}} \sum_{\substack{j \\ j\neq i}} (r_i f_{ij} + r_j f_{ji}) \rangle \tag{5.6}$$

The calculation is similar with the previous non-bonded term one except the counted forces arise from the bond between atom i and atom j.

The expressions of per-atom pressure for 2-body virial term in equation 5.5 and 5.6 are equivalent to Harasima (H) expression for the local pressure tensor for

the virial term (Sonne et al., 2005). Basically, in terms of a pair of atoms in two different slabs, Harasima expression depicts that the half lateral pressure arising from the interaction between atom i and atom j is assigned to the slab where atom i exists, and the other half of the lateral pressure arising from the same pair is assigned to the slab where j exists. In addition to the Harasima expression, another more popular expression for the local pressure tensor is the Irving and Kirkwood (IK) (Sonne et al., 2005). The IK expression distribute the viral terms evenly on the slabs where the straight line connecting atom i and atom j goes through. Therefore the contribution to the local pressure from this interaction is the same in all slabs that are in the region between the two atoms. According to the previous study by Sonne et al. (2005), both the pressure profiles obtained from the H and the IK expressions qualitatively reproduced the essential features for lipid bilayer obtained in previous studies (Goetz and Lipowsky, 1998, Lindahl and Edholm, 2000b, Gullingsrud and Schulten, 2004) . Moreover, it was observed that there were no qualitative and negligible quantitative differences in the lateral pressure profiles obtained by H method compared to the results by IK approach. The H approach is used in present study because its well-tested implementation in LAMMPS package (*LAMMPS website*, Plimpton, 1995, Orsi and Essex, 2013).

5.3 Results and discussion

5.3.1 The lateral pressure in the DPPC bilayer without cholesterol

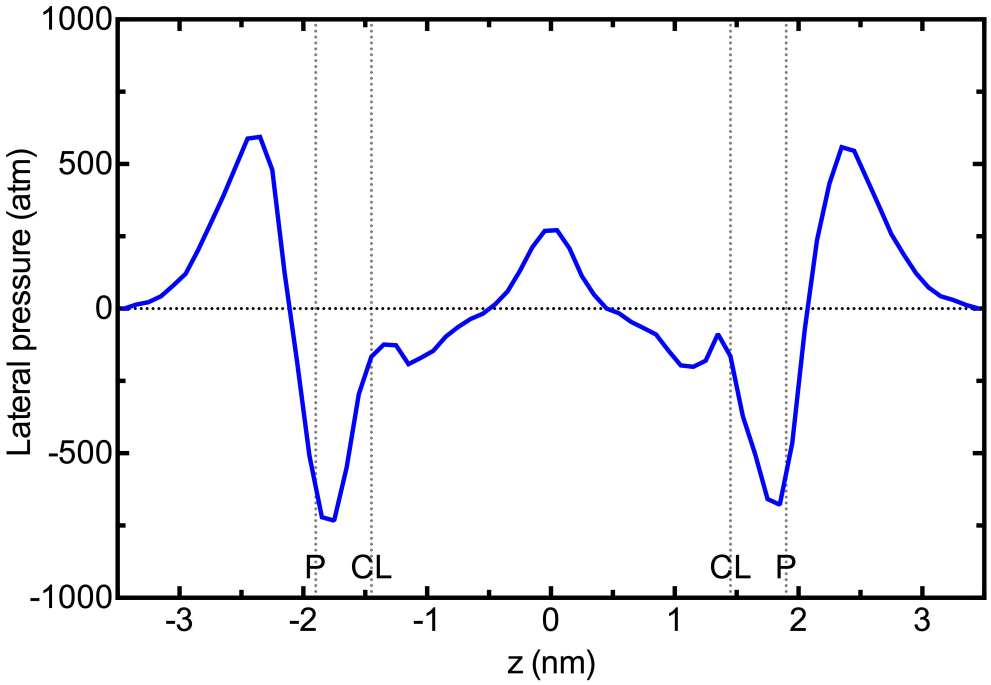

Figure 21 The lateral pressure profile of pure DPPC bilayer

The vertical dotted lines represent the average position of the corresponding atoms. The label P and CL represent the average position of phosphorus and the carbonyl carbon respectively.

The lateral pressure arises from the average local forces acting on the atoms as well as the kinetic motions of the atoms in each slab. Since the DPPC bilayer is inhomogeneous in the norm direction of the bilayer, the local pressures at different depth are expected to be various. As shown in Figure 21, the obtained

lateral pressure for the pure DPPC bilayer system shows alternating positive and negative regions along bilayer normal, where the positive regions represent the tendency of expansion and the negative regions correspond to contraction in the lateral plane, respectively.

In the lateral pressure profile of DPPC, both positive peaks and negative troughs were found in the hydrophilic head group region, and a shallow positive region at the bilayer centre where the terminal methyl groups of the hydrocarbon chains reside. The result obtained here is consistent with the conventionally identified regimes for the interactions across lipid membrane. At the outmost of the bilayer, a repulsive contribution occurs in the hydrophilic head group due to electrostatic and steric interaction, and hydrogen repulsion. Then a bit further down in the bilayer-water interfacial region, there exists an attractive interaction arising from the interfacial energy between the water and hydrophobic core of the lipid bilayer. At last, a repulsive contribution exists inside the membrane due to steric interactions between the hydrocarbon chains (Israelachvili et al., 1980, Marsh, 1996, Samuli Ollila et al., 2007). In present study, the positive pressure at bilayer centre was found to be over 250 atm, suggesting that the hydrocarbon chains tried to distance from each other. While in the membrane-water interfacial region, the lateral pressure drops quickly from positive 500 atm to negative pressure 700 atm. The solvation energy between water and the polar head is dominant in this region, and the strong attraction in the

membrane-water interfacial region suggests that the bilayer tries to reduce the area to prevent more water penetrate inside the hydrophobic region. Most of the attractive pressure is compensated by the repulsive pressure between water molecules, because water molecules becomes ordered due to the electrostatic field produced by zwitterionic polar head, and then they attempt to gain entropy (Lindahl and Edholm, 2000b, Patra, 2005). Despite pressure in this region appears to be huge compared with external pressure (1 atm), the local pressure of this order has been predicted in earlier theoretical estimation based on the thickness of the membrane-water interfacial region and the corresponding interfacial tension(Cantor, 1997, Cantor, 1999b, Gullingsrud and Schulten, 2004).

Compared with the other similar studies, the lateral pressure profile found here shows a reasonable agreement with the results from previous atomic-level simulation studies (Lindahl and Edholm, 2000b, Patra, 2005, Sonne et al., 2005, Samuli Ollila et al., 2007), though slightly differences occur in quantities. The differences can be caused for many reasons, such as force fields, simulation conditions (Sonne et al., 2005) and so on. It was noticed that using different force field in simulation could result in discrepancies in the profile. In the previous study by Patra (2005), DPPC molecules were described with the united-atom force filed (Berger et al., 1997). In the model, the hydrogen atoms in DPPC were implicitly considered to increase computational efficiency, and importantly, no partial charges were assigned to the particles in the hydrocarbon chains. Using

this model, Patra (2005) observed a positive region near the carbonyl group in DPPC, indicating repulsive interactions between water molecules and hydrocarbon chains due to hydrophobicity. Whereas in my study, the local pressure at the same position only shows an increasing trend but still remains negative (in Figure 21), and similar results were observed in another study by Sonne et al. (2005), who used all-atom CHARMM27 force field, the predecessor of CHARMM36 force field. Therefore, different force fields do have an impact on lateral pressure profiles. In real membrane, it's not clear how the local pressure at this position would perform due to technical limitations, but it's sensible to argue that there exist noticeable attractive interactions in this region, since hydrogen bonding can be formed between water molecules and carbonyl oxygen atoms (Ohvo-Rekila et al., 2002, Starke-Peterkovic et al., 2006, Olsen et al., 2009, Rog et al., 2009, Berkowitz, 2009, Rog and Vattulainen, 2014).

5.3.2 The lateral pressure in the DPPC bilayer with cholesterol

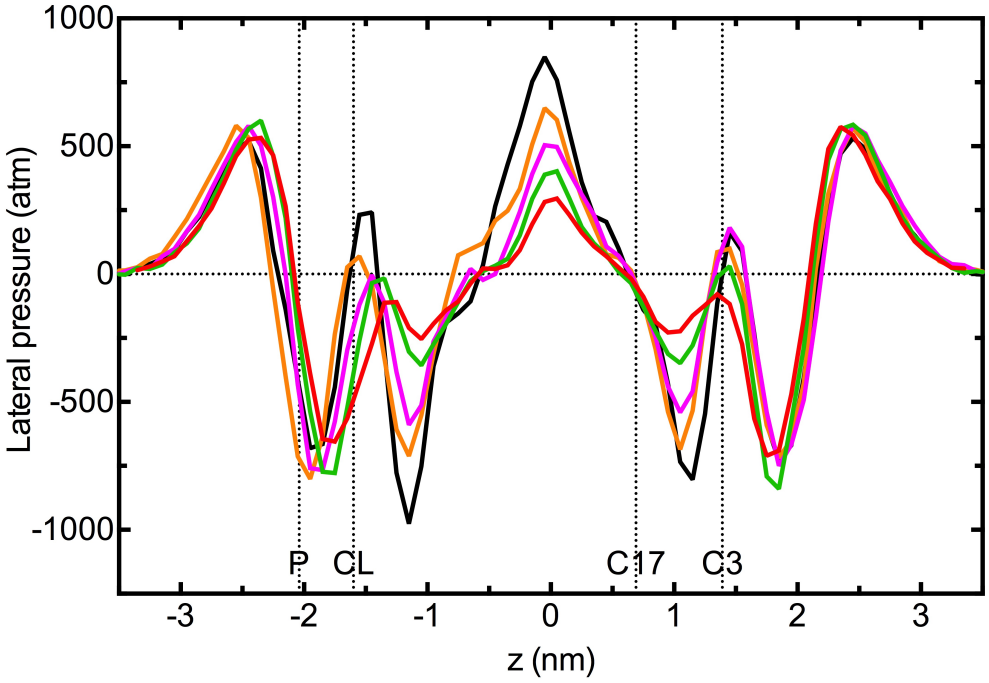

Figure 22 The lateral pressure profiles of the DPPC-cholesterol mixture bilayers. Cholesterol concentrations include 5 % (Red), 10 % (Green), 20 %(Magenta), 30 % (Orange), 40 % (Black) cholesterol. And the vertical dotted lines represent the average position of the corresponding atoms in the 40% cholesterol system. P and CL represent the phosphorus and carbonyl carbon in DPPC, respectively, and C3 and C17 represent carbon atoms in the ring structure of cholesterol.

As for the lateral pressure profile in the DPPC bilayers with cholesterol, the calculated lateral pressure profiles are shown in Figure 22. Upon increasing cholesterol concentration, pronounced changes in the profiles were observed in the region where cholesterol resides. In the four-ring region, which is roughly

the region between C3 and C17 shown in Figure 22, well-pronounced negative troughs were gradually developed at the middle part of the ring structure of the cholesterol, while they were not present in the lateral pressure profile of pure DPPC bilayer. And the magnitude of the lateral pressure in the region was monotonically increased by almost a factor of 5, reaching about negative 1000 atm. A bit further down at the bilayer centre, the local pressure was enhanced to be over 800 atm in the 40% cholesterol bilayer, whereas it was only 250 atm in pure DPPC bilayer.

Apparently, the amplified magnitudes of the local pressures in the regions are closely associated with cholesterol in the bilayer. In cholesterol, the fused ring structure provides much more complicated chemical structure compared with the linear tails of DPPC molecules, and the polar hydroxyl group attached on the steroid ring makes it even more complex by offering hydrophilic property to the ring. It was reported that the interactions of lipids with cholesterol largely depends on the attractive van der Waals interactions between the steroid rings of cholesterol and the acyl chains, and the attractive interactions of cholesterol with unsaturated lipids can be weakened due to the presence of kinks in the *cis*-bond (Ohvo-Rekila et al., 2002). In present study, the obtained attractive local pressures in the region with cholesterol ring are consistent with the above arguments. It is sensible to consider that the negative pressure in this region further reduces the cross-sectional area of the interfacial region, and results in

ordering in the tails of DPPC, especially in the upper segment of the tails. Then in the region close to the bilayer centre, the local pressures displayed stronger repulsions among the tails to compensate the attraction. It was reported that the repulsion is due to steric interaction, while I would argue that the entropy in the nonpolar hydrophobic region is an important factor for the expanding trend, since the ordered tails have lost degree of freedom in motion due to the Van der Waals attraction with the cholesterol ring structure. In fact, the two explanations are consistent in essence, since both imply an expanding tread in this region.

By contrast, as shown in Figure 21 and Figure 22, the local pressures in the regions of the polar head of DPPC were barely affected with increasing cholesterol content. The observation is reasonable since cholesterol molecules can hardly access to the polar head region, where the solvation between water and the polar head groups is the dominant interactions (Marsh, 2002, Patra, 2005). The finding here is consistent with the argument in the previous investigation Marsh (2002), which suggested that the lateral pressure of this region was weakly associated with the cholesterol concentration because the hydration energy in this region is weakly dependent on the area per lipid. However, Patra (2005) found that the local pressures in the region of head group were also strongly influenced, and the magnitudes of pressure were increased by up to thousands of bars upon at high cholesterol concentrations. It was explained as a generic and unspecific effect associated with reduction in surface area of

bilayer. Indeed, the condensing effect of cholesterol in his study is much stronger than the study here. Nevertheless, it was reported that the condensation at this level is overestimated (Rog et al., 2009, Ferreira et al., 2013, Rog and Vattulainen, 2014). So it can be concluded that the obtained results here have shown to be more reasonable than previous simulation studies (Chiu et al., 2002, Hofsass et al., 2003, Patra, 2005, Ollila et al., 2007a).

5.4 Summary

In this chapter, I investigated the lateral pressure profile of the pure DPPC bilayer and also the DPPC-cholesterol mixed bilayer. It was found the cholesterol introduced specific characteristics in the lateral pressure, and the obtained lateral pressure profiles are reasonably agreed with previous investigations qualitatively. In addition, it was found different force fields have noticeable impacts on the lateral pressure by comparing current study with previous ones, especially in the cholesterol-containing systems. However, it's not clear how the local pressure is distributed in real membrane due to no proper probes for accurate measurement of the local pressure inside a bilayer. It needs further developments in experimental techniques to produce more reliable experimental data to validate the simulated systems.

Chapter 6 Elastic properties of the lipid bilayer with and without cholesterol

6.1 Introduction

The elastic properties of lipid membranes have been suggested to be critical in modulating the conformational properties and functions of the proteins (Zimmerberg and Kozlov, 2006, Andersen and Koeppe, 2007, Marsh, 2007, Soubias et al., 2010). Previous investigations on lipid rafts have found that cholesterol-enriched domains possessed the distinguished mechanical properties. Moreover, Lipid rafts have been suggested to be thicker and relatively rigid toward bending compared with the more fluid non-raft bilayer region (Mouritsen and Zuckermann, 2004, Andersen and Koeppe, 2007, McIntosh and Simon, 2006, Khelashvili and Harries, 2013a). Earlier studies on structural properties of cholesterol-containing lipid bilayer have found that the cholesterol molecules in lipid bilayer are oriented by a preferred tilt angle with respect to the bilayer normal, and the tilt angles are closely related to the cholesterol concentration (Mouritsen and Zuckermann, 2004, Veatch, 2007, Korade and Kenworthy, 2008, Marsh, 2009, Elson et al., 2010, Khelashvili et al., 2010a, Khelashvili et al., 2010b).

On the basis of analysing the MD simulation trajectory, Khelashvili et al. (2010b) recently proposed an energetic parameter, cholesterol tilt modulus χ, to quantify the energetic cost of tilting cholesterol inside the lipid bilayers. Cholesterol tilt modulus is derived from the distribution of cholesterol orientations with respect to bilayer normal in the lipid membrane, and it establishes a link between the structural, thermodynamics and mechanical properties of the cholesterol-containing bilayers. Moreover, sterol tilt modulus can be considered as a quantitative measure of the sterol-induced aligning field in lipid bilayer. Then, the authors further extended the methodology to estimate the splay modulus χ_{12} for pairwise interactions, which is associated with the free energy cost for splaying one lipid molecule with respect to another. Different from cholesterol tilt modulus χ, the splay modulus χ_{12} is derived based on the splay angle between two closely located molecules. For instance, in a DPPC-cholesterol binary system, three different pairs can be found to calculate the splay modulus χ_{12}: DPPC-DPPC, cholesterol-cholesterol, DPPC-cholesterol. Then the contributions from the corresponding splay modulus of each molecular pair can be analogously weighed to extract the overall bending modulus of the membrane (Khelashvili et al., 2013, Khelashvili et al., 2014). In fact, the global membrane deformation stems from the local lipid splay deformation, which is most significant microscopic mode of the deformations in lipid bilayer. Moreover, the idea is common to many classical theories of statistical and condensed matter physics by making the connection between the macroscopic material

properties of a many particle system and the average pairwise interactions (Chaikin and Lubensky, 2000).

It was found that the method (Khelashvili et al., 2013) had shown advantageous aspects over another popular method for bending modulus prediction based on the spectral analysis of bilayer undulations (Goetz et al., 1999, Lindahl and Edholm, 2000a, Chiu et al., 2003, Olsen et al., 2009, Brandt et al., 2011, Khelashvili et al., 2011). The spectral analysis method has been applied to calculate bending modulus for the single-component phospholipid bilayers in fluid phase (L_d), and the result was in good agreement with experimental value (Lindahl and Edholm, 2000a, Chiu et al., 2003, Brandt et al., 2011). However, the limitations of the spectral analysis method have been reported previously. This approach requires large enough simulated membranes to sustain long-wavelength undulations, and it also requires sufficiently long simulation time-length to efficiently sample the shape fluctuations (Lindahl and Edholm, 2000a, Hofsass et al., 2003). In addition, it was reported that these limitations result in a statistical error of 20-24% for the bending moduli, and this method greatly underestimated the bending rigidity for the cholesterol-containing liquid ordered (L_o) lipid bilayer (Hofsass et al., 2003, Khelashvili et al., 2011). It is interpretable as the fact that this technique relies on large amount of sampling of membrane undulations. However, it has been known that cholesterol can lead condensing effect in lipid bilayer, so such undulations in the liquid-ordered (L_o)

bilayer are highly suppressed. Therefore it is still very hard to assess in simulations, even for large bilayer systems and very long simulation time. In contrast, the method proposed by Khelashvili et al. (2013) can obtain the bending modulus parameter for lipid membranes of arbitrary lipid composition irrespective of the phase behaviours of the membrane. In addition to the fact that it has predicted the bending rigidity for a ternary lipid bilayer with remarkable consistency with the experimental values, the method can quantitatively evaluate the contributions from the splaying of different pairs of molecules in the ternary bilayer to the overall bending rigidity. Furthermore, It was reported that the computational framework, taking advantages of local splaying interactions, is extendable to more complex systems such as lipid membranes decorated with peptides or even multi-helical proteins (Khelashvili et al., 2013).

In this chapter, I will calculate the bending modulus for DPPC bilayer systems with and without cholesterol in the novel approach (Khelashvili et al., 2013), thus to evaluate how cholesterol influences the elastic properties of DPPC bilayers. Before investigating the splay modulus for each pairwise interaction, I first discussed the cholesterol tilt and its implications on energetic aspect of the cholesterol-containing lipid bilayers. Then the splay moduli and bending moduli of each simulated bilayer systems were studied.

6.2 Method

6.2.1 Deriving bending modulus from the splay moduli

The calculations of bending rigidities K_c for all simulated bilayer systems were carried out with myself-coded tool (Appendix B) following the method proposed by Khelashvili et al. (2013). The basic idea for the method is based on the fact that the bending deformation in lipid bilayers is closely associated with the localized pairwise splay interactions. To evaluate the local splay deformation, the splay modulus χ_{12} was proposed as an energetic parameter that quantifies the free energy costs for splaying one molecule away from the other one. Then the splay modulus for all possible pairs of molecules in the lipid bilayer is calculated, respectively. For instance, three different pair types are found in binary DPPC-cholesterol mixture, namely DPPC-DPPC, cholesterol-cholesterol, DPPC-cholesterol. Finally, the bending rigidity K_{C} of the lipid bilayer can be determined by weighting the corresponding splay contributions (Khelashvili et al., 2013).

$$\frac{1}{k_{\mathrm{m}}} = \frac{1}{\varphi_{\mathrm{total}}} \sum_{\langle i,j \rangle} \frac{\varphi_{ij}}{\chi_{12}^{ij}} \tag{6.1}$$

where $k_{\mathrm{m}} = K_{\mathrm{C}}/2$ is the monolayer bending modulus, χ_{12}^{ij} denotes the splay modulus per monolayer between molecular pairs of types i and j, and φ_{ij} is the number of near-neighbouring ij encounters, derived from the simulation

trajectories; At last, $\varphi_{\text{total}} = \sum_{\langle ij \rangle} \varphi_{ij}$ represents the total number of encounters in the simulations for all possible near-neighbouring pairwise contributions $\langle i, j \rangle$, for which the splay angles considered.

6.2.2 Calculations of splay modulus

To obtain the splay modulus χ_{12}^{ij}, which measures the energetic cost for splaying $\langle i, j \rangle$ molecular type pairs, the local lipid direction vector $\vec{t}$ should be defined first to calculate the splay angle α of the near-neighbouring encounters. The direction vector $\vec{t}$ for DPPC molecule is the vector that connects from the geometric centre-of-mass of the three terminal carbons to the midpoints between phosphorus and the glycerol C2 atoms. For cholesterol molecule, the director vector connects the C23 in the middle segment of the hydrocarbon chain to the C3 at the hydroxyl group of cholesterol. Then, the splay angles α between different $\vec{t}$ vectors for all possible pairs (i.e. DPPC-DPPC, DPPC-cholesterol, DPPC-cholesterol) were collected from simulation trajectories. After that, the corresponding splay angle probability distributions $P(\alpha)$ for each pair were constructed by creating a normalized splay angular histogram in the range of [0°; 90°].

According to the Helfrich continuum elastic theory of membrane deformation (Helfrich, 1973, Kozlovsky and Kozlov, 2002, May et al., 2004, Fosnaric et al.,

2006), the splay energy, f_{splay}, is proportional to the quadratic expansion $(\nabla \cdot \theta)^2$ in local direction vector $\vec{t}$ (Kozlovsky and Kozlov, 2002):

$$f_{\text{splay}} = \frac{k_s}{2}(\nabla \cdot \theta)^2 \approx \frac{k_s}{2}(\nabla \cdot \alpha)^2 \tag{6.2}$$

where k_s represents the splay modulus, and θ is the tilt angle between vector $\vec{t}$ and the bilayer norm. Since the expression of f_{splay} is strictly valid for the small splay angles α range (Kozlovsky and Kozlov, 2002, Khelashvili et al., 2014), the $P(\alpha)$ probability distributions only count the pairs where at least one of the participant molecules is tilted no more than $\theta = 10°$ away from the bilayer norm vector. Moreover, to limit the splay analysis to near neighbours, only the pairs of molecules within 10 Å from each other were considered. At last, the χ_{12}^{ij} splay modulus can be obtained by performing a quadratic fitting over small α angle range in potential of mean-force function, $\text{PMF} = -k_{\text{B}}T \ln(P(\alpha)/\sin\alpha)$. PMF (α) describes the free energy cost for pairwise splaying, and $\sin\alpha$ in PMF represents the probability distribution for a hypothetical system of non-interacting molecules (Kessel et al., 2001)]. The value of the splay modulus χ_{12}^{ij} for splaying $\langle i, j \rangle$ corresponds to the coefficient of the quadratic term of the best fit. In this approach, the obtained splay modulus χ_{12}^{ij} obtained is consistent with k_s in equation (6.2) (Khelashvili et al., 2014) .

6.2.3 Methodological issues for calculating splay moduli

In terms of the reliability of the resultant splay moduli with the fitting procedure, the method is required to start with a simulation trajectory where the bilayer system is well equilibrated and it requires adequate sampling of splay angles for calculating splay moduli. In present study, the last 60ns segment in simulations trajectories were taken from the simulations introduced in Chapter 3 for bending rigidities analysis. Before the trajectories were collected, all of the systems have run at least more than 120 ns simulation, so the simulations used for analyses are deemed as dynamical equilibrium periods.

6.2.3.1 Evaluating sampling quality of splay angle for $P(\alpha)$

In present study, the DPPC/cholesterol bilayer systems span a wide range of cholesterol concentrations, and systems containing small fractions of cholesterol can result in statistically poor sampling of pairwise splay angles, especially for the splay pair cholesterol-cholesterol. However, the calculation of the splay modulus requires adequate samplings of slay angles for performing quadratic fitting to PMF (α). In practice, the sampling quality was evaluated by monitoring the number of times that the specific splay pair visits a certain $[\alpha + \delta\alpha]$ angular bin. Regarding to the poor sampled splay pairs, the contributions from them to

the overall bending rigidities were ignored. For instance, in either 5% or 10% cholesterol systems, the splay angles of cholesterol-cholesterol pair visit each angular bin less than 80 times during the 60 ns simulations, while the times of visit to the angular bins for the DPPC-cholesterol and DPPC-DPPC splay pairs are significantly larger than that for cholesterol pair. So the contributions to the global bending rigidities from the cholesterol pairs in such systems can be safely ignored. As for the 20%, 30% and 40% cholesterol systems, it was found that the cholesterol splay pairs visit each bin in angular range [5°, 40°] at least 200 times, so the $P(\alpha)$ distributions are considered to be well-converged, at least for $\alpha \in [5°, 40°]$.

6.2.3.2 Quadratic fitting intervals and estimation of uncertainties in splay moduli

As for fitting procedure in present study, the [12°, 24°] was taken as the interval of small splay angle for quadratic fitting to PMF (α) in relatively more ordered systems with 20%, 30% and 40% cholesterol, and the interval [15°, 30°] was used in relatively disordered systems with 0%, 5%, 10% cholesterol. The fitting intervals here are consistent with those used in previous similar studies [2014 Jan, 2012 tilt, 2013 sterol tilt]. In addition, the chosen intervals were compared to the confidence angular intervals in $P(\alpha)$ distribution, which were estimated by fitting Gaussian distribution to corresponding $P(\alpha)$. The chosen angular

ranges [12°, 24°] and [15°, 30°] are mostly within the ranges of the calculated confidence intervals for all systems. Therefore the intervals used here represent the best-sampled regions with relatively high probability density, and also remain within small angle range eligible for deriving splay moduli from quadratic fitting (Kozlovsky and Kozlov, 2002, Khelashvili et al., 2014) .

To estimate uncertainties in obtained splay moduli, the quadratic fitting procedures were repeated by using smaller angular window within the original interval, and drifting the fitting windows. Then the standard deviations were calculated from this series of fits. For example, the original fitting was performed in the [12°, 24°] range, then a series of 10° angular intervals were used for repeating the quadratic fitting in [12°, 22°], [13°, 23°], and [14°, 24°] ranges. Similarly, for [15°, 30°] interval, a series of fitting intervals with angular range of 12° can be used for the quadratic fitting to calculate the standard deviations. The approach used here is similar with many previous studies (Khelashvili and Harries, 2013b, Khelashvili et al., 2013, Khelashvili et al., 2014, Khelashvili et al., 2010b).

Since the splay moduli are derived from the local splaying interactions, the obtained errors are related to monolayer rigidity k_{m}. So the error bars for the bending rigidity K_c of the bilayer were set as $\sqrt{2} \times \sigma_{error}$, where σ_{error} is the standard error in monolayer rigidity k_{m}, following the approximation approach

introduced by Khelashvili et al. (2014).

6.3 Result and discussion

6.3.1 Molecular orientations of cholesterol and DPPC in the membrane

As it was investigated in Chapter 3, cholesterol condenses the DPPC bilayers with reduced area per lipid, thickened bilayers and increased order parameters. In addition, condensing effect is also reflected in the molecular orientations, which is represented by the tilt angle θ. The tilt angle θ is defined as the angle between the molecule's direction vector $\vec{t}$ and the bilayer normal (z-axis), hereby $\theta = 0°$ represents that the molecule is oriented parallel to the bilayer normal. To analyse the orientation of molecules in each bilayer system, tilt angles θ for DPPC and cholesterol were obtained from the respective simulation trajectories and then the tilt angles were constructed into histogram in the angular intervals of [0°; 90°]. The normalized histograms for tilt angles (P (θ)) represent the probability for finding a molecule that is oriented at a tilt angle θ with respect to bilayer normal. Figure 23 shows the calculated tilt angle distributions P (θ) of DPPC and cholesterol in all systems. In addition, the lower panel of Figure 23 also includes the hypothetical probability distribution $P_0(\theta)$ of tilt angles for cholesterols in an ideal condition, where non-interacting cholesterol molecules

are oriented randomly and the number of accessible orientation states is maximized. The assumption was proposed by (Khelashvili et al., 2010b), who defined the random distribution as $P_0(\theta) = \sin\theta$, since the molecule tilted at an angle θ with respective to bilayer normal can possess more possible orientational states compared to the position that is upright in the normal direction, and the degeneracy is proportion to $\sin\theta$.

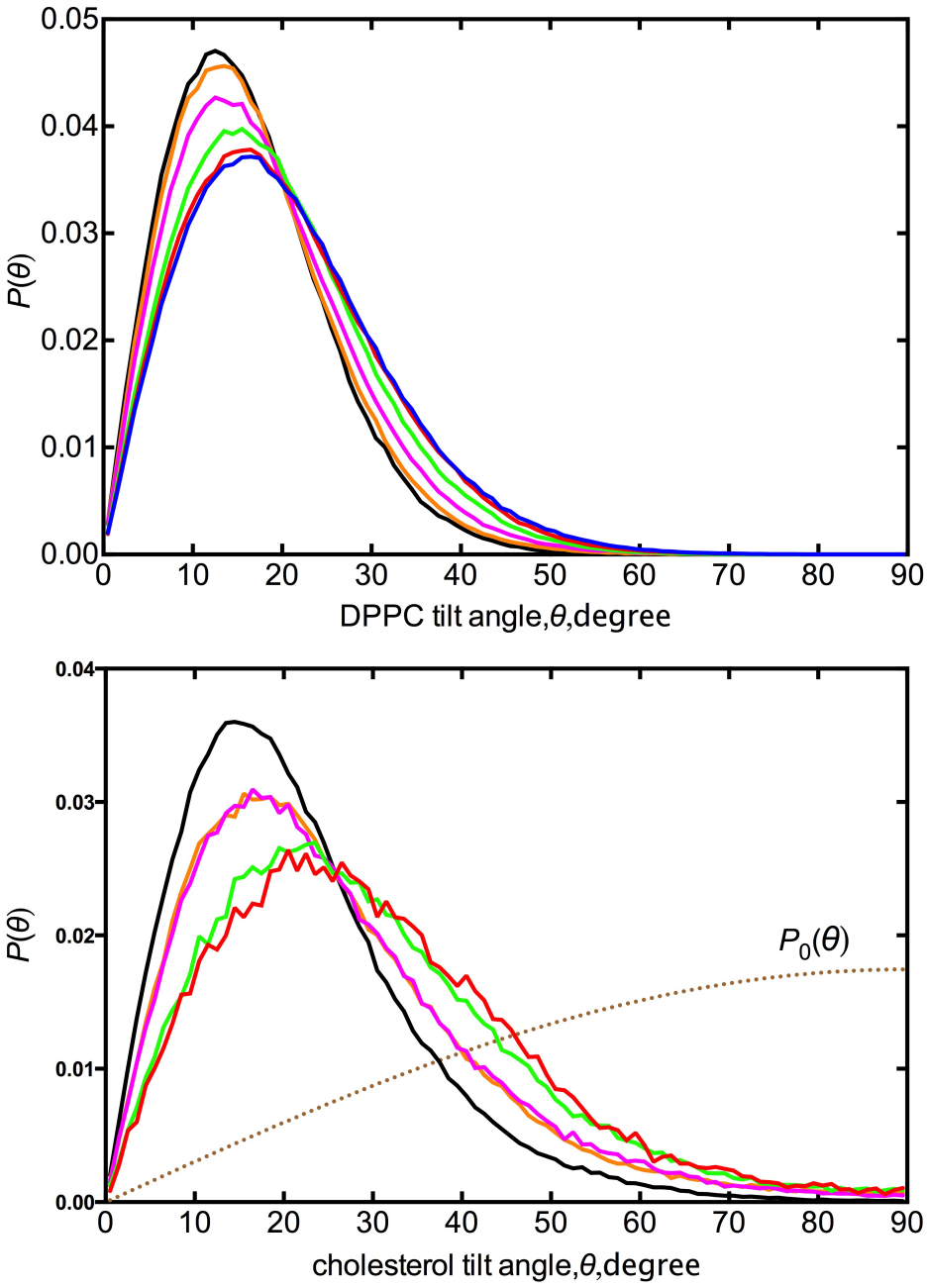

Figure 23 Probability distributions of tilt angle θ with respect to the bilayer normal $P(\theta)$ for DPPC (upper panel) and cholesterol (lower panel) in DPPC bilayers with 0% (blue), 5% (red), 10% (green), 20% (magenta), 30% (orange), 40% (black) cholesterol concentrations.

Upon increasing cholesterol concentration (in Figure 23), the tilt angle distributions $P(\theta)$ for both of DPPC and cholesterol become narrower and

develop well-defined peaks at decreasingly lower tilt angles. The narrowing $P(\theta)$ distributions indicate that both of DPPC and cholesterol molecules become more aligned along bilayer normal with cholesterol concentration increasing. It is noted that all of the distributions $P(\theta)$ of cholesterol are relatively broader than those of DPPC, especially in the systems at low cholesterol concentrations. It is not surprising that DPPC molecules possess narrow tilt angle distributions. As DPPC is responsible for sustaining the bilayer structure so that they appear to be well organised. In contrast, the cholesterol shows stronger dependence on its concentration in the DPPC bilayers. At low concentrations (in Figure 23), non-zero distributions of cholesterol are observed, indicating that cholesterol molecules can be found at pretty large tilt angles. Then non-zero regions disappeared when cholesterol concentration goes up, and cholesterol molecules are preferentially oriented at relatively smaller tilt angles. This behaviour of the alignment is analogous with the isotropic-nematic (I-N) transition in liquid crystals (de Gennes and Prost, 1993), where hard-rod molecules are aligned with preferred orientations with its increased concentration.

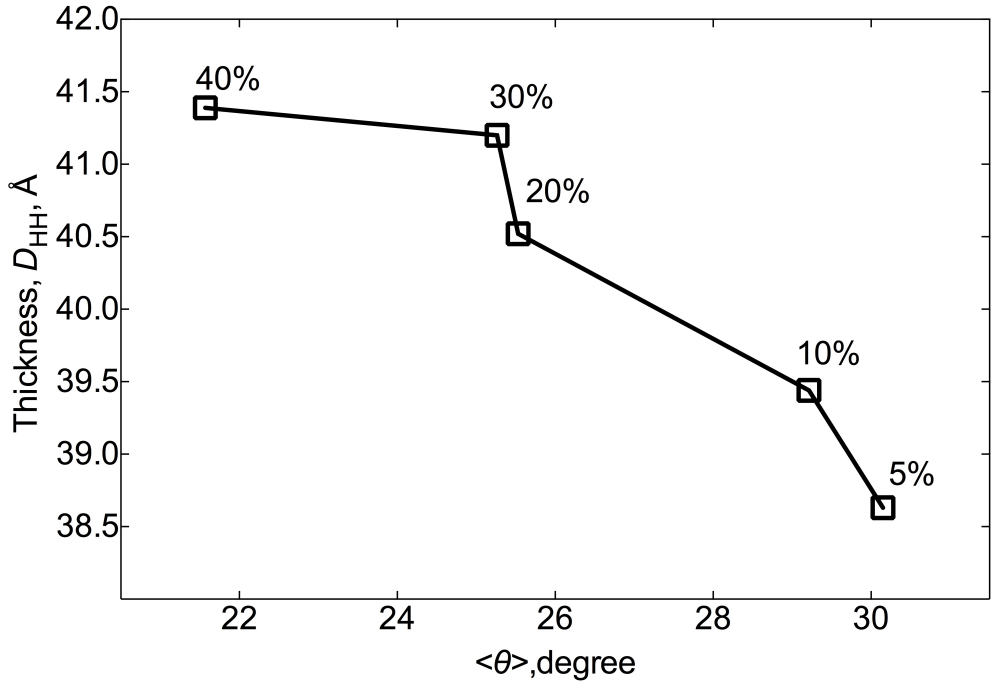

Figure 24 Correlation between average cholesterol tilt angle $\langle\theta\rangle$ and bilayer thickness D_{HH} in the DPPC/cholesterol systems at different cholesterol concentrations.

$\langle\theta\rangle$ was obtained from the $P(\theta)$ shown in Figure 23, and D_{HH} was defined as the average distance between the phosphorus atoms from the opposite monolayers, and data adapted from Chapter 3.

The alignment of cholesterol upon increasing cholesterol concentration can be correlated with changes in structural properties of the bilayers. The cholesterol alignment states can be monitored by the average cholesterol tilt angle $\langle\theta\rangle$, which is defined by $\langle\theta\rangle = \int_0^{90^\circ} \theta P(\theta)\, d\theta$. Here, the cholesterol $\langle\theta\rangle$ at different cholesterol concentration is correlated with bilayer thickness D_{HH}, since thickness is closely associated with the ordering in the lipid tails. Figure 24 shows that cholesterol tilt is strongly anti-correlated with the bilayer thickness

D_{HH} over the 5%-30% cholesterol concentrations. Then it seems to be less correlated when cholesterol concentration increasing from 30% to 40%, since tilt angles $\langle\theta\rangle$ decreases from 25.3° to 21.6° while thickness only increases slightly. It may suggest the system may enter liquid-ordered thermodynamic state at and above 30% cholesterol, where the lipid molecules have been condensed and ordered to an extent so that the thickening procedure becomes relatively independent from cholesterol tilt angle. Basically, cholesterol tilt can be deemed as an effective indicator of the ordering effect induced by cholesterol (Olsen et al., 2009, Aittoniemi et al., 2006, Rog and Vattulainen, 2014).

6.3.2 Mechanisms of cholesterol alignment along bilayer normal in membrane

To explore the mechanisms of cholesterol alignment in lipid bilayer, energetic and entropic factors can be considered to account for the orientation of cholesterol molecules (Khelashvili et al., 2011). Since interactions between cholesterols are less energetic favourable compared with those between cholesterol and DPPC, cholesterol molecules tend to be apart from themselves upon increasing cholesterol content in the membrane. In turn, the energetically preferred interactions between DPPC and cholesterol contribute to forming stable complexes in bilayer (Simons and Vaz, 2004), which is closely associated with forming lipid raft. Aside from the energetic consideration, each molecule

owns degrees of freedom associated with translational and orientational entropy of the molecule within the bilayer structure. When a molecule that is tilted by an angle θ with respect to the bilayer normal, the molecule can span more configurations than the molecule positioned upright in the bilayer. On the basis of pure orientational entropy considerations, cholesterol molecules tend to be oriented away from the bilayer normal direction by 'lying down' in the bilayer to maximize the number of possible orientations, and thus gain degrees of freedom in rotations. Khelashvili et al. (2010b) found that the cholesterol tilt angle $P(\theta)$ for 1% cholesterol DMPC/cholesterol system shares partly overlapped probabilities in the angular interval [45°; 60°] with the hypothetic tilt angle distribution $P_0(\theta) = \sin\theta$, which indicates random angle distribution of the non-interacting molecules. The idealized non-interacting state is solely governed by entropic tendencies, and it only exists in a hypothetical system. In present study, I followed the assumption for the randomly distributed system as the reference state.

Upon increasing in cholesterol content, cholesterol molecules undergo transition from 'lying down' to 'standing up' in the bilayer. It largely relies on the interplay between the energetic and entropic contributions discussed above. The tendency is first due to cholesterol trying to gain ''free volume'' and thereby attain translational entropy. But it compromises by orientational entropy loss. Besides that, the tendency can also be partly attributed to lipid-mediated unfavourable

cholesterol-cholesterol interactions (Khelashvili et al., 2005). In an attempt to distance themselves from each other, cholesterol molecules adopt the nematic-like ordering means to be aligned, and become preferentially engaged in interacting with the surrounding lipids. In such a way, the molecules in the membrane become well packed and condensed, and the lipid tails become more ordered, accordingly.

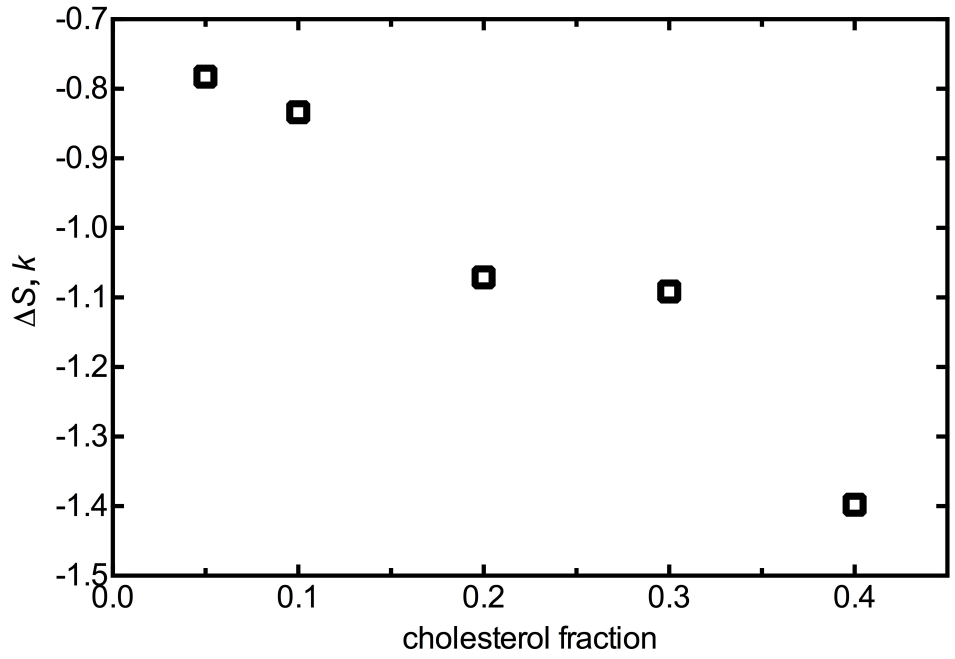

Figure 25 Cholesterol orientational entropy loss ΔS with increasing cholesterol concentration in units of Boltzmann's constant *k*.

6.3.3 Cholesterol orientational entropy loss upon increasing cholesterol concentration

The losses in cholesterol orientational entropy (ΔS) upon increasing cholesterol concentration can be quantified by the approach proposed by (Khelashvili et al.,

2011)., and ΔS is defined as:

$$\Delta S = -\mathrm{K_B} \int_{0^\circ}^{90^\circ} P\,(\theta) \ln\left(\frac{P\,(\theta)}{\sin\theta}\right) \mathrm{d}\theta \qquad (6.3)$$

The definition ΔS is zero for the hypothetic non-interacting molecules, which is regarded as the reference state. However, for the realistic anisotropic oriented cholesterol molecules, ΔS is expected to be non-zero and negative. Figure 25 shows the calculated ΔS for all DPPC/cholesterol bilayers at different cholesterol concentrations. Upon increasing cholesterol concentration, the ΔS decreases monotonically. At low cholesterol concentrations (5% and 10%), ΔS remains relatively high with slight decrease, then the pronounced drops can be found at 10%-20%, and 30%-40% cholesterol concentrations intervals, respectively. The results obtained here show great qualitative and quantitative consistency with previous studies on DMPC/cholesterol systems [(Khelashvili et al., 2010b)]. With cholesterol fraction increasing, the cholesterol molecules undergo transition of 'lying down' to 'standing up', and procedure sacrifices degrees of freedom in orientation. Therefor transition is expected to gain free energy in other forms to compensate for the entropy loss. Earlier study on free energy estimation of transferring cholesterol from a disordered lipid bilayer to an ordered lipid bilayer suggested the transfer is energetic favourable (Zhang et al., 2008). Moreover, another study by Bennett el al. found the process of cholesterol desorption from an ordered lipid bilayer consisting of saturated lipids costs more energy than that from a less ordered lipid bilayer containing

poly-unsaturated lipid species (Bennett et al., 2009). The findings are consistent with the observed loss in orientational entropy upon increasing the cholesterol concentration in present study. Therefore, ΔS additionally provides an energetic insight into the condensation of lipid bilayer induced by cholesterol. The losses in cholesterol orientational entropy are closely associated with the condensation states of the lipid bilayer.

6.3.4 Splay angle probability distribution

It was reported that cholesterol tilt deformation was an important contributor to the mechanical properties of lipid bilayer, and it can be quantified with cholesterol tilt modulus χ (Khelashvili et al., 2013). Based on that point of view, pairwise splaying deformations between molecules in membrane are more related to the mechanical properties. Indeed, the molecules in a membrane undergoing bending deformation comply with the deforming trend via rearrangement of their orientations in the bilayer, therefore it is sensible that the molecules possess a more splayed configurations with respect to each other. The pairwise splaying deformation in lipid bilayers can be energetically evaluated by splay modulus χ_{12}^{ij}, which predicts the energy cost for splaying one molecule with respect to each other in lipid pairs of type i and j. Furthermore, evaluating splaying deformation in this approach can consider not only the cholesterol molecules but also any other components in the membrane. (Khelashvili et al.,

2013, Khelashvili et al., 2014)

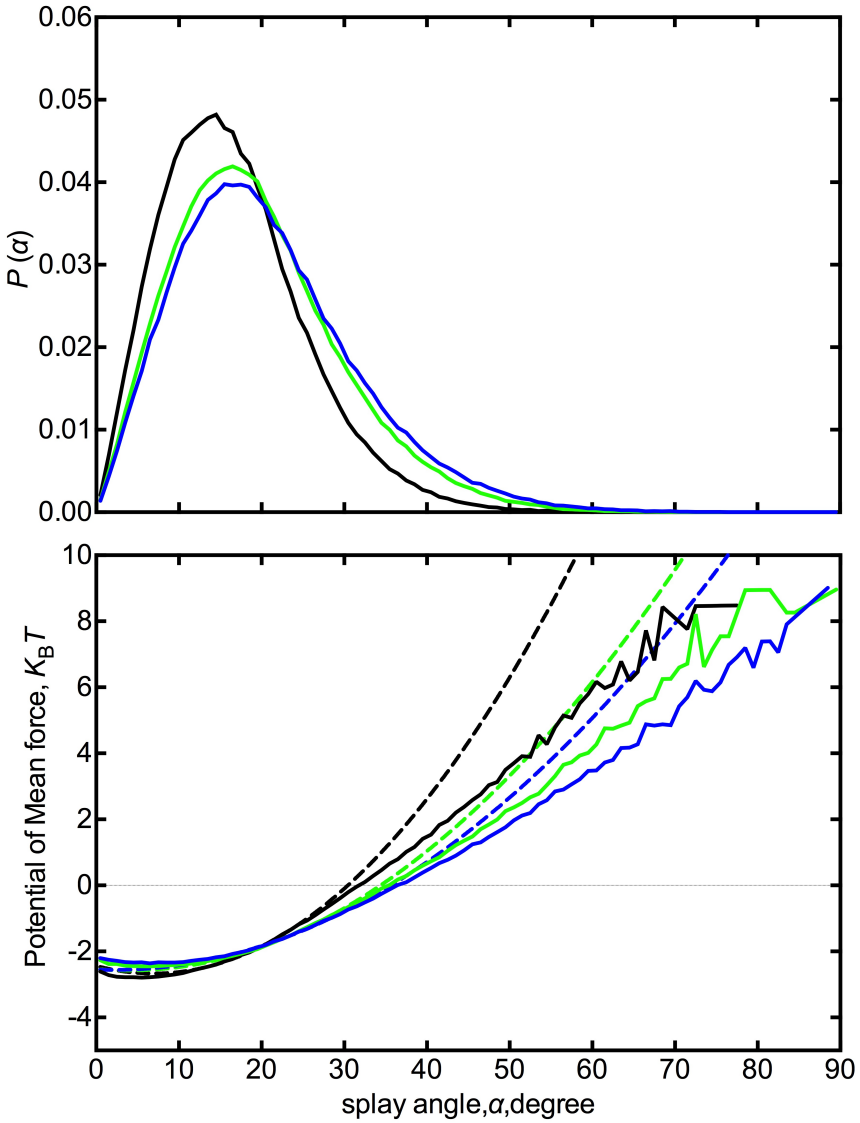

Figure 26 Quadratic fittings in the intervals of small angular range for splay moduli of the pair of DPPC and DPPC

(Upper panel) the normalized probability densities $P(\alpha)$ of finding a pair of DPPC and DPPC at an angle α with respect to each other in DPPC bilayers at 0% (blue), 10% (green), 40% (black) cholesterol concentration. (Lower panel) the solid curves presents the potential of mean force (PMF (α)) corresponding to $P(\alpha)$ distributions shown in upper graph, and the dashed curves represent the best quadratic fits for PMF curves. The [15°, 30°] interval was used for fitting in 0% and 10% cholesterol systems, and the [12°, 24°] interval was used in 40% cholesterol systems.

In present study, three different splaying pairs occur in the cholesterol-containing DPPC bilayers, including DPPC/DPPC, DPPC/Chol, and Chol/Chol (Chol for cholesterol). Figure 26 illustrates the procedure to derive splay modulus χ_{12} for the example of all DPPC pairs in 0%, 10% and 40% cholesterol systems. The splay angle probability distributions $P(\alpha)$ for DPPC pairs in Figure 26 show similar trend with the DPPC tilt angle distributions $P(\theta)$ (in Figure 23). The splay angles between DPPC molecules are decreasingly lower upon increasing cholesterol content, thereby the molecules are aligned with each other. Different from $P(\theta)$, more limitations were applied to $P(\alpha)$ to ensure that only local splay fluctuations were counted. The analysis is limited to the near-neighbouring pairs so that only pairs of molecules within 10 Å from each other are taken into account. Moreover, considerations were only given to the DPPC pairs, for which at least one DPPC molecule in each pair should be tilted by no more than 10° with respect to the bilayer normal. As it was introduced earlier, such a limitation is required to validate the small angle regime for splay modulus calculation from the quadratic fitting to PMF (α). Using the probability distributions of splay angle, potential of mean forces for splaying two DPPC molecules was calculated with $\mathrm{PMF} = -k_{\mathrm{B}}T\ln(P(\alpha)/\sin\alpha)$, shown in Figure 26 (bottom), where PMF (α) curves appear to be quadratic not only in the intervals of small angles but also throughout the angular range. Then the dashed curves in the same graph represent the best quadratic fits performed in small α ranges of the PMF (α) for the corresponding bilayer systems, respectively. Apparently,

the plots of quadratic fitting became steeper upon increasing cholesterol concentrations, which indicates the higher energy cost for splaying two DPPC molecules.

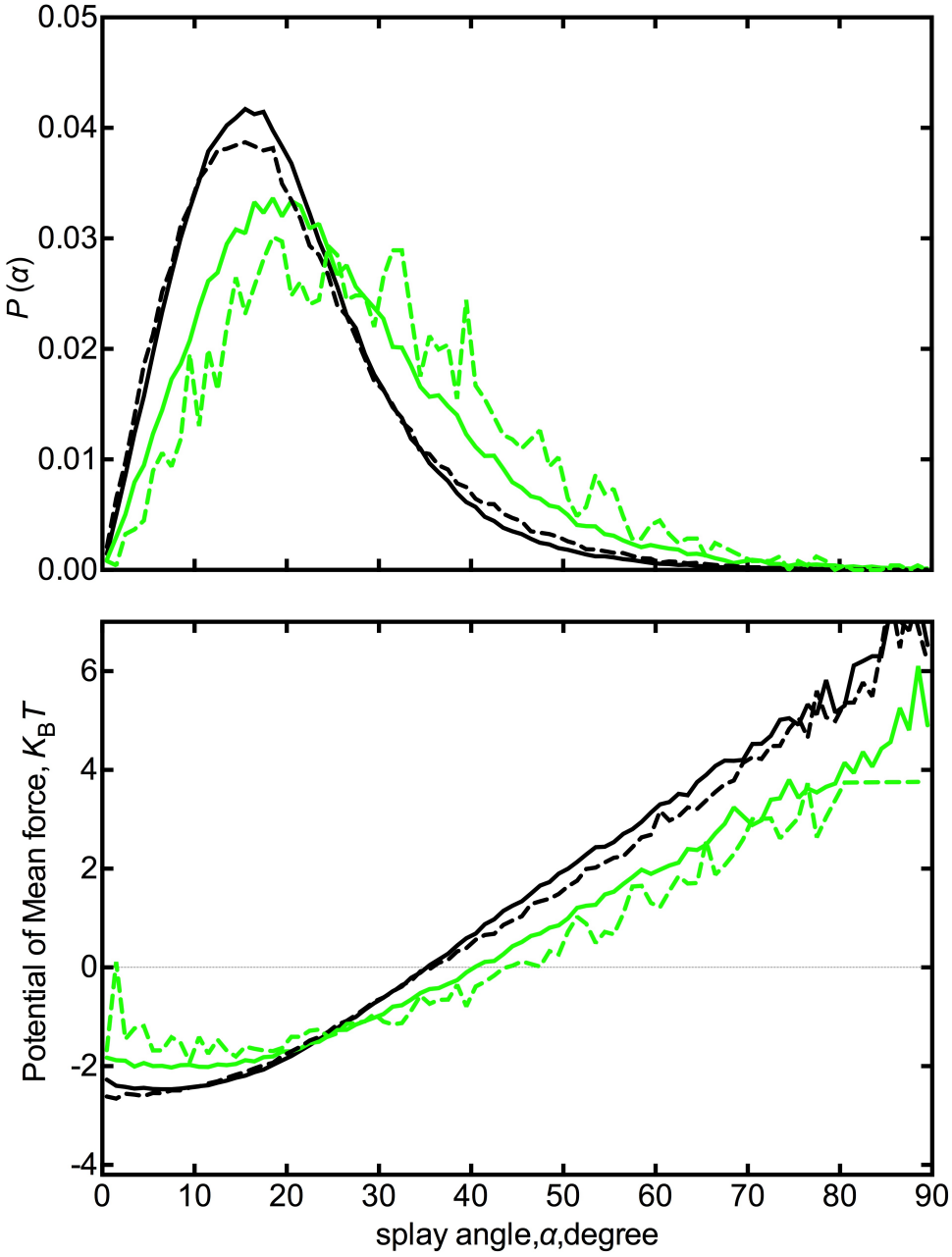

Figure 27 Quadratic fittings in the intervals of small angular range for splay moduli of the pair of DPPC and cholesterol

(Upper panel) the normalised probability density $P(\alpha)$ of finding a pair of DPPC/cholesterol (solid curves) and cholesterol/cholesterol (dashed curves) at an

angle α with respect to each other in DPPC bilayers at 10% (green), 40% (black) cholesterol concentrations. (Lower panel) the potential of mean forces (PMF (α)) for corresponding $P(\alpha)$ distributions shown in upper graphs.

As for the cholesterol-involved splay pairs, Figure 27 illustrates the examples of $P(\alpha)$ and PMF (α) for the cholesterol-involved splay pairs in 10% and 40% cholesterol systems. The $P(\alpha)$ distributions for Chol/Chol and DPPC/Chol (in Figure 27) are slightly wider than that for DPPC/DPPC. It is expected that cholesterol-involved splay pairs have wider angle distributions since cholesterol molecules are orientated not as aligned along bilayer normal as DPPC molecules are (in Figure 23).

It is noticeable in Figure 27 where curves for Chol/Chol splay pair in 10% cholesterol system are pretty zigzagging, indicating that the splay angles are not adequately sampled. The quality of the sampled data for $P(\alpha)$ and PMF (α) need be carefully examined to get reliable results of splay moduli. As it was discussed in method section, the sampling quality of cholesterol-cholesterol splay angles was found to be pretty poor in low cholesterol concentration systems (5%, 10%) due to the small amount of cholesterol molecules existing in these systems. Furthermore, the encounters of cholesterol/cholesterol splay pair in 5% and 10% bilayers only takes up very limited fraction, in comparison with those of DPPC pair and DPPC/cholesterol pair. Therefore, it is sensible to approximately estimate the overall bending moduli without considering the

contributions of the Chol/Chol pair in such systems.

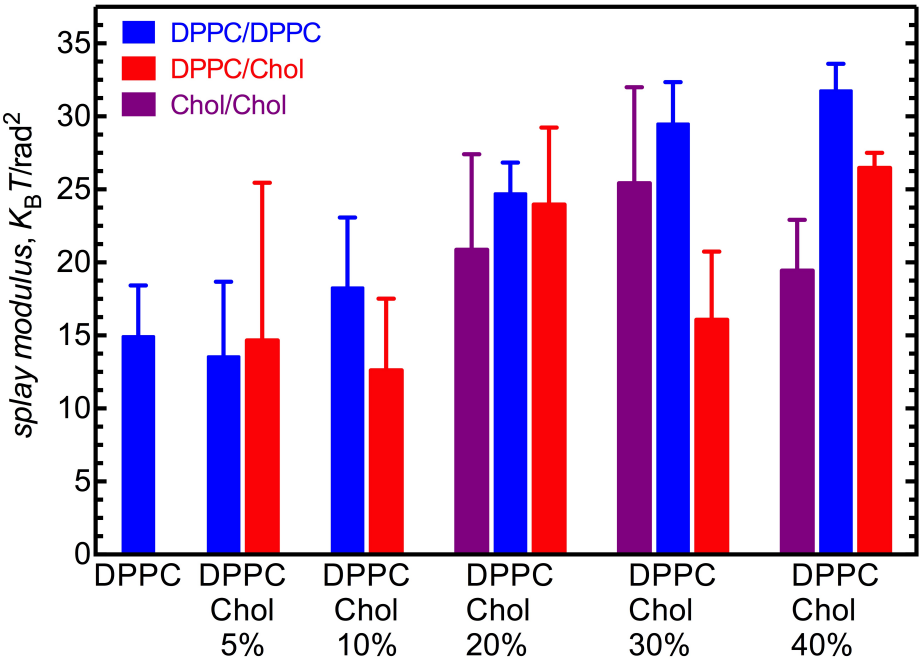

Figure 28 Splay moduli for all possible pairs.

DPPC/DPPC (blue), DPPC/cholesterol (red) and cholesterol/cholesterol (purple) in the corresponding DPPC bilayer systems containing 0%, 5%, 10%, 20%, 30% 40% cholesterol. Error bars present the standard deviations from similar fitting over [12°, 22°], [13°, 23°], and [14°, 24°] for 20%, 30% and 40% cholesterol systems, and [15°, 27°], [16°, 28°], [17°, 29°] and [18°, 30°] for pure DPPC, 5% and 10% cholesterol systems.

6.3.5 Cholesterol stiffens the DPPC bilayer

The values of splay moduli χ_{12} correspond to the coefficients of the quadratic fitting to PMF (α) in the interval of small splay angle. In all cases, the interval [15°, 30°] was used for fitting in 0%, 5% and 10% cholesterol systems, and the interval [12°, 24°] was used in the bilayer at high cholesterol concentrations 30%

and 40%. Those chosen intervals represent the best-sampled region in corresponding $P(\alpha)$, and remain within small angle ranges eligible for deriving splay modulus from quadratic fitted plots.

Figure 28 shows the calculated splay moduli χ_{12} for all possible splaying pairs in the simulated DPPC bilayers with and without cholesterol. As discussed above, splay moduli for cholesterol pair in 5% and 10% were not shown and not included in calculating the overall bending rigidities. Upon increasing cholesterol concentration, splay moduli of the DPPC pair were increased by a factor of 2, indicating substantial increase in the energy cost for splaying a DPPC molecule from the other one. Compared with previous investigations on the DOPC bilayer with cholesterol (Khelashvili et al., 2014), the DPPC splay moduli obtained in present study are in excellent agreement with their results. The splay moduli of DPPC obtained here are slightly higher by about $3\sim5$ in $K_{\mathrm{B}}T$ units than those of POPC pair at each available cholesterol concentration. The finding is consistent with the fact that POPC bilayer is more fluid-like at the same cholesterol concentration due to its mono-unsaturated hydrocarbon chain [(Pan et al., 2008, Pan et al., 2009, Khelashvili and Harries, 2013a).

It was found that the DPPC/DPPC pair in general has highest splay modulus among the three splay pairs at different concentrations, except for the 5% cholesterol bilayer. Moreover, the splay pair of DPPC molecules is the major

contributor to the overall bending rigidities due to the high probability of the DPPC/DPPC encounter in these bilayer systems. It was observed that the uncertainties in cholesterol-involved splay moduli are pretty large, which is probably because the orientation distributions of the cholesterol molecules are rather dispersing in the low cholesterol content system, while the splay moduli of DPPC/DPPC appear to be relatively reliable. These statistical errors can be attributed to the chosen fitting intervals and error estimation approach (Khelashvili et al., 2014). In previous simulation studies using different approaches, similar levels of the uncertainties were also observed (Khelashvili et al., 2013). Though there are noticeable errors in the present study, an increasing trend in splay moduli for each pair was observed in the systems with cholesterol concentration increasing, and also the obtained values are in reasonably agreement with the results from previous studies (Khelashvili and Harries, 2013a, Khelashvili et al., 2014).

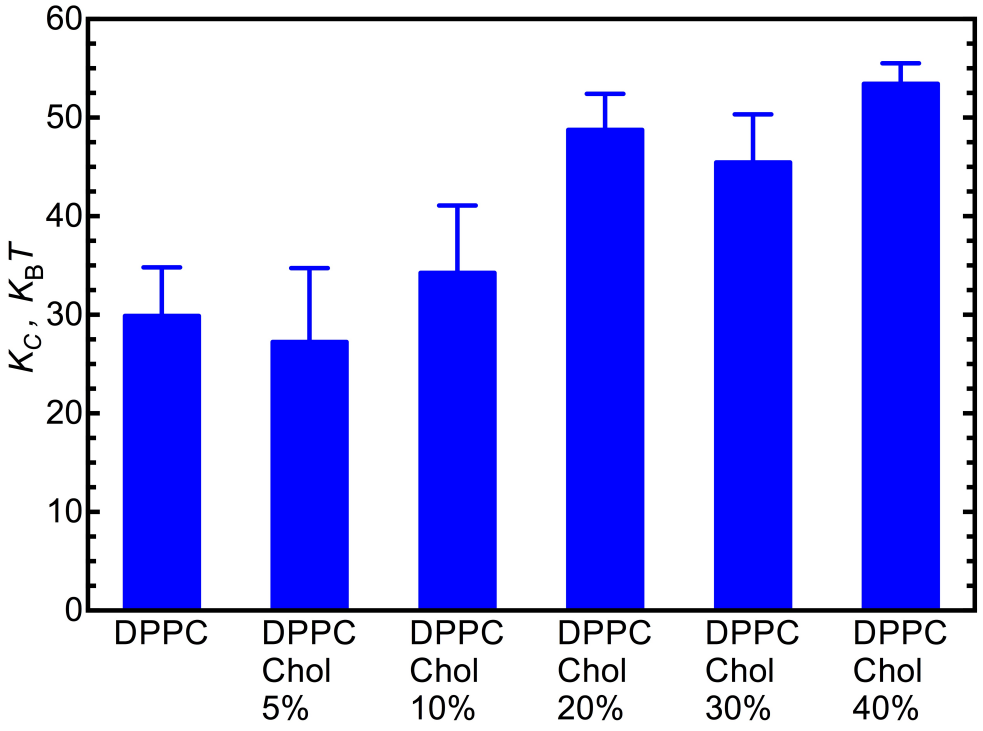

Figure 29 Bilayer bending rigidities K_C, for DPPC/cholesterol bilayers with cholesterol concentrations from 0% to 40%

Figure 29 shows the corresponding bending rigidity K_C in the simulated DPPC bilayers with or without cholesterol. The bending rigidities were calculated using equation (6.1) by weighing the contributions of each splay modulus, K_C for pure DPPC bilayer is about 30 K_BT, and then it increases substantially to 54 K_BT in the DPPC bilayer containing 40% cholesterol. The results indicate that the cholesterol substantially stiffens the DPPC bilayer by almost a factor of 2 with increasing cholesterol concentration from 0 to 40 %.

In comparison with experimental studies, since DPPC bilayer, whose transition temperature is about 41 ℃, is at gel-like state at room temperature, many of the

experiments were carried out at room temperature. It was reported in literature that the bending modulus of DPPC bilayer at room temperature is about 200 $K_{\mathrm{B}}T$ (Lee et al., 2001). In the same study, the DPPC bilayer was melted into fluid phase, and the corresponding the bending modulus was found to decrease by almost tenfold, hence it is roughly about 20~30 $K_{\mathrm{B}}T$. In addition to that, the elasticity of the fluid-like DPPC bilayer at 47.5 ℃ was reported to be about 34.6 $K_{\mathrm{B}}T$ (Heimburg, 1998). Overall, the obtained bending modulus for the pure DPPC bilayer is comparable with these compared experimental data.

As for the DPPC/cholesterol bilayer system, to my knowledge, relevant experimental data were not available in literature. But the experiment studies of the lipid bilayer composed of other lipid types were available for comparison. For instance, the X-ray scattering study of DMPC/Cholesterol bilayer were performed by Pan et al. (2009), and the bending rigidity for DMPC/cholesterol at 30% cholesterol was found to be increased by a factor of 4, reaching about 65 $K_{\mathrm{B}}T$. By comparing their data with the obtained results here, the stiffening effect of cholesterol on DMPC bilayer in experiment is noticeably stronger than that in current simulation study. However, I would argue that the difference in stiffening effect could be reasonably explained. As the transition temperature for pure DMPC bilayer is much lower than that for pure DPPC bilayer, the DPPC bilayer with cholesterol was simulated at constant 323 K, while the experiment of the DMPC system was performed at room temperature about 300K. Accordingly, it is

expected that the cholesterol is more dynamic at higher temperature than that at lower temperature. Therefore, it is reasonable to deduce that the more dynamic cholesterol may weaken its stiffening effect on the bending rigidity of the DPPC bilayer.

6.4 Summary

In summary, upon increasing cholesterol concentration, the molecules in the bilayer became more aligned with the bilayer normal, and then the average splay angles in each pair became smaller concomitantly. Moreover, it was found that splaying a pair of more aligned molecules cost more energy, so the corresponding splay modulus was increased at high cholesterol concentration. By weighing the contributions of the different splay pairs, the bending moduli of the all simulated bilayer were obtained, and the results showed that cholesterol stiffened the DPPC bilayer substantially.

Chapter 7 Discussion and future work

7.1 Cholesterol effects on DPPC bilayer

The obtained results from the project advance our knowledge of the effect of cholesterol on the DPPC phospholipid bilayer. Several concerned aspects of the bilayer property were investigated with the molecular dynamics simulation method, including the structural properties, the dynamics properties, the local lateral pressure profile and the mechanical properties of the lipid bilayer.

From study of the structural properties of the bilayers with and without cholesterol, the two most discussed condensing effect and ordering effect of cholesterol were observed in present study. The ordering effect of cholesterol was characterized with more ordered hydrocarbon chains of DPPC molecules, and the condensing effect was characterized with the decreased partial area occupied by individual DPPC molecule. Accordingly, the dynamical properties of the lipid molecules in the bilayer were affected by cholesterol. In presence of cholesterol, the lateral diffusion of DPPC was slowed. Moreover, it was found that the motion of cholesterol in the bilayer was special, since it could not only diffuse laterally but also undergo flip-flop motion across the two monolayers. Besides that, it was found that cholesterol had diverse effects on the intra-molecular dynamics for different parts of DPPC molecules. The enhanced dynamics of the

head groups of DPPC was observed, whereas the rotation dynamics of the backbone and tail region of DPPC was damped. The completely opposite effects of cholesterol seem to be closely related to its position in the DPPC bilayer.

The condensing effect and ordering effect of cholesterol can be closely associated with the lateral pressure profile across the bilayer. The lateral pressure profile of the pure DPPC bilayer showed both strong repulsive and attractive interactions in the hydrophilic region of the bilayer. Moreover, it is the huge attractive interaction in the membrane-water interfacial region that contributes to preventing the bilayer structure from falling apart, and accordingly, it is the most condensed region with highest electron density over the rest part of the bilayer. In presence of cholesterol, extra remarkable negative attractions were introduced in the region where cholesterol's ring structure is located, and the stronger repulsion occur at the bilayer centre. Furthermore, it was found that cholesterol barely influenced the local lateral pressure of the region where it couldn't physically assess. Therefore, it can be concluded that the condensing effect mostly relies on the interactions between the fused ring structure of cholesterol and the hydrocarbon chains of DPPC.

All of the mentioned findings above can be reasonably connected with the effect of cholesterol on the mechanical properties of the simulated bilayers. Taking advantages of the novel method by Khelashvili et al. (2013), the membrane

bending moduli of different bilayer systems were obtained from the local pairwise spaying fluctuations of the membrane components, and it was found that the DPPC bilayer was substantially stiffened in presence of cholesterol. Moreover, the increased bending rigidity is closely correlated with the ordering effect of cholesterol. Since the bending modulus is derived from the splay deformations between two molecules, the more ordered molecules tend to have a smaller splay angle with each other, and the energy for splaying the more-aligned pair is higher accordingly. In addition, the findings about the lipid dynamics suggest that cholesterol may increase the bending rigidity of the bilayer via enhancing the stiffness of region where cholesterol resides, because the head groups of DPPC became more dynamic with existence of cholesterol in bilayer system. The deduction is also consistent with the findings from the local lateral pressure.

7.2 The implications of the location of cholesterol

Based on the findings from current study, many of cholesterol effects on the DPPC bilayer are closely related to the vertical location of cholesterol ring structure. As it was found in the order parameter investigations in the Chapter 3, the carbon groups in upper segment of the tails became more ordered than those in lower part in presence of cholesterol. Actually, the hydroxyl group of cholesterol is located very close to the carbonyl groups of the chains, and the

ring structure corresponds to the segment of the tails near the glycerol backbone of DPPC. In addition, at the ring-located depth of bilayer, pronounced monotonic increase in electro density profile was observed, and huge attractive tendency were observed in the lateral pressure profile. Therefore, it can be concluded that the cholesterol-induced condensation probably occurs in the region below the membrane-water interface where the head groups of DPPC are located. The conclusion here is consistent with a recent simulation study by Alwarawrah et al. (2010), who suggested that the condensing effect of cholesterol was mostly resulted from the packing at the depth where the steroid ring was located.

From this point of view on the condensation location, the current study showed an excellent example on estimating the partitioned surface area for DPPC and cholesterol in binary bilayer. In present study, the Voronoi tessellation approach was used to estimate surface area partition for DPPC and cholesterol, respectively. However, as the Voronoi tessellation approach is strongly influenced by the positions of the selected key atoms and the number of atoms for each molecule, it's hard to find out a perfect strategy for choosing key atoms. In the previous study by Edholm and Nagle (2005), some improper settings for Voronoi tessellation method have been discussed. For instance, one typical form is using the centre of mass of each molecule to project and tessellate its area on plane, which has been explicitly criticised for over weighting the area of smaller molecules. In contrast, the present study considered three atoms in glycerol

group for DPPC, and three atoms for cholesterol are located almost at the same level. More importantly, the chosen atoms are mostly located in the effective region for the condensations led by cholesterol. In this way, the obtained partial areas for DPPC are directly associated the condensations in lipid bilayer, and the obtained areas for cholesterol mostly reflect the vertical location and the orientation of ring structure. Therefore, the chosen key atoms are appropriate for constructing Voronoi diagrams in present case of the DPPC bilayer with cholesterol, and the obtained the partial areas of DPPC and cholesterol have shown great consistency with the experimental data.

7.3 The implications of the orientation of cholesterol

Besides the important findings about cholesterol's location, a more interesting aspect of cholesterol, the orientation of cholesterol, was not explicitly discussed in present study. The orientation of cholesterol was often evaluated by the cholesterol tilt angle with respect to the bilayer normal. In fact, the cholesterol tilt is closely correlated with its vertical location in lipid bilayer. As it was discussed in the Chapter 6 that cholesterol molecules underwent transition from 'lying down' to 'standing up' in the lipid bilayer upon increasing cholesterol concentration. During the process, the vertical location of cholesterol was correlated with the increasing thickness, and the polar hydroxyl group migrated towards the water phase with a smaller tilt angle. Compared to the vertical

location, cholesterol tilt angle as a parameter is more convenient for quantitative comparison with results from other studies.

Recently, the importance of cholesterol tilt has been reviewed in literatures (Khelashvili et al., 2010b, Khelashvili et al., 2011, Khelashvili and Harries, 2013b, Khelashvili and Harries, 2013a), cholesterol tilt or sterol tilt has become an increasingly concerned parameter that correlates with the degrees of condensing effect and ordering effect of cholesterol on lipid bilayer (Aittoniemi et al., 2006, Olsen et al., 2009). Aittoniemi et al. (2006) first showed that a sterol with smaller tilt angle corresponds to a stronger ordering effect on the acyl chain of nearby lipids. In the recent study by Khelashvili et al. (2010b), the possible mechanism for the changes of cholesterol tilt with increasing cholesterol concentration has been explained by the interplay between the entropy, which is related to the tendency for cholesterol orienting randomly, and the energetically unfavourable interactions between cholesterol molecules. Based on the findings, they first built the connection between the mechanical properties of the lipid bilayer and cholesterol tilt, and then they proposed the method to calculate the bending rigidity of a multi-component lipid bilayer from the splaying fluctuations between any pair of the molecules in the bilayer (Khelashvili et al., 2013). In another recent study by de Joannis et al. (2011) , the importance of cholesterol tilt was studied in simulations of ternary mixtures containing saturated DPPC, unsaturated DOPC, and cholesterol, where cholesterol tilt was found correlated

with the relative affinity of DPPC and DOPC in cholesterol-rich domain, and higher affinity was observed in the interactions between DPPC and cholesterol. All in all, the importance of cholesterol tilt has been realized, so more concerns should be given in cholesterol-involved lipid bilayer research in future.

7.4 Force field issue for lipid bilayer simulation

Force field (FF) is determinant for simulation results, and the development of FF is a particularly dynamic topic for MD simulation studies (Monticelli and Tieleman, 2013, Antila and Salonen, 2013, Rog and Vattulainen, 2014). The recently optimized force field CHARMM (version 36) for DPPC and cholesterol (Lim et al., 2012, Klauda et al., 2012, Klauda et al., 2010) were used in present simulations, and the obtained results showed reasonable agreement with experimental data in most cases. Compared with earlier simulation studies using other force fields, the CHARMM36 produced more reasonable results. In addition, the parameters sets for other lipid types for lipid bilayer research were also available with proper modification as well, such as raft-forming lipid sphingomeylin, which is actively involved of forming raft-like domains. The parameterisation of the CHARMM force field was based on computationally demanding high-level quantum-mechanical calculations, and the resultant force field was validated against experimental NMR data (Klauda et al., 2004).

In terms of the force field for cholesterol, most atomistic simulations of cholesterol-containing lipids bilayer have used the default parameters for given atom types in cholesterol molecule. This simple approach has shown reasonable results with the Slipids force field, with the order parameter data of acyl chains consistent with experimental observations (Jambeck and Lyubartsev, 2013, Rog and Vattulainen, 2014). However, in combination of the popular Berger lipids force fields (Hofsass et al., 2003, Berger et al., 1997), the cholesterol model described with the GROMOS force field is reasonable to reproduce comparable order parameters of hydrocarbon chains and the short chain of cholesterol at small cholesterol concentrations, to overestimate the cholesterol-led condensation level at higher concentrations (over 30 mol%) (Rog et al., 2009, Ferreira et al., 2013, Rog and Vattulainen, 2014). Moreover, another study by Tieleman et al. (2006), suggested that the interactions between Berger lipids' tails and peptides, which were parameterised with the GROMOS force field, resulted in overestimated membrane condensations. The two cases suggested the incompatibility in the widely used combination between the Berger lipids and GROMOS force field. By contrast, the parameters for cholesterol in present study were thoroughly re-parameterized for the CHARMM force field C36(Lim et al., 2012). As to validation of the model, the updated parameters were validated in a series of simulations of a mixture of heptane representing the hydrocarbon chain and decalin representing the first two rings of cholesterol, and the obtained molar volumes were found to be reasonably consistent with

experimental data. The findings suggested sufficient accuracy of the non-bonded parameters in the model though small deviations between simulation and experimental data were observed.

Back to the present study of the DPPC bilayer with cholesterol in framework of CHARMM force field (Klauda et al., 2004, Klauda et al., 2010, Lim et al., 2012, Klauda et al., 2012), the obtained results showed better consistency than many existing cholesterol-related bilayer simulation studies. For instance, the ordering and condensing effects of cholesterol on lipid membrane were found with more reasonable degree of condensation than previous simulations (Chiu et al., 2002, Hofsass et al., 2003, Ollila et al., 2007a, Ollila et al., 2007b). As for the cholesterol effect on lipid lateral diffusion, the calculated diffusion coefficients here are more comparable with NMR experimental data (Lindblom et al., 2006, Ollila et al., 2007b) than those found in the study by Falck et al. (2004). Moreover, the obtained lateral pressure across the lipid bilayer showed relatively explainable profiles over the findings from simulation work by Patra (2005). Overall, the current simulations with the latest released CHARMM force field for lipid and cholesterol produced comparable results with experimental data, and the obtained data here have shown to be more reasonable than previous simulation studies using other popular force fields.

7.5 Conclusion and future work

The aim of the project has been achieved, as cholesterol effects on the DPPC bilayer have been systematically studied in present study. Despite that the cholesterol effect has been studied extensively in earlier experiments and simulations for the past decades, the current simulation study further advances our understanding on the effects of cholesterol on several aspects of bilayer properties. The obtained results here provided evidences for the most distinctive condensing effect of cholesterol on lipid bilayer from different concerned aspects, and built connections between cholesterol condensing effect and its remarkable effects on other aspects, such as lipid dynamics, lateral pressure, and mechanical properties of the membrane. Moreover, the findings highlighted the importance of cholesterol tilt in influencing the properties of the lipid bilayer. Besides the findings of the cholesterol effects, the present work also filled the gap for the cholesterol-containing lipid bilayer simulation study using the latest CHARMM36 force field (Klauda et al., 2010, Lim et al., 2012), and the findings here have suggested that simulations with CHARMM36 can produce relatively reliable results as complementary information for lipid bilayer research in experiments.

Future work can be concerned with more complex lipid bilayers with cholesterol and larger in size of the membrane systems, since the real biological membranes are composed of a complex mixture of numerous lipid species (Niemela et al.,

2009). In a recent study, it was found that thousands of lipid species existed in a single sample of adipose tissue (Pietilainen et al., 2011). Huge diversity of lipids arises from variations in polar head groups, length and degree of saturation in the hydrocarbon chains. Obviously, it is not possible to reproduce the diversity of lipids in a real biological membrane, but generally a proper mixture of cholesterol, saturated and unsaturated lipids is representative to cover most lipid species properties. In model membranes, the behaviour of this lipid mixture is well characterized (Almeida, 2009) Moreover, it is known that cholesterol can separate saturated lipids into a liquid-ordered (L_o) phase by forming a relatively stable complex, which was often referred as lipid rafts, whereas the unsaturated lipids segregate into a liquid-disordered (L_d) phase (Rheinstädter and Mouritsen, 2013). In simulations, evidences from coarse-grained simulations of a ternary mixture have shown that cholesterol is preferentially interacted with long saturated lipid types over polyunsaturated lipids. Typically, unsaturated lipid bilayer is characterized by a lower transition temperature, and addition of unsaturated lipids into bilayer mixture with cholesterol was found to increase the fluidity of the membrane (Ollila et al., 2007b). Furthermore, it was found that the orientation of cholesterol in saturated DMPC bilayer occurred different from its orientation in polyunsaturated lipids (Kucerka et al., 2010). From the point of view of raft-like domain, the atomistic simulations with ternary or higher lipid mixture are very interesting and they may potentially shed light on the underpinnings for forming raft-like domain in future.

In addition, the cholesterol has been suggested to be involved of modulating the properties of membrane proteins via direct and indirect approach. The indirect effect of cholesterol on properties is mainly associated with the changes of the membrane properties. The membrane thickness is involved of hydrophobic matching with trans-membrane properties, and the lateral pressure profile is correlated with the elasticity of the membrane. In addition, the dynamics property of membrane is engaged to the lifetime of functional complexes formed by lipids and proteins. Aside from the indirect effect, the functions of the properties are also affected by the direct interactions between cholesterol and proteins' functional units. In many cases, there is no distinguished boundary between direct and indirect cholesterol effects, and it is hard to determine which effect is main contributing factor for the altered protein conformation and function. As it was found that cholesterol effects mostly occurred in the hydrophobic region where the ring structure is located, the future work may focus on the hydrophobic matching between proteins and lipids. It is reasonable to start with simulations of the relatively simpler peptides embedded in the cholesterol-containing lipid bilayer, and then move to more complicated interactions with proteins. In future work, the cholesterol tilt parameter, which is potentially indicative for protein functions, should be highly concerned with respect to the changes of the proteins conformation.

Reference

Aittoniemi, J., Rog, T., Niemela, P., Pasenkiewicz-Gierula, M., Karttunen, M. and Vattulainen, I. (2006) 'Tilt: major factor in sterols' ordering capability in membranes', *J Phys Chem B,* 110(51), pp. 25562-4.

Allen, J. A., Halverson-Tamboli, R. A. and Rasenick, M. M. (2007) 'Lipid raft microdomains and neurotransmitter signalling', *Nature Reviews Neuroscience,* 8(2), pp. 128-140.

Almeida, P. F. F. (2009) 'Thermodynamics of lipid interactions in complex bilayers', *Biochimica Et Biophysica Acta-Biomembranes,* 1788(1), pp. 72-85.

Almeida, P. F. F., Vaz, W. L. C. and Thompson, T. E. (1992) 'LATERAL DIFFUSION IN THE LIQUID-PHASES OF DIMYRISTOYLPHOSPHATIDYLCHOLINE CHOLESTEROL LIPID BILAYERS - A FREE-VOLUME ANALYSIS', *Biochemistry,* 31(29), pp. 6739-6747.

Alwarawrah, M., Dai, J. and Huang, J. (2010) 'A molecular view of the cholesterol condensing effect in DOPC lipid bilayers', *J Phys Chem B,* 114(22), pp. 7516-23.

Andersen, H. C. (1983) 'RATTLE - A VELOCITY VERSION OF THE SHAKE ALGORITHM FOR MOLECULAR-DYNAMICS CALCULATIONS', *Journal of Computational Physics,* 52(1), pp. 24-34.

Andersen, O. S. and Koeppe, R. E., II (2007) 'Bilayer thickness and membrane protein function: An energetic perspective', *Annual Review of Biophysics and Biomolecular Structure Annual Review of Biophysics*, pp. 107-130.

Antila, H. S. and Salonen, E. (2013) 'Polarizable force fields', *Methods Mol Biol,* 924, pp. 215-41.

Baran, M. and Mazerski, J. (2002) 'Molecular modelling of membrane sterols with the use of the GROMOS 96 force field', *Chemistry and Physics of Lipids,* 120(1-2), pp. 21-31.

Bennett, W. F. D., MacCallum, J. L., Hinner, M. J., Marrink, S. J. and Tieleman, D. P. (2009) 'Molecular View of Cholesterol Flip-Flop and Chemical Potential in Different Membrane Environments', *Journal of the American Chemical Society,* 131(35), pp. 12714-12720.

Bennett, W. F. D. and Tieleman, D. P. (2013) 'Computer simulations of lipid membrane domains', *Biochimica Et Biophysica Acta-Biomembranes,* 1828(8), pp. 1765-1776.

Berendsen, H. J. C., Postma, J. P. M., Vangunsteren, W. F., Dinola, A. and Haak, J. R. (1984) 'MOLECULAR-DYNAMICS WITH COUPLING TO AN EXTERNAL BATH', *Journal of Chemical Physics,* 81(8), pp. 3684-3690.

Berger, O., Edholm, O. and Jahnig, F. (1997) 'Molecular dynamics simulations of a fluid bilayer of dipalmitoylphosphatidylcholine at full hydration, constant pressure, and constant temperature', *Biophys J,* 72(5), pp. 2002-13.

Berkowitz, M. L. (2009) 'Detailed molecular dynamics simulations of model

biological membranes containing cholesterol', *Biochim Biophys Acta,* 1788(1), pp. 86-96.

Bloom, M., Evans, E. and Mouritsen, O. G. (1991) 'Physical properties of the fluid lipid-bilayer component of cell membranes: a perspective', *Q Rev Biophys,* 24(3), pp. 293-397.

Brandt, E. G., Braun, A. R., Sachs, J. N., Nagle, J. F. and Edholm, O. (2011) 'Interpretation of fluctuation spectra in lipid bilayer simulations', *Biophys J,* 100(9), pp. 2104-11.

Brzozowska, I. and Figaszewski, Z. A. (2002) 'The equilibrium of phosphatidylcholine-cholesterol in monolayers at the air/water interface', *Colloids and Surfaces B-Biointerfaces,* 23(1), pp. 51-58.

Bucciantini, M., Rigacci, S. and Stefani, M. (2014) 'Amyloid Aggregation: Role of Biological Membranes and the Aggregate-Membrane System', *Journal of Physical Chemistry Letters,* 5(3), pp. 517-527.

Cantor, R. S. (1997) 'The lateral pressure profile in membranes: A physical mechanism of general anesthesia', *Biochemistry,* 36(9), pp. 2339-2344.

Cantor, R. S. (1999a) 'The influence of membrane lateral pressures on simple geometric models of protein conformational equilibria', *Chemistry and Physics of Lipids,* 101(1), pp. 45-56.

Cantor, R. S. (1999b) 'Lipid composition and the lateral pressure profile in bilayers', *Biophys J,* 76(5), pp. 2625-39.

Carrillo-Tripp, M. and Feller, S. E. (2005) 'Evidence for a mechanism by which

omega-3 polyunsaturated lipids may affect membrane protein function', *Biochemistry,* 44(30), pp. 10164-10169.

Chaikin, P. M. and Lubensky, T. C. (2000) *Principles of Condensed Matter Physics.* Cambridge,UK: Cambridge University Press.

Chiu, S. W., Jakobsson, E., Mashl, R. J. and Scott, H. L. (2002) 'Cholesterol-induced modifications in lipid bilayers: a simulation study', *Biophys J,* 83(4), pp. 1842-53.

Chiu, S. W., Vasudevan, S., Jakobsson, E., Mashl, R. J. and Scott, H. L. (2003) 'Structure of sphingomyelin bilayers: A simulation study', *Biophysical Journal,* 85(6), pp. 3624-3635.

Clarke, R. J. (2001) 'The dipole potential of phospholipid membranes and methods for its detection', *Advances in Colloid and Interface Science,* 89, pp. 263-281.

Darden, T., York, D. and Pedersen, L. (1993) 'PARTICLE MESH EWALD - AN N.LOG(N) METHOD FOR EWALD SUMS IN LARGE SYSTEMS', *Journal of Chemical Physics,* 98(12), pp. 10089-10092.

David W. Ball, J. W. H., Rhonda J. Scott (2011) *The Basics of General, Organic, and Biological Chemistry.* Irvington, NY: Flat World Knowledge.

de Gennes, P. and Prost, J. (1993) *The physics of liquid crystals.* Oxford: Clarendon Press.

de Joannis, J., Coppock, P. S., Yin, F., Mori, M., Zamorano, A. and Kindt, J. T. (2011) 'Atomistic simulation of cholesterol effects on miscibility of saturated and

unsaturated phospholipids: implications for liquid-ordered/liquid-disordered phase coexistence', *J Am Chem Soc,* 133(10), pp. 3625-34.

deKruijff, B. (1997) 'Biomembranes - Lipids beyond the bilayer', *Nature,* 386(6621), pp. 129-130.

Deserno, M. and Holm, C. (1998) 'How to mesh up Ewald sums. I. A theoretical and numerical comparison of various particle mesh routines', *Journal of Chemical Physics,* 109(18), pp. 7678-7693.

Dickson, C. J., Madej, B. D., Skjevik, A. A., Betz, R. M., Teigen, K., Gould, I. R. and Walker, R. C. (2014) 'Lipid14: The Amber Lipid Force Field', *Journal of Chemical Theory and Computation,* 10(2), pp. 865-879.

Durrant, J. D. and McCammon, J. A. (2011) 'Molecular dynamics simulations and drug discovery', *Bmc Biology,* 9.

Eckenhoff, R. G. (2001) 'Promiscuous ligands and attractive cavities: how do the inhaled anesthetics work?', *Mol Interv,* 1(5), pp. 258-68.

Edholm, O. and Nagle, J. F. (2005) 'Areas of molecules in membranes consisting of mixtures', *Biophys J,* 89(3), pp. 1827-32.

Eeman, M. and Deleu, M. (2010) 'From biological membranes to biomimetic model membranes', *Biotechnologie Agronomie Societe Et Environnement,* 14(4), pp. 719-736.

Elson, E. L., Fried, E., Dolbow, J. E. and Genin, G. M. (2010) 'Phase Separation in Biological Membranes: Integration of Theory and Experiment', in Rees,

D.C., Dill, K.A. & Williamson, J.R. (eds.) *Annual Review of Biophysics, Vol 39 Annual Review of Biophysics*, pp. 207-226.

Essmann, U., Perera, L., Berkowitz, M. L., Darden, T., Lee, H. and Pedersen, L. G. (1995) 'A SMOOTH PARTICLE MESH EWALD METHOD', *Journal of Chemical Physics,* 103(19), pp. 8577-8593.

Falck, E., Patra, M., Karttunen, M., Hyvonen, M. T. and Vattulainen, I. (2004) 'Lessons of slicing membranes: Interplay of packing, free area, and lateral diffusion in phospholipid/cholesterol bilayers', *Biophysical Journal,* 87(2), pp. 1076-1091.

Ferreira, T. M., Coreta-Gomes, F., Ollila, O. H., Moreno, M. J., Vaz, W. L. and Topgaard, D. (2013) 'Cholesterol and POPC segmental order parameters in lipid membranes: solid state 1H-13C NMR and MD simulation studies', *Phys Chem Chem Phys,* 15(6), pp. 1976-89.

Fosnaric, M., Iglic, A. and May, S. (2006) 'Influence of rigid inclusions on the bending elasticity of a lipid membrane', *Physical Review E,* 74(5).

Gallova, J., Uhrikova, D., Islamov, A., Kuklin, A. and Balgavy, P. (2004) 'Effect of cholesterol on the bilayer thickness in unilamellar extruded DLPC and DOPC liposomes: SANS contrast variation study', *General Physiology and Biophysics,* 23(1), pp. 113-128.

Goetz, R., Gompper, G. and Lipowsky, R. (1999) 'Mobility and elasticity of self-assembled membranes', *Physical Review Letters,* 82(1), pp. 221-224.

Goetz, R. and Lipowsky, R. (1998) 'Computer simulations of bilayer membranes:

Self-assembly and interfacial tension', *Journal of Chemical Physics,* 108(17), pp. 7397-7409.

Grouleff, J., Irudayam, S. J., Skeby, K. K. and Schiott, B. (2015) 'The influence of cholesterol on membrane protein structure, function, and dynamics studied by molecular dynamics simulations', *Biochimica Et Biophysica Acta-Biomembranes,* 1848(9), pp. 1783-1795.

Gullingsrud, J. and Schulten, K. (2004) 'Lipid bilayer pressure profiles and mechanosensitive channel gating', *Biophys J,* 86(6), pp. 3496-509.

Heimburg, T. (1998) 'Mechanical aspects of membrane thermodynamics. Estimation of the mechanical properties of lipid membranes close to the chain melting transition from calorimetry', *Biochimica Et Biophysica Acta-Biomembranes,* 1415(1), pp. 147-162.

Helfrich, W. (1973) 'ELASTIC PROPERTIES OF LIPID BILAYERS - THEORY AND POSSIBLE EXPERIMENTS', *Zeitschrift Fur Naturforschung C-a Journal of Biosciences,* C 28(11-1), pp. 693-703.

Hockney, R. W. and Eastwood, J. W. (1988) *Computer Simulation Using Particles.*

Hofsass, C., Lindahl, E. and Edholm, O. (2003) 'Molecular dynamics simulations of phospholipid bilayers with cholesterol', *Biophys J,* 84(4), pp. 2192-206.

Hoover, W. G. (1985) 'CANONICAL DYNAMICS - EQUILIBRIUM PHASE-SPACE DISTRIBUTIONS', *Physical Review A,* 31(3), pp. 1695-1697.

Hyslop, P. A., Morel, B. and Sauerheber, R. D. (1990) 'ORGANIZATION AND INTERACTION OF CHOLESTEROL AND PHOSPHATIDYLCHOLINE IN

MODEL BILAYER-MEMBRANES', *Biochemistry,* 29(4), pp. 1025-1038.

Israelachvili, J. N., Marcelja, S. and Horn, R. G. (1980) 'Physical principles of membrane organization', *Quarterly Reviews of Biophysics,* 13(2), pp. 121-200.

Jambeck, J. P. M. and Lyubartsev, A. P. (2013) 'Another Piece of the Membrane Puzzle: Extending Slipids Further', *Journal of Chemical Theory and Computation,* 9(1), pp. 774-784.

Jensen, M. O., Mouritsen, O. G. and Peters, G. H. (2001) 'Dipolar and chain-linking effects on the rheology of grafted chains in a nanopore under shear at different grafting densities', *Physical Review E,* 64(1).

Karplus, M. and McCammon, J. A. (2002) 'Molecular dynamics simulations of biomolecules', *Nature Structural Biology,* 9(9), pp. 646-652.

Kessel, A., Ben-Tal, N. and May, S. (2001) 'Interactions of cholesterol with lipid bilayers: The preferred configuration and fluctuations', *Biophysical Journal,* 81(2), pp. 643-658.

Khelashvili, G. and Harries, D. (2013a) 'How cholesterol tilt modulates the mechanical properties of saturated and unsaturated lipid membranes', *J Phys Chem B,* 117(8), pp. 2411-21.

Khelashvili, G. and Harries, D. (2013b) 'How sterol tilt regulates properties and organization of lipid membranes and membrane insertions', *Chem Phys Lipids,* 169, pp. 113-23.

Khelashvili, G., Johner, N., Zhao, G., Harries, D. and Scott, H. L. (2014) 'Molecular

origins of bending rigidity in lipids with isolated and conjugated double bonds: The effect of cholesterol', *Chemistry and Physics of Lipids,* 178, pp. 18-26.

Khelashvili, G., Kollmitzer, B., Heftberger, P., Pabst, G. and Harries, D. (2013) 'Calculating the Bending Modulus for Multicomponent Lipid Membranes in Different Thermodynamic Phases', *J Chem Theory Comput,* 9(9), pp. 3866-3871.

Khelashvili, G., Mondal, S., Andersen, O. S. and Weinstein, H. (2010a) 'Cholesterol Modulates the Membrane Effects and Spatial Organization of Membrane-Penetrating Ligands for G-Protein Coupled Receptors', *Journal of Physical Chemistry B,* 114(37), pp. 12046-12057.

Khelashvili, G., Pabst, G. and Harries, D. (2010b) 'Cholesterol Orientation and Tilt Modulus in DMPC Bilayers', *Journal of Physical Chemistry B,* 114(22), pp. 7524-7534.

Khelashvili, G., Rappolt, M., Chiu, S. W., Pabst, G. and Harries, D. (2011) 'Impact of sterol tilt on membrane bending rigidity in cholesterol and 7DHC-containing DMPC membranes', *Soft Matter,* 7(21), pp. 10299-10312.

Khelashvili, G. A., Pandit, S. A. and Scott, H. L. (2005) 'Self-consistent mean-field model based on molecular dynamics: Application to lipid-cholesterol bilayers', *Journal of Chemical Physics,* 123(3).

Klauda, J. B., Garrison, S. L., Jiang, J. W., Arora, G. and Sandler, S. I. (2004) 'HM-IE:

Quantum chemical hybrid methods for calculating interaction energies', *Journal of Physical Chemistry A,* 108(1), pp. 107-112.

Klauda, J. B., Monje, V., Kim, T. and Im, W. (2012) 'Improving the CHARMM force field for polyunsaturated fatty acid chains', *J Phys Chem B,* 116(31), pp. 9424-31.

Klauda, J. B., Venable, R. M., Freites, J. A., O'Connor, J. W., Tobias, D. J., Mondragon-Ramirez, C., Vorobyov, I., MacKerell, A. D., Jr. and Pastor, R. W. (2010) 'Update of the CHARMM all-atom additive force field for lipids: validation on six lipid types', *J Phys Chem B,* 114(23), pp. 7830-43.

Korade, Z. and Kenworthy, A. K. (2008) 'Lipid rafts, cholesterol, and the brain', *Neuropharmacology,* 55(8), pp. 1265-1273.

Kozlovsky, Y. and Kozlov, M. M. (2002) 'Stalk model of membrane fusion: Solution of energy crisis', *Biophysical Journal,* 82(2), pp. 882-895.

Kucerka, N., Marquardt, D., Harroun, T. A., Nieh, M. P., Wassall, S. R., de Jong, D. H., Schafer, L. V., Marrink, S. J. and Katsaras, J. (2010) 'Cholesterol in bilayers with PUFA chains: doping with DMPC or POPC results in sterol reorientation and membrane-domain formation', *Biochemistry,* 49(35), pp. 7485-93.

Kucerka, N., Nieh, M.-P. and Katsaras, J. (2011) 'Fluid phase lipid areas and bilayer thicknesses of commonly used phosphatidylcholines as a function of temperature', *Biochimica Et Biophysica Acta-Biomembranes,* 1808(11), pp. 2761-2771.

Kupiainen, M., Falck, E., Ollila, S., Niemela, P., Gurtovenko, A. A., Hyvonen, M. T., Patra, M., Karttunen, M. and Vattulainen, I. (2005) 'Free volume properties of sphingomyelin, DMPC, DPPC, and PLPC bilayers', *Journal of Computational and Theoretical Nanoscience,* 2(3), pp. 401-413.

LAMMPS website. Available at: http://lammps.sandia.gov.

Lee, C. H., Lin, W. C. and Wang, J. P. (2001) 'All-optical measurements of the bending rigidity of lipid-vesicle membranes across structural phase transitions', *Physical Review E,* 64(2), pp. 4.

Lim, J. B., Rogaski, B. and Klauda, J. B. (2012) 'Update of the cholesterol force field parameters in CHARMM', *J Phys Chem B,* 116(1), pp. 203-10.

Lindahl, E. and Edholm, O. (2000a) 'Mesoscopic undulations and thickness fluctuations in lipid bilayers from molecular dynamics simulations', *Biophysical Journal,* 79(1), pp. 426-433.

Lindahl, E. and Edholm, O. (2000b) 'Spatial and energetic-entropic decomposition of surface tension in lipid bilayers from molecular dynamics simulations', *Journal of Chemical Physics,* 113(9), pp. 3882-3893.

Lindblom, G. and Oradd, G. (2009) 'Lipid lateral diffusion and membrane heterogeneity', *Biochimica Et Biophysica Acta-Biomembranes,* 1788(1), pp. 234-244.

Lindblom, G., Oradd, G. and Filippov, A. (2006) 'Lipid lateral diffusion in bilayers with phosphatidylcholine, sphingomyelin and cholesterol - An NMR study

of dynamics and lateral phase separation', *Chemistry and Physics of Lipids,* 141(1-2), pp. 179-184.

Lukat, G., Krueger, J. and Sommer, B. (2013) 'APL@Voro: A Voronoi-Based Membrane Analysis Tool for GROMACS Trajectories', *Journal of Chemical Information and Modeling,* 53(11), pp. 2908-2925.

Marsh, D. (1996) 'Lateral pressure in membranes', *Biochimica Et Biophysica Acta-Reviews on Biomembranes,* 1286(3), pp. 183-223.

Marsh, D. (2002) 'Membrane water-penetration profiles from spin labels', *European Biophysics Journal with Biophysics Letters,* 31(7), pp. 559-562.

Marsh, D. (2007) 'Lateral pressure profile, spontaneous curvature frustration, and the incorporation and conformation of proteins in membranes', *Biophysical Journal,* 93(11), pp. 3884-3899.

Marsh, D. (2009) 'Cholesterol-induced fluid membrane domains: A compendium of lipid-raft ternary phase diagrams', *Biochimica Et Biophysica Acta-Biomembranes,* 1788(10), pp. 2114-2123.

Marsh, D. and Smith, I. C. P. (1973) 'INTERACTING SPIN LABEL STUDY OF FLUIDIZING AND CONDENSING EFFECTS OF CHOLESTEROL ON LECITHIN BILAYERS', *Biochimica Et Biophysica Acta,* 298(2), pp. 133-144.

Martinez, L., Andrade, R., Birgin, E. G. and Martinez, J. M. (2009) 'PACKMOL: A Package for Building Initial Configurations for Molecular Dynamics Simulations', *Journal of Computational Chemistry,* 30(13), pp. 2157-2164.

May, S., Kozlovsky, Y., Ben-Shaul, A. and Kozlov, M. M. (2004) 'Tilt modulus of a

lipid monolayer', *European Physical Journal E,* 14(3), pp. 299-308.

McIntosh, T. J. (1978) 'EFFECT OF CHOLESTEROL ON STRUCTURE OF PHOSPHATIDYLCHOLINE BILAYERS', *Biochimica Et Biophysica Acta,* 513(1), pp. 43-58.

McIntosh, T. J., Magid, A. D. and Simon, S. A. (1989) 'CHOLESTEROL MODIFIES THE SHORT-RANGE REPULSIVE INTERACTIONS BETWEEN PHOSPHATIDYLCHOLINE MEMBRANES', *Biochemistry,* 28(1), pp. 17-25.

McIntosh, T. J. and Simon, S. A. (2006) 'Roles of bilayer material properties in function and distribution of membrane proteins', *Annual Review of Biophysics and Biomolecular Structure Annual Review of Biophysics*, pp. 177-198.

Monticelli, L. and Tieleman, D. P. (2013) 'Force fields for classical molecular dynamics', *Methods Mol Biol,* 924, pp. 197-213.

Mouritsen, O. G. and Zuckermann, M. J. (2004) 'What's so special about cholesterol?', *Lipids,* 39(11), pp. 1101-1113.

Nagle, J. F. and Tristram-Nagle, S. (2000) 'Structure of lipid bilayers', *Biochimica Et Biophysica Acta-Reviews on Biomembranes,* 1469(3), pp. 159-195.

Niemela, P. S., Castillo, S., Sysi-Aho, M. and Oresic, M. (2009) 'Bioinformatics and computational methods for lipidomics', *Journal of Chromatography B-Analytical Technologies in the Biomedical and Life Sciences,* 877(26), pp. 2855-2862.

Nose, S. and Klein, M. L. (1983) 'CONSTANT PRESSURE MOLECULAR-DYNAMICS

FOR MOLECULAR-SYSTEMS', *Molecular Physics,* 50(5), pp. 1055-1076.

Ohvo-Rekila, H., Ramstedt, B., Leppimaki, P. and Slotte, J. P. (2002) 'Cholesterol interactions with phospholipids in membranes', *Prog Lipid Res,* 41(1), pp. 66-97.

Ollila, O. H. S., Rog, T., Karttunen, M. and Vattulainen, I. (2007a) 'Role of sterol type on lateral pressure profiles of lipid membranes affecting membrane protein functionality: Comparison between cholesterol, desmosterol, 7-dehydrocholesterol and ketosterol', *Journal of Structural Biology,* 159(2), pp. 311-323.

Ollila, S., Hyvonen, M. T. and Vattulainen, I. (2007b) 'Polyunsaturation in lipid membranes: Dynamic properties and lateral pressure profiles', *Journal of Physical Chemistry B,* 111(12), pp. 3139-3150.

Olsen, B. N., Schlesinger, P. H. and Baker, N. A. (2009) 'Perturbations of membrane structure by cholesterol and cholesterol derivatives are determined by sterol orientation', *J Am Chem Soc,* 131(13), pp. 4854-65.

Orsi, M. and Essex, J. W. (2013) 'Physical properties of mixed bilayers containing lamellar and nonlamellar lipids: insights from coarse-grain molecular dynamics simulations', *Faraday Discussions,* 161, pp. 249-272.

Paila, Y. D. and Chattopadhyay, A. (2010) 'Membrane cholesterol in the function and organization of G-protein coupled receptors', *Sub-cellular biochemistry,* 51, pp. 439-66.

Pan, J., Mills, T. T., Tristram-Nagle, S. and Nagle, J. F. (2008) 'Cholesterol perturbs

lipid bilayers nonuniversally', *Physical Review Letters,* 100(19).

Pan, J., Tristram-Nagle, S. and Nagle, J. F. (2009) 'Effect of cholesterol on structural and mechanical properties of membranes depends on lipid chain saturation', *Physical Review E,* 80(2).

Pare, C. and Lafleur, M. (1998) 'Polymorphism of POPE/cholesterol system: A H-2 nuclear magnetic resonance and infrared spectroscopic investigation', *Biophysical Journal,* 74(2), pp. 899-909.

Patra, M. (2005) 'Lateral pressure profiles in cholesterol-DPPC bilayers', *Eur Biophys J,* 35(1), pp. 79-88.

Patra, M., Karttunen, M., Hyvonen, M. T., Falck, E. and Vattulainen, I. (2004) 'Lipid bilayers driven to a wrong lane in molecular dynamics simulations by subtle changes in long-range electrostatic interactions', *Journal of Physical Chemistry B,* 108(14), pp. 4485-4494.

Petrache, H. I., Dodd, S. W. and Brown, M. F. (2000) 'Area per lipid and acyl length distributions in fluid phosphatidylcholines determined by H-2 NMR spectroscopy', *Biophysical Journal,* 79(6), pp. 3172-3192.

Pietilainen, K. H., Rog, T., Seppanen-Laakso, T., Virtue, S., Gopalacharyulu, P., Tang, J., Rodriguez-Cuenca, S., Maciejewski, A., Naukkarinen, J., Ruskeepaa, A. L., Niemela, P. S., Yetukuri, L., Tan, C. Y., Velagapudi, V., Castillo, S., Nygren, H., Hyotylainen, T., Rissanen, A., Kaprio, J., Yki-Jarvinen, H., Vattulainen, I., Vidal-Puig, A. and Oresic, M. (2011) 'Association of lipidome remodeling in the adipocyte membrane with acquired obesity in humans', *PLoS Biol,*

9(6), pp. e1000623.

Plimpton, S. (1995) 'FAST PARALLEL ALGORITHMS FOR SHORT-RANGE MOLECULAR-DYNAMICS', *Journal of Computational Physics,* 117(1), pp. 1-19.

Polson, J. M., Vattulainen, I., Zhu, H. and Zuckermann, H. (2001) 'Simulation study of lateral diffusion in lipid-sterol bilayer mixtures', *European Physical Journal E,* 5(4), pp. 485-497.

Repakova, J., Holopainen, J. M., Karttunen, M. and Vattulainen, I. (2006) 'Influence of pyrene-labeling on fluid lipid membranes', *Journal of Physical Chemistry B,* 110(31), pp. 15403-15410.

Rheinstädter, M. C. and Mouritsen, O. G. (2013) 'Small-scale structure in fluid cholesterol–lipid bilayers', *Current Opinion in Colloid & Interface Science,* 18(5), pp. 440-447.

Robinson, D., Besley, N. A., O'Shea, P. and Hirst, J. D. (2011) 'Water Order Profiles on Phospholipid/Cholesterol Membrane Bilayer Surfaces', *Journal of Computational Chemistry,* 32(12), pp. 2613-2618.

Rog, T., Pasenkiewicz-Gierula, M., Vattulainen, I. and Karttunen, M. (2009) 'Ordering effects of cholesterol and its analogues', *Biochim Biophys Acta,* 1788(1), pp. 97-121.

Rog, T. and Vattulainen, I. (2014) 'Cholesterol, sphingolipids, and glycolipids: what do we know about their role in raft-like membranes?', *Chem Phys Lipids,* 184, pp. 82-104.

Sackmann, E. (1995) *Biological membranes architecture and function. Handbook of Biological Physics, Vol. 1; Structure and dynamics of membranes: From cells to vesicles*.

Safran, S. (1994) *Statistical Thermodynamics of Surfaces, Interfaces, and Membranes.* New York: Addison-Wesley.

Saiz, L., Bandyopadhyay, S. and Klein, M. L. (2002) 'Towards an understanding of complex biological membranes from atomistic molecular dynamics simulations', *Bioscience Reports,* 22(2), pp. 151-173.

Samuli Ollila, O. H., Rog, T., Karttunen, M. and Vattulainen, I. (2007) 'Role of sterol type on lateral pressure profiles of lipid membranes affecting membrane protein functionality: Comparison between cholesterol, desmosterol, 7-dehydrocholesterol and ketosterol', *J Struct Biol,* 159(2), pp. 311-23.

Schneider, T. and Stoll, E. (1978) 'Molecular-dynamics study of a three-dimensional one-component model for distortive phase transitions', *Physical Review B,* 17(3), pp. 1302-1322.

Scott, H. L. (2002) 'Modeling the lipid component of membranes', *Current Opinion in Structural Biology,* 12(4), pp. 495-502.

Shaw, D. E., Deneroff, M. M., Dror, R. O., Kuskin, J. S., Larson, R. H., Salmon, J. K., Young, C., Batson, B., Bowers, K. J., Chao, J. C., Eastwood, M. P., Gagliardo, J., Grossman, J. P., Ho, C. R., Ierardi, D. J., Kolossvary, I., Klepeis, J. L., Layman, T., McLeavey, C., Moraes, M. A., Mueller, R., Priest, E. C., Shan, Y., Spengler, J., Theobald, M., Towles, B. and Wang, S. C. (2008) 'Anton, a

special-purpose machine for molecular dynamics simulation', *Communications of the Acm,* 51(7), pp. 91-97.

Simons, K. and Ikonen, E. (1997) 'Functional rafts in cell membranes', *Nature,* 387(6633), pp. 569-572.

Simons, K. and Vaz, W. L. C. (2004) 'Model systems, lipid rafts, and cell membranes', *Annual Review of Biophysics and Biomolecular Structure,* 33, pp. 269-295.

Singer, S. J. and Nicolson, G. L. (1972) 'The fluid mosaic model of the structure of cell membranes', *Science,* 175(4023), pp. 720-31.

Siu, S. W. I., Vacha, R., Jungwirth, P. and Boeckmann, R. A. (2008) 'Biomolecular simulations of membranes: Physical properties from different force fields', *Journal of Chemical Physics,* 128(12).

Smaby, J. M., Brockman, H. L. and Brown, R. E. (1994) 'CHOLESTEROLS INTERFACIAL INTERACTIONS WITH SPHINGOMYELINS AND PHOSPHATIDYLCHOLINES - HYDROCARBON CHAIN STRUCTURE DETERMINES THE MAGNITUDE OF CONDENSATION', *Biochemistry,* 33(31), pp. 9135-9142.

Smaby, J. M., Momsen, M., Kulkarni, V. S. and Brown, R. E. (1996) 'Cholesterol-induced interfacial area condensations of galactosylceramides and sphingomyelins with identical acyl chains', *Biochemistry,* 35(18), pp. 5696-5704.

Smaby, J. M., Momsen, M. M., Brockman, H. L. and Brown, R. E. (1997)

'Phosphatidylcholine acyl unsaturation modulates the decrease in interfacial elasticity induced by cholesterol', *Biophysical Journal,* 73(3), pp. 1492-1505.

Sonne, J., Hansen, F. Y. and Peters, G. H. (2005) 'Methodological problems in pressure profile calculations for lipid bilayers', *J Chem Phys,* 122(12), pp. 124903.

Soubias, O., Teague, W. E., Jr., Hines, K. G., Mitchell, D. C. and Gawrisch, K. (2010) 'Contribution of Membrane Elastic Energy to Rhodopsin Function', *Biophysical Journal,* 99(3), pp. 817-824.

Starke-Peterkovic, T., Turner, N., Vitha, M. F., Waller, M. P., Hibbs, D. E. and Clarke, R. J. (2006) 'Cholesterol effect on the dipole potential of lipid membranes', *Biophys J,* 90(11), pp. 4060-70.

Stimson, L., Dong, L., Karttunen, M., Wisniewska, A., Dutka, M. and Rog, T. (2007) 'Stearic acid spin labels in lipid bilayers: Insight through atomistic Simulations', *Journal of Physical Chemistry B,* 111(43), pp. 12447-12453.

Swope, W. C., Andersen, H. C., Berens, P. H. and Wilson, K. R. (1982) 'A COMPUTER-SIMULATION METHOD FOR THE CALCULATION OF EQUILIBRIUM-CONSTANTS FOR THE FORMATION OF PHYSICAL CLUSTERS OF MOLECULES - APPLICATION TO SMALL WATER CLUSTERS', *Journal of Chemical Physics,* 76(1), pp. 637-649.

Templer, R. H., Castle, S. J., Curran, A. R., Rumbles, G. and Klug, D. R. (1998) 'Sensing isothermal changes in the lateral pressure in model membranes

using di-pyrenyl phosphatidylcholine', *Faraday Discuss,* (111), pp. 41-53; discussion 69-78.

Terama, E., Ollila, O. H. S., Salonen, E., Rowat, A. C., Trandum, C., Westh, P., Patra, M., Karttunen, M. and Vattulainen, I. (2008) 'Influence of ethanol on lipid membranes: From lateral pressure profiles to dynamics and partitioning', *Journal of Physical Chemistry B,* 112(13), pp. 4131-4139.

Tieleman, D. P., Maccallum, J. L., Ash, W. L., Kandt, C., Xu, Z. and Monticelli, L. (2006) 'Membrane protein simulations with a united-atom lipid and all-atom protein model: lipid-protein interactions, side chain transfer free energies and model proteins', *J Phys Condens Matter,* 18(28), pp. S1221-34.

Tieleman, D. P., Marrink, S. J. and Berendsen, H. J. (1997) 'A computer perspective of membranes: molecular dynamics studies of lipid bilayer systems', *Biochim Biophys Acta,* 1331(3), pp. 235-70.

Tildesley, M. P. A. a. D. J. (1987) *Computer Simulations of Liquds.* Oxford.

Vanommeslaeghe, K., Hatcher, E., Acharya, C., Kundu, S., Zhong, S., Shim, J., Darian, E., Guvench, O., Lopes, P., Vorobyov, I. and Mackerell, A. D., Jr. (2010) 'CHARMM general force field: A force field for drug-like molecules compatible with the CHARMM all-atom additive biological force fields', *J Comput Chem,* 31(4), pp. 671-90.

Vattulainen, I. and Mouritsen, O. G. (2004) *In Diffusion in Condensed Matter: Methods, Materials, Models* Berlin: Springer.

Veatch, S. L. (2007) 'From small fluctuations to large-scale phase separation: Lateral organization in model membranes containing cholesterol', *Seminars in Cell & Developmental Biology,* 18(5), pp. 573-582.

Vist, M. R. and Davis, J. H. (1990) 'PHASE-EQUILIBRIA OF CHOLESTEROL DIPALMITOYLPHOSPHATIDYLCHOLINE MIXTURES - H-2 NUCLEAR MAGNETIC-RESONANCE AND DIFFERENTIAL SCANNING CALORIMETRY', *Biochemistry,* 29(2), pp. 451-464.

Yang, J., Calero, C. and Marti, J. (2014) 'Diffusion and spectroscopy of water and lipids in fully hydrated dimyristoylphosphatidylcholine bilayer membranes', *Journal of Chemical Physics,* 140(10).

Yeagle, P. L. (1985) 'CHOLESTEROL AND THE CELL-MEMBRANE', *Biochimica Et Biophysica Acta,* 822(3-4), pp. 267-287.

Yeagle, P. L. (1989) 'Lipid regulation of cell membrane structure and function', *FASEB J,* 3(7), pp. 1833-42.

Yeagle, P. L. (2004) *The structure of Biological Membranes, Second Edition.* CRC Press.

Zhang, Z., Lu, L. and Berkowitz, M. L. (2008) 'Energetics of cholesterol transfer between lipid bilayers', *Journal of Physical Chemistry B,* 112(12), pp. 3807-3811.

Zimmerberg, J. and Kozlov, M. M. (2006) 'How proteins produce cellular membrane curvature', *Nature Reviews Molecular Cell Biology,* 7(1), pp. 9-19.

Appendix A

This python programme is used to track cholesterol that most likely underwent flip-flop motions via checking how much times one switch its orientation along z-axis over last 60ns production simulations.

MDAnalysis software library was used in this code. (Michaud-Agrawal et al., 2011)

Michaud-Agrawal, N., Denning, E. J., Woolf, T. B. and Beckstein, O. (2011) 'Software News and Updates MDAnalysis: A Toolkit for the Analysis of Molecular Dynamics Simulations', *Journal of Computational Chemistry,* 32(10), pp. 2319-2327.

```
#------Codes start-----------------

import sys, string
import numpy as np
from MDAnalysis import *

if len(sys.argv) !=4 :
   print "Syntax: flip_flop.py psf.file dcd.file mol% "
   sys.exit()

skip = 1

time_interval=0.010*skip

universe = Universe(sys.argv[1],sys.argv[2])

box=universe.trajectory.ts.dimensions[:3]
```

```
x_half=box[0]/2
y_half=box[1]/2
z_half=box[2]/2

selection_C25 = "resname CHL1 and name C25"
C25_group = universe.selectAtoms(selection_C25)
C25_data = universe.trajectory.timeseries(C25_group, &
                &format="afc", skip=skip)

selection_O3 = "resname CHL1 and name O3"
O3_group = universe.selectAtoms(selection_O3)
O3_data = universe.trajectory.timeseries(O3_group,&
              &format="afc", skip=skip)

no_frame=C25_data.shape[1]
no_mol=C25_data.shape[0]
chol_vector=np.zeros((no_mol,no_frame,3))

count_pbc=0.00

for i in range (no_mol):
      for j in range(no_frame):
            if C25_data[i,j,0]-O3_data[i,j,0]>x_half:
                  C25_data[i,j,0]=C25_data[i,j,0]-2*x_half

            elif C25_data[i,j,0]-O3_data[i,j,0]<-x_half:
                  C25_data[i,j,0]=C25_data[i,j,0]+2*x_half

            if C25_data[i,j,1]-O3_data[i,j,1]>y_half:
                  C25_data[i,j,1]=C25_data[i,j,1]-2*y_half

            elif C25_data[i,j,1]-O3_data[i,j,1]<-y_half:
```

```
                C25_data[i,j,1]=C25_data[i,j,1]+2*y_half

            if C25_data[i,j,2]-O3_data[i,j,2]>z_half:
                C25_data[i,j,2]=C25_data[i,j,2]-2*z_half

            elif C25_data[i,j,2]-O3_data[i,j,2]<-z_half:
                C25_data[i,j,2]=C25_data[i,j,2]+2*z_half


chol_vector=O3_data-C25_data

chol_length=np.sqrt(np.sum(np.power(chol_vector,2),axis=-1))

unit_chol=np.zeros((no_mol,no_frame,3))

for i in range(no_mol):
    for j in range(no_frame):
        unit_chol[i,j,:]=chol_vector[i,j,:]/chol_length[i,j]
chol=chol_vector

cos_theta=np.dot(unit_chol,(0,0,1))
theta=np.arccos(cos_theta)
theta=np.rad2deg(theta)

#print cos_theta.shape,theta.shape

flip_flop=[]

for i in range(no_mol):
    for j in range(no_frame):
        if chol[i,j,2]>0:
            flip_flop.append(int(1))
```

```
            elif chol[i,j,2]<0:
                flip_flop.append(int(-1))
flip_flop=np.asarray(flip_flop)

flip_flop=flip_flop.reshape(no_mol,no_frame,1)

no_flips=np.zeros((no_mol,1))


for i in range(no_mol):
    count_flip=0
    for j in range(no_frame):
        if j==0:
            ref_direction=flip_flop[i,0]

        if flip_flop[i,j] == -ref_direction:
            count_flip=count_flip+1
            ref_direction = flip_flop[i,j]

    no_flips[i]=count_flip

total_flips=0

fliped_chol=0
for i in range(no_mol):
    if no_flips[i]!=0:
        fliped_chol=fliped_chol+1
    total_flips=total_flips+no_flips[i]

print 'total flips:',total_flips
print 'no_flipped chol', fliped_chol, ',in total number of cholesterol', no_mol
print 'no of occurance of flip-flop:\n',no_flips
```

```
out=open('%s_traj_for_most_flipped.dat'%(sys.argv[3]),'w')
out2=open('%s_angular_for_most_flipped.dat'%(sys.argv[3]),'w')
max_flip=max(no_flips)

for i in range(no_mol):
    if no_flips[i] == max_flip:
        for j in range(no_frame):
            out.write('%f \t %f \t %f \n'%(j*&
                &time_interval, O3_data[i,j,2],C25_data [i,j,2]))
            out2.write('%f \t %f \n'%(j*time_interval,cos_theta[i,j]))
out.close()
out2.close()

#------Codes end----------
```

Appendix B

This python code is used to collect splay angles of three pairs: DPPC-DPPC, DPPC-cholesterol, and cholesterol-cholesterol pairs in a cholesterol-containing DPPC bilayer. The last 60ns trajectory file was used for the collection.

MDAnalysis software library was used in this code. (Michaud-Agrawal et al., 2011)

Michaud-Agrawal, N.,
Denning, E. J., Woolf, T. B. and Beckstein, O. (2011) 'Software News and Updates MDAnalysis: A Toolkit for the Analysis of Molecular Dynamics Simulations', *Journal of Computational Chemistry,* 32(10), pp. 2319-2327.

```
#------Codes start-----------------

import sys
from MDAnalysis import *
from numpy import *
from MDAnalysis.core.distances import *
from scipy.stats import norm

skip=1
if len(sys.argv) !=4 :
   print "Syntax: splay_angle_collection.py psf_file dcd_123 mol%_info"
   sys.exit()

limit_tilt=10    #limit tilt angle for DPPC in splay angle pairing
limit_tilt_chl=10 #limit tilt angle for cholesterol in splay angle pairing
limit_dis=10    #limit molecular lateral distance for DPPC in splay angle pairing
```

```
#########reading trajectory data files #############

u=Universe(sys.argv[1],sys.argv[2])

box = u.trajectory.ts.dimensions[:3]

#-----------------------------Reading DPPC data-------------------------

pc_head_P=u.selectAtoms('resname DPPC and name P')
pc_head_C=u.selectAtoms('resname DPPC and name C2')

pc_tail_2C1=u.selectAtoms('resname DPPC and name C216')
pc_tail_2C2=u.selectAtoms('resname DPPC and name C215')
pc_tail_2C3=u.selectAtoms('resname DPPC and name C214')

pc_tail_1C1=u.selectAtoms('resname DPPC and name C316')
pc_tail_1C2=u.selectAtoms('resname DPPC and name C315')
pc_tail_1C3=u.selectAtoms('resname DPPC and name C314')



pc_HP=u.trajectory.timeseries(pc_head_P,format='fac',skip=skip)
pc_HC=u.trajectory.timeseries(pc_head_C,format='fac',skip=skip)

pc_T_2C1=u.trajectory.timeseries(pc_tail_2C1,format='fac',skip=skip)
pc_T_2C2=u.trajectory.timeseries(pc_tail_2C2,format='fac',skip=skip)
pc_T_2C3=u.trajectory.timeseries(pc_tail_2C3,format='fac',skip=skip)

pc_T_1C1=u.trajectory.timeseries(pc_tail_1C1,format='fac',skip=skip)
pc_T_1C2=u.trajectory.timeseries(pc_tail_1C2,format='fac',skip=skip)
pc_T_1C3=u.trajectory.timeseries(pc_tail_1C3,format='fac',skip=skip)

shape_pc=pc_HC.shape
frame=shape_pc[0]
```

```
natoms_pc=shape_pc[1]

#--------------remove PBC and prepare DPPC vector----------------------

#remove PBC
x_half=box[0]/2
y_half=box[1]/2
z_half=box[2]/2

pc_head=zeros((frame,natoms_pc,3))
pc_tail=zeros((frame,natoms_pc,3))

#before get the midpoint, need to remove periodic boundary conditions #for each molecule
#to do that, need chose one reference point, and calculate the distance in #x,y,z direction,respectively.
#this is the easiest way to obtain that.chose Phosphate P as the reference point

Candidates=[pc_HC,pc_T_1C1,pc_T_1C2,pc_T_1C3,pc_T_2C1,pc_T_2C2,pc_T_2C3]

for i in range(frame):
    for j in range(natoms_pc):
        for z in range(len(Candidates)):
            if pc_HP[i,j,0]-Candidates[z][i,j,0]>x_half:
                Candidates[z][i,j,0]=Candidates[z][i,j,0]+2*x_half

            elif pc_HP[i,j,0]-Candidates[z][i,j,0]<-x_half:
                Candidates[z][i,j,0]=Candidates[z][i,j,0]-2*x_half

            if pc_HP[i,j,1]-Candidates[z][i,j,1]>y_half:
                Candidates[z][i,j,1]=Candidates[z][i,j,1]+2*y_half

            elif pc_HP[i,j,1]-Candidates[z][i,j,1]<-y_half:
```

```
                Candidates[z][i,j,1]=Candidates[z][i,j,1]-2*y_half

            if pc_HP[i,j,2]-Candidates[z][i,j,2]>z_half:

                Candidates[z][i,j,2]=Candidates[z][i,j,2]+2*z_half

            elif pc_HP[i,j,2]-Candidates[z][i,j,2]<-z_half:
                Candidates[z][i,j,2]=Candidates[z][i,j,2]-2*z_half

#----get PC midpoint in head and get geometric center of terminal three C #from both tails -------

for i in range(frame):
    for j in range(natoms_pc):
        pc_head[i,j,:]=(pc_HP[i,j,:]+pc_HC[i,j,:])/2.0
        pc_tail[i,j,:]=(pc_T_1C1[i,j,:]+pc_T_1C2[i,j,:]+pc_T_1C3[i,j,:]&
                &+pc_T_2C1[i,j,:]+pc_T_2C2[i,j,:]+pc_T_2C3[i,j,:])/6.0

del(pc_head_P,pc_head_C,pc_tail_2C1,pc_tail_2C2,pc_tail_2C3,&
  &pc_tail_1C1, pc_tail_1C2, pc_tail_1C3)
del(pc_T_2C1,pc_T_2C2,pc_T_2C3,pc_T_1C1,pc_T_1C2,pc_T_1C3,&
  &pc_HP,pc_HC)

#DPPC orientation vector, point from the center of bilayer to edge
pc_vector=zeros((frame,natoms_pc,3))

pc_vector=pc_head-pc_tail       #DPPC 's direction vector t

#------------------------------PC tilt angle calculation----------------------

length_pc=zeros((frame,natoms_pc))
z_dis_pc=abs(pc_vector[:,:,2])
```

```
for i in range(frame):
      length_pc[i,:]=sqrt((pc_vector[i,:,0])**2+pc_vector[i,:,1]**2+&
                        &pc_vector[i,:,2] **2)

cos_theta_pc=z_dis_pc/length_pc

theta_pc=arccos(cos_theta_pc)
theta_pc=rad2deg(theta_pc)      #convert radian into degrees

angle_length=open('first_frame_length_angle.dat','w')
angle_length.write('atom_no_j    length_PC    theta_PC \n')

for j in range(natoms_pc):
       angle_length.write('%d %f %f \n'%(j+1,length_pc[0,j],theta_pc[0,j]))

#------------read data for CHOL from trajectory -----------------

chl_3=u.selectAtoms('resname CHL1 and name C3')
chl_17=u.selectAtoms('resname CHL1 and name C23')     ## redefined C3-C23
vector for cholesterol
chl_c3=u.trajectory.timeseries(chl_3,format='fac',skip=skip)
chl_c17=u.trajectory.timeseries(chl_17,format='fac',skip=skip)

shape_chol=chl_c3.shape
frame_chol=shape_chol[0]
natoms_chl=shape_chol[1]

#------------Chol vector preparation: remove PBC-----------------

chl_x_pbc=0
chl_y_pbc=0
chl_z_pbc=0
```

```
for i in range(frame):
    for j in range(natoms_chl):
        #---------for x-direction-----------------

        if chl_c3[i,j,0]-chl_c17[i,j,0]>x_half:
            chl_c17[i,j,0]=chl_c17[i,j,0]+2*x_half
            chl_x_pbc=chl_x_pbc+1
        elif chl_c3[i,j,0]-chl_c17[i,j,0]<-x_half:
            chl_c17[i,j,0]=chl_c17[i,j,0]-2*x_half
            chl_x_pbc=chl_x_pbc+1

        #---------for y-direction-----------------
        if chl_c3[i,j,1]-chl_c17[i,j,1]>y_half:
            chl_c17[i,j,1]=chl_c17[i,j,1]+2*y_half
            chl_y_pbc=chl_y_pbc+1
        elif chl_c3[i,j,1]-chl_c17[i,j,1]<-y_half:
            chl_c17[i,j,1]=chl_c17[i,j,1]-2*y_half
            chl_y_pbc=chl_y_pbc+1

        #---------for z-direction-----------------
        if chl_c3[i,j,2]-chl_c17[i,j,2]>z_half:
            chl_c17[i,j,2]=chl_c17[i,j,2]+2*z_half
            chl_z_pbc=chl_z_pbc+1
        elif chl_c3[i,j,2]-chl_c17[i,j,2]<-z_half:
            chl_c17[i,j,2]=chl_c17[i,j,2]-2*z_half
            chl_z_pbc=chl_z_pbc+1

chl_vector=chl_c3-chl_c17

#------------------------CHOL tilt angle calculation-----------------------

theta_chl=zeros((frame_chol,natoms_chl))
length_chl=zeros((frame_chol,natoms_chl))
```

```
z_dis_chl=abs(chl_vector[:,:,2])

for i in range(frame_chol):
    length_chl[i,:]=sqrt((chl_vector[i,:,0])**2+&
                    &chl_vector[i,:,1]**2+chl_vector[i,:,2]**2)

cos_theta_chl=z_dis_chl/length_chl

theta_chl=arccos(cos_theta_chl)
theta_chl=rad2deg(theta_chl)



#---------------DPPC-Cholesterol splay angle calculation-----------------
angle_a_upper=[]
angle_a_lower=[]
angle_a_total=[]

##upper_layer
for i in range(frame):
      for j in range(natoms_pc):
            if pc_vector[i,j,2]>0:
                  for k in range(natoms_chl):
                        if chl_vector[i,k,2]>0:
                              if theta_pc[i,j]<=limit_tilt
                              or theta_chl[i,k]<=limit_tilt_chl:
                                    vector_jk=pc_head[i,j,:]-chl_c3[i,k,:]
                                    if vector_jk[0]>x_half:
                                          vector_jk[0]=vector_jk[0]-2*x_half
                                    elif vector_jk[0]<-x_half:
                                          vector_jk[0]=vector_jk[0]+2*x_half

                                    if vector_jk[1]>y_half:
```

```
                    vector_jk[1]=vector_jk[1]-2*y_half
                elif vector_jk[1]<-y_half:
                    vector_jk[1]=vector_jk[1]+2*y_half
                jk_distance=sqrt(vector_jk[0]**2+&
                            &vector_jk[1]**2+vector_jk[2]**2)
                if jk_distance <=limit_dis:

                    cos_a=dot(pc_vector[i,j],chl_vector[i,k])/&
                            &(length_pc[i,j]*length_chl[i,k])
                    angle_a=arccos(cos_a)
                    angle_a=rad2deg(angle_a)

                    angle_a_upper.append(angle_a)
                    angle_a_total.append(angle_a)

##lower_layer
for i in range(frame):
    for j in range(natoms_pc):
        if pc_vector[i,j,2]<0:
            for k in range(natoms_chl):
                if chl_vector[i,k,2]<0:
                    if theta_pc[i,j]<=limit_tilt
                    or theta_chl[i,k]<=limit_tilt_chl:
                        vector_jk=pc_head[i,j,:]-chl_c3[i,k,:]

                        if vector_jk[0]>x_half:
                            vector_jk[0]=vector_jk[0]-2*x_half
                        elif vector_jk[0]<-x_half:
                            vector_jk[0]=vector_jk[0]+2*x_half

                        if vector_jk[1]>y_half:
                            vector_jk[1]=vector_jk[1]-2*y_half
                        elif vector_jk[1]<-y_half:
```

```
                    vector_jk[1]=vector_jk[1]+2*y_half

                jk_distance=sqrt(vector_jk[0]**2+&
                    &vector_jk[1]**2+vector_jk[2]**2)
                if jk_distance <=limit_dis:
                    cos_a=dot(pc_vector[i,j],chl_vector[i,k])&
                        &/(length_pc[i,j]*length_chl[i,k])
                    angle_a=arccos(cos_a)
                    angle_a=rad2deg(angle_a)

                    angle_a_lower.append(angle_a)
                    angle_a_total.append(angle_a)

angle_a_upper=asarray(angle_a_upper)
angle_a_lower=asarray(angle_a_lower)
angle_a_total=asarray(angle_a_total)

bin_z=arange(0,91,1)

his_z=histogram(angle_a_total,bin_z,normed=False)

pdf_alpha=his_z[0]

file_tilt_angle=open('%s_PC_CHL_angle.dat'%sys.argv[3],'w')

for i in range(len(pdf_alpha)):
    file_tilt_angle.write('%i '%(bin_z[i+1])+' %.8f'%pdf_alpha[i]+'\n')

file_tilt_angle.close()
del(angle_a_upper,angle_a_lower,angle_a_total)

#------------DPPC-DPPC splay angle calculation--------
angle_a_upper=[]
```

```
angle_a_lower=[]
angle_a_total=[]

##upper_layer
for i in range(frame):
    for j in range(natoms_pc-1): #go over all pairs of pc-pc pairs
        if pc_vector[i,j,2]>0:      #to discard flipped lipids
            #up_1=up_1+1
             for k in range(j+1,natoms_pc): # over all pairs of pc-pc pairs
                 if pc_vector[i,k,2]>0:    #discard flipped lipids

                     #filter out theta over 10 degree
                      if theta_pc[i,j]<=limit_tilt
                      or theta_pc[i,k]<=limit_tilt:
                          vector_jk=pc_head[i,j,:]-pc_head[i,k,:]

                          if vector_jk[0]>x_half:
                              vector_jk[0]=vector_jk[0]-2*x_half
                          elif vector_jk[0]<-x_half:
                              vector_jk[0]=vector_jk[0]+2*x_half

                          if vector_jk[1]>y_half:
                              vector_jk[1]=vector_jk[1]-2*y_half
                          elif vector_jk[1]<-y_half:
                              vector_jk[1]=vector_jk[1]+2*y_half

                          jk_distance=sqrt(vector_jk[0]**2&
                              &+vector_jk[1]**2+vector_jk[2]**2)
                          if jk_distance <=limit_dis:

                              cos_a=dot(pc_vector[i,j],pc_vector[i,k])/&
                                    &(length_pc[i,j]*length_pc[i,k])
                              angle_a=arccos(cos_a)
```

```
                                angle_a=rad2deg(angle_a)

                                angle_a_upper.append(angle_a)
                                angle_a_total.append(angle_a)

##lower_layer
for i in range(frame):
    for j in range(natoms_pc-1):
        if pc_vector[i,j,2]<=0:
            for k in range(j+1,natoms_pc):
                if pc_vector[i,k,2]<=0:
                    #filter the theta over limit_tilt
                     if theta_pc[i,j]<=limit_tilt
                     or theta_pc[i,k]<=limit_tilt:
                        vector_jk=pc_head[i,j,:]-pc_head[i,k,:]
                        if vector_jk[0]>x_half:
                            vector_jk[0]=vector_jk[0]-2*x_half
                        elif vector_jk[0]<-x_half:
                            vector_jk[0]=vector_jk[0]+2*x_half

                        if vector_jk[1]>y_half:
                            vector_jk[1]=vector_jk[1]-2*y_half
                        elif vector_jk[1]<-y_half:
                            vector_jk[1]=vector_jk[1]+2*y_half

                        jk_distance=sqrt(vector_jk[0]**2+&
                                    &vector_jk[1]**2+vector_jk[2]**2)
                        if jk_distance <=limit_dis:
                            cos_a=dot(pc_vector[i,j],pc_vector[i,k])/&
                                    &(length_pc[i,j]*length_pc[i,k])
                            angle_a=arccos(cos_a)
                            angle_a=rad2deg(angle_a)
```

```
                                    angle_a_lower.append(angle_a)
                                    angle_a_total.append(angle_a)

angle_a_upper=asarray(angle_a_upper)
angle_a_lower=asarray(angle_a_lower)
angle_a_total=asarray(angle_a_total)

bin_z=arange(0,91,1)    #create a bin array from 0 to 90

his_z=histogram(angle_a_total,bin_z,normed=False)    # not normalized

pdf_alpha=his_z[0]      #get the probability distribution data

file_tilt_angle=open('%s_PC_PC_angle.dat'%sys.argv[3],'w')

for i in range(len(pdf_alpha)):
      file_tilt_angle.write('%i '%(bin_z[i+1])+' %.8f'%pdf_alpha[i]+'\n')

file_tilt_angle.close()

del(angle_a_upper,angle_a_lower,angle_a_total)

#-----------------CHL-CHL splay angle calculation-------------------------
angle_a_upper=[]
angle_a_lower=[]
angle_a_total=[]

up_1=0
up_2=0
##upper_layer
for i in range(frame):
      for j in range(natoms_chl-1):
            if chl_vector[i,j,2]>0:
```

```
                up_1=up_1+1
                for k in range(j+1,natoms_chl):
                    if chl_vector[i,k,2]>0:
                        if theta_chl[i,j]<=limit_tilt_chl or &
                        & theta_chl[i,k]<=limit_tilt_chl

                            vector_jk=chl_c3[i,j,:]-chl_c3[i,k,:] #
                            if vector_jk[0]>x_half:
                                vector_jk[0]=vector_jk[0]-2*x_half
                            elif vector_jk[0]<-x_half:
                                vector_jk[0]=vector_jk[0]+2*x_half

                            if vector_jk[1]>y_half:
                                vector_jk[1]=vector_jk[1]-2*y_half
                            elif vector_jk[1]<-y_half:
                                vector_jk[1]=vector_jk[1]+2*y_half



                            jk_distance=sqrt(vector_jk[0]**2+&
                                    &vector_jk[1]**2+vector_jk[2]**2)
                            if jk_distance <=limit_dis:

                                cos_a=dot(chl_vector[i,j],chl_vector[i,k])&
                                        &/(length_chl[i,j]*length_chl[i,k])
                                angle_a=arccos(cos_a)
                                angle_a=rad2deg(angle_a)

                                angle_a_upper.append(angle_a)
                                angle_a_total.append(angle_a)

low_1=0
##lower_layer
for i in range(frame):
```

```
    for j in range(natoms_chl-1):
        if chl_vector[i,j,2]<0:
            low_1=low_1+1
            for k in range(j+1,natoms_chl):
                if chl_vector[i,k,2]<0:
                    if theta_chl[i,j]<=limit_tilt_chl or &
                    & theta_chl[i,k]<= limit_tilt_chl:

                        vector_jk=chl_c3[i,j,:]-chl_c3[i,k,:]
                        if vector_jk[0]>x_half:
                            vector_jk[0]=vector_jk[0]-2*x_half
                        elif vector_jk[0]<-x_half:
                            vector_jk[0]=vector_jk[0]+2*x_half

                        if vector_jk[1]>y_half:
                            vector_jk[1]=vector_jk[1]-2*y_half
                        elif vector_jk[1]<-y_half:
                            vector_jk[1]=vector_jk[1]+2*y_half

                        jk_distance=sqrt(vector_jk[0]**2+&
                              &vector_jk[1]**2+vector_jk[2]**2)
                        if jk_distance <=limit_dis:

                            cos_a=dot(chl_vector[i,j],chl_vector[i,k])&
                                  &/ (length_chl[i,j]*length_chl[i,k])
                            angle_a=arccos(cos_a)
                            angle_a=rad2deg(angle_a)

                            angle_a_lower.append(angle_a)
                            angle_a_total.append(angle_a)



angle_a_upper=asarray(angle_a_upper)
```

```
angle_a_lower=asarray(angle_a_lower)
angle_a_total=asarray(angle_a_total)

bin_z=arange(0,91,1)

his_z=histogram(angle_a_total,bin_z,normed=False)

pdf_alpha=his_z[0]

file_tilt_angle=open('%s_CHL_CHL_angle.dat'%sys.argv[3],'w')

for i in range(len(pdf_alpha)):
    file_tilt_angle.write('%i '%(bin_z[i+1])+' %.8f'%pdf_alpha[i]+'\n')

file_tilt_angle.close()
del(angle_a_upper,angle_a_lower,angle_a_total)

#------Codes End-----------------
```